Vol. 05 / Issue. 02 / 2016

ENGINEERING EDGE

Accelerate Innovation with CFD & Thermal Characterization

Optimizing a Championship NASCAR Racing Machine
Page 14

Fujifilm Camera Design
Page 24

Robert Bosch India Drives ECU Temperatures Down
Page 37

mentor.com/mechanical

Mentor Graphics®
Mechanical Analysis

FloMASTER™ V8

Increase the Speed & Accuracy of Product Simulations with Simulation Based Characterization

3D CFD meets System Level Simulation

Uncompromised Performance

Data at Speed

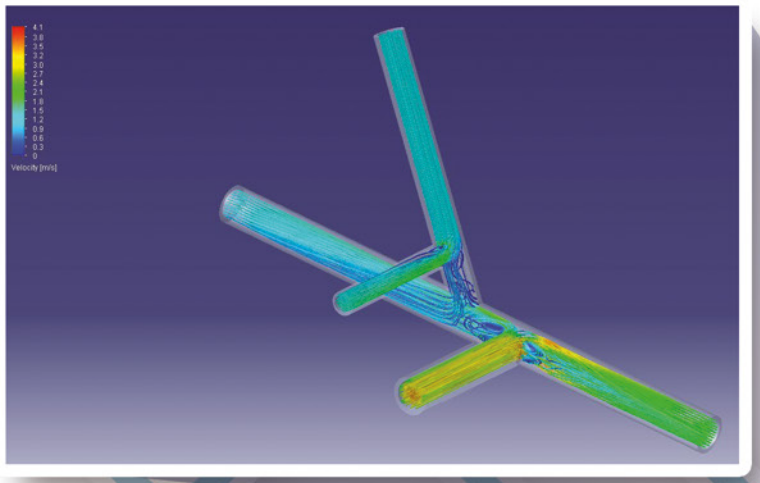

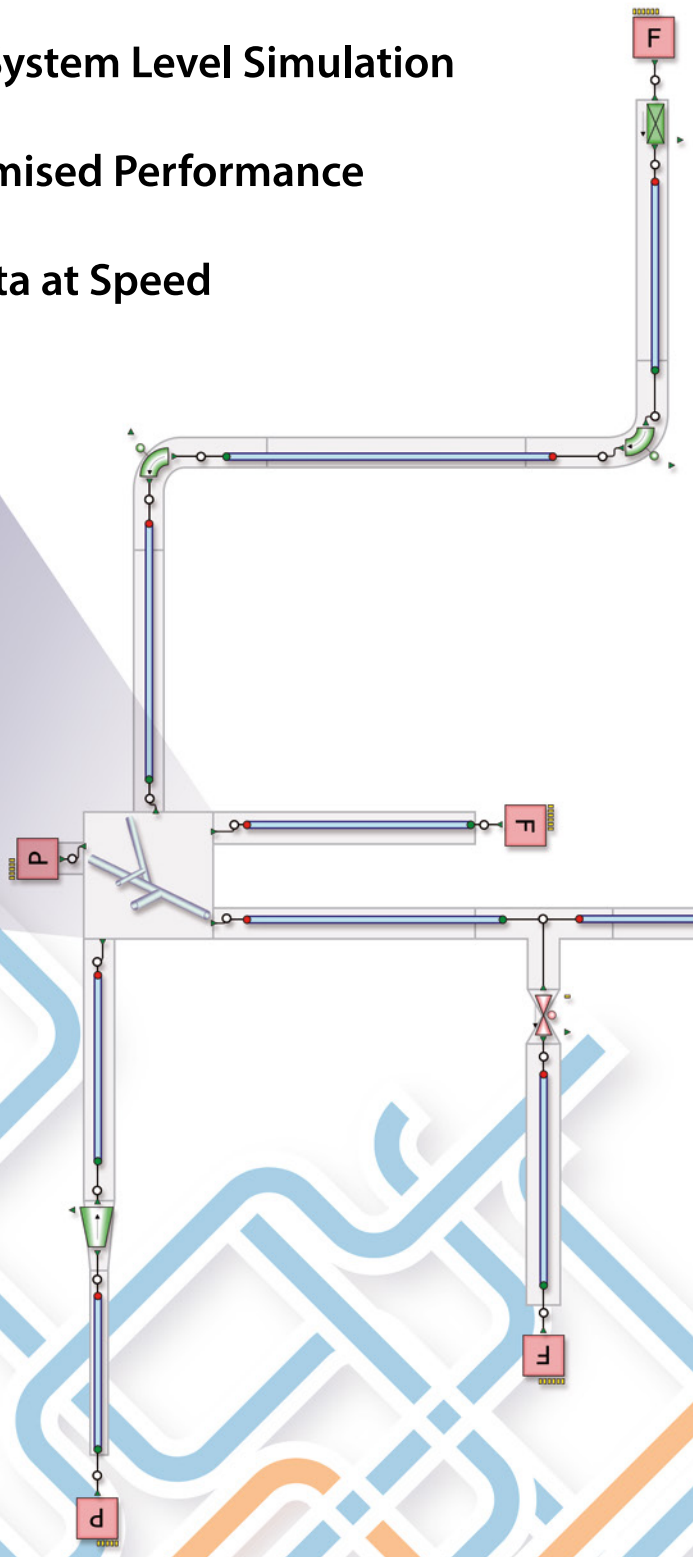

Visit the website for more:
www.mentor.com/mechanical

Mentor Graphics®

Mechanical Analysis

Mentor Graphics
Mechanical Analysis

Mentor Graphics Corporation
Pury Hill Business Park,
The Maltings,
Towcester, NN12 7TB,
United Kingdom
Tel: +44 (0)1327 306000
email: ee@mentor.com

Editor:
Keith Hanna

Managing Editor:
Natasha Antunes

Copy Editor:
Jane Wade

Contributors:
Sergio Antioquia, Robin Bornoff, Mike Croegaert, Mike Gruetzmacher, Keith Hanna, Doug Kolak, Boris Marovic, John Murray, Sawako Ofuchi, John Parry, Nazita Saye, Tatiana Trebunskikh, Gang Wang

With special thanks to:
Anthony Kumpen,
Axis Engineering,
CSEG,
Esteq,
Fujifilm,
Hyundai Heavy Industries Analysis of Pressure Surge in Offshore Floating Production Unit,
Institute of Microelectronics, Singapore,
Laboratoire IMS,
Mitsubishi Materials,
Robert Bosch India,
Shin-Etsu Chemicals Co., Ltd.,
Tamturbo Oy,
TsAGI & Irkut Corporation, and
Voxdale bvba

Perspective

Vol. 05, Issue. 02

Greetings readers! It is nearly five years since the Flowmaster® product-line joined Mentor Graphics and this edition celebrates its first major release, V8.0 which has also been rebranded to: FloMASTER™. This is a major overhaul of the product (see Product News page 8) with a new user experience Launchpad interface, a new Simulation Based Characterization (SBC) capability that is unique to a 1D thermo-fluid system simulation tool, and physics improvements in a number of areas, not least of which a new Waste Heat Recovery capability. SBC is effectively a 3D CFD capability (based on FloEFD™ technology) embedded within a 1D CFD code. This unites two of our strengths – system level thermo-fluid modeling and fast CAD-embedded 3D CFD component simulation and characterization. This will transform the way that 1D systems engineers engage with 3D CFD, make systems simulations more accurate, and speed up the 3D to 1D CFD workflow dramatically. Nothing else like it exists on the CFD market.

I am also pleased to report that our Don Miller Award for Excellence in Thermo-Fluid System Simulation in its second year has been awarded to Chrysler India Automotive for their great experimental validation of Flowmaster in various automotive thermal management applications. Our new 2016 Frontloading CFD Award for the best applications of FloEFD early in a design process has been awarded to Automotive Lighting in America who had a body of work on how they improved their headlight design process. This year we hosted a FloEFD User Conference in Frankfurt, Germany, in early November which was a great forum for FloEFD users to hear of the advances going on with this next-wave CFD product and to network with other FloEFD users.

The breadth of customer stories in this edition of Engineering Edge is truly broad with automotive and ground transportation taking prominence. Delphi, Robert Bosch India, Continental, Voxdale, CSEG and EC-Power all feature in this industry sector with applications ranging from HEV battery modeling to NASCAR and a Wind Tunnel design. Fujifilm describe how they develop camera electronics using FloTHERM. Mitsubishi Materials have developed a clever multi-software simulation approach to designing liquid cooling of machining tools. ShinEtsu, IMS in Bordeaux and our own AE, Gang Wang, in China describe T3Ster® applications ranging from TIM materials to Lasers and automotive headlights showing the versatility of our MicReD® thermal testing technology. Two great Flowmaster stories are included: Hyundai Heavy Industries in Korea and Robin Bornoff's N-Arm How to Guide as well as the use of FloEFD to simulate turbochargers at Tamturbo in Finland.

Finally, we recently joined the power electronics Wide Band Gap initiative (WBGi) consortium in Japan led by Professors Suganuma and Funaki of Osaka University. This cements our ongoing commitment to this sector globally with our MicReD hardware and electronics cooling software product-lines.

Roland Feldhinkel, General Manager,
Mechanical Analysis Division, Mentor Graphics

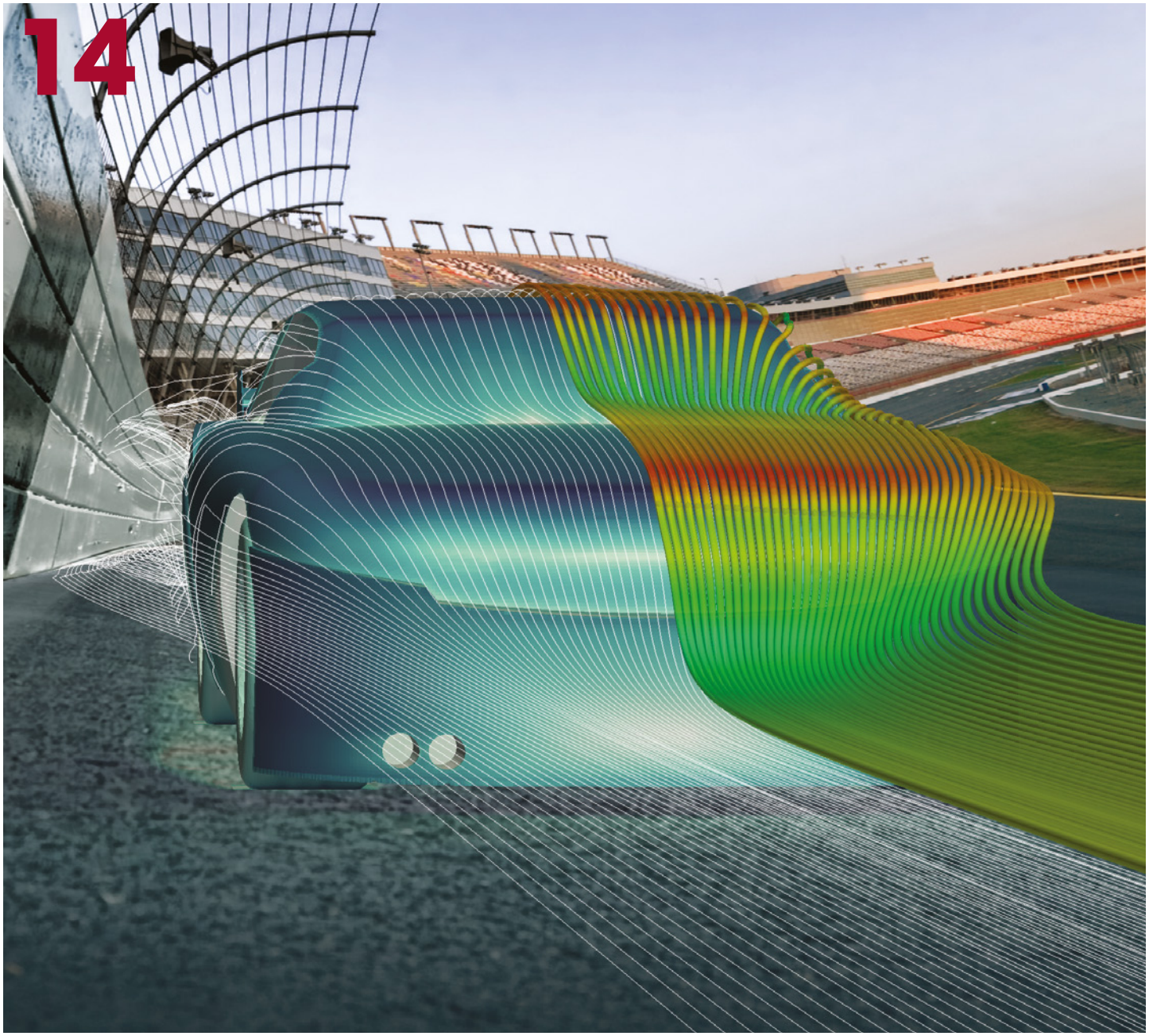

News

Engineering Edge

Contents

Technology & Knowledge Bank

Regular Features

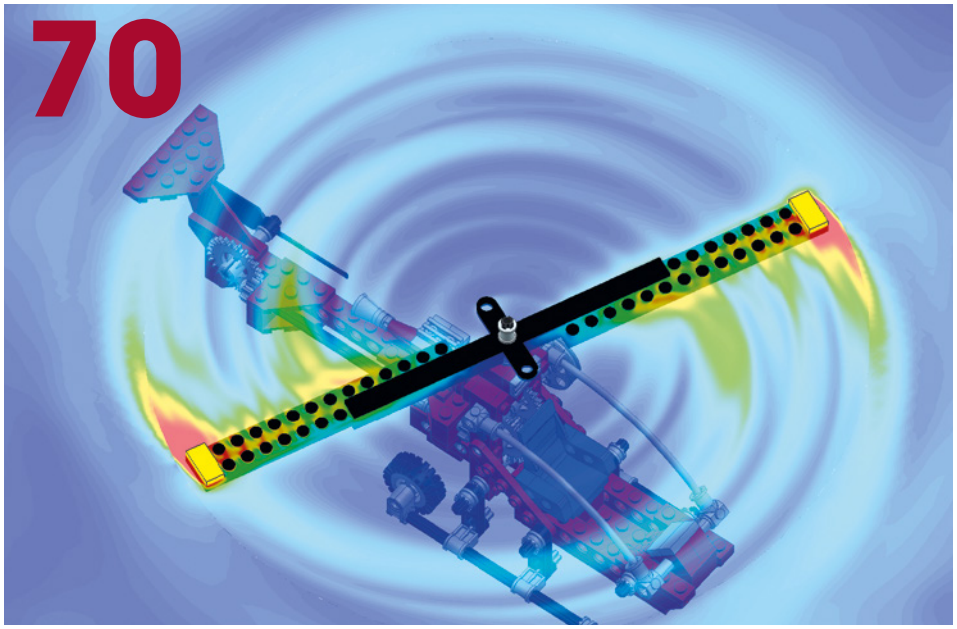

New Release: FloEFD 16

The newest release of the leading frontloading Computational Fluid Dynamics (CFD) product, FloEFD™ targets complex design challenges. Frontloading CFD refers to the practice of moving CFD simulation early into the design process, enabling design engineers to examine and evaluate design options, resulting in optimized product performance and reliability. The new FloEFD release provides the industry's first simulation solution for water vapor absorption alongside several other lighting related functionalities.

- **Water Sorption by Plastics:** With the latest version of FloEFD, users can now simulate the sorption (when one substance permeates another) and desorption (changing from an adsorbed state to a gaseous or liquid state) processes. For example, plastic absorbs water and then releases it when environmental conditions change. This functionality is important for several key markets such as automotive lighting design where moisture needs to be minimized in light housings. Other automotive lighting related capabilities include radiation and spectrum for direction source modeling, and LED thermal-optical modeling to simulate LEDs with non-linear dependence of parameters on temperature.

While we continue to make the software faster and more efficient, the focus of FloEFD 16 is on power and the ability to handle even more complex tasks:

- **Linked Data from Components:** Often the design of complex devices assumes a multi-level simulation approach when analysis is initiated from a simple component, followed by an assembly of components, then finally the full system comprise many components and sub-assemblies. Using the new FloEFD product, users can move from level to level, and re-use the component task definition of an assembly, saving a great amount of time by eliminating the need to repeat component or sub-assembly definition. Users simply link to a previously created project in just seconds, minimizing the risk of manual entry errors. In addition, users can create a library of components by saving model components with FloEFD conditions for future use, to be shared with other designers in the organization.

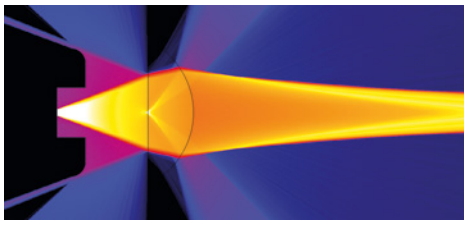

Figure 1. Radiation Spectrum and Pattern Essential for Laser Diode Simulation

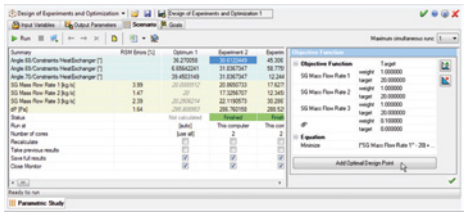

Figure 3. DoE and Response Surface Optimization

- **Radiation and LED Enhancements:** The radiation modeling capability for FloEFD has been further extended to include radiation pattern and spectrum definitions for directional sources. The LED thermal-optical model is now capable of simulating LEDs with non-linear dependency of parameters on temperature. These improvements are ideal for automotive lighting design and simulation.
- **Transient Explorer:** The new method of results data compression saves large amounts of disc space while it provides access to transient data immediately. Users can combine the transient animation of plots and parameter charts into a single view.
- **Design of Experiment (DOE) and Optimization:** True optimization of designs requires that multiple criteria be considered concurrently; as such its implementation can consume substantial resources (such as time and computing power). With the addition of this functionality now users can take advantage of DoE and Response Surface optimization.

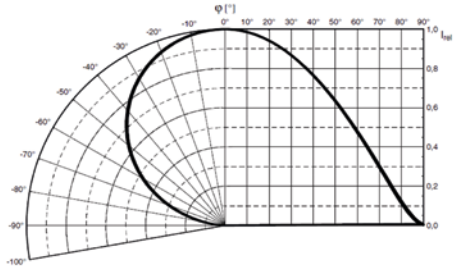

Figure 2. LED Radiation Pattern

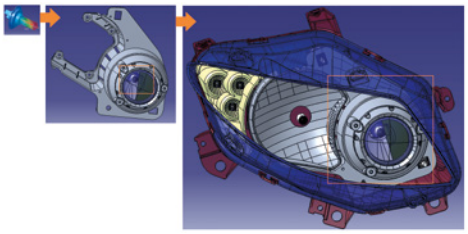

Figure 4. Project Conditions from a Component for Simulation of the Entire Assembly

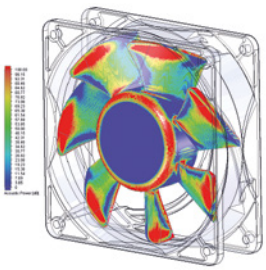

Figure 5. Acoustic Power Level – a new Feature in FloEFD 16 to Estimate Broadband Noise

- **Korean Localization:** FloEFD is now the only CFD software with user interfaces in Japanese, Chinese, French, German, Russian, English and now Korean, allowing engineers to experience FloEFD in their preferred language.

"Our customers require fast and accurate simulation results for their complex engineering problems," said Roland Feldhinkel, General Manager of Mentor Graphics Mechanical Analysis Division. "Our latest FloEFD product provides the power, special functionality and performance required by engineers to obtain meaningful answers to their questions without disrupting their design process."

For additional product information, visit the website: www.mentor.com/floefd

FloEFD for Solid Edge

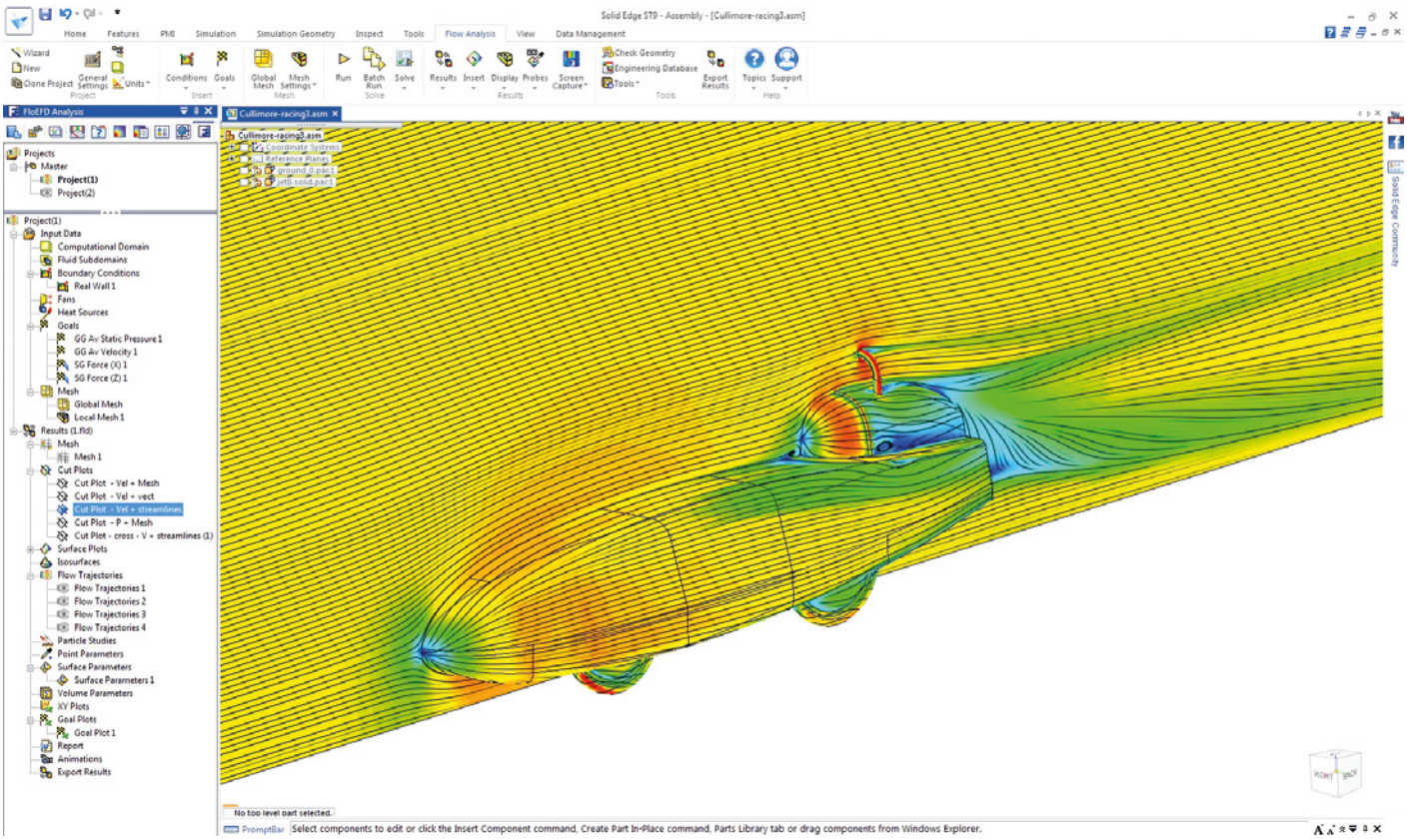

Mentor Graphics® is pleased to announce the only fully-embedded Computational Fluid Dynamics (CFD) solution for Solid Edge® users. Solid Edge is a product lifecycle management (PLM) suite of software tools addressing all aspects of the product development process, from 3D design through to manufacturing from Siemens Corporation. For the first time, Solid Edge customers can take advantage of Mentor Graphics FloEFD™ frontloading CFD product and use simulation in their design process. The FloEFD solution for Solid Edge is especially well suited for use during the design process as it reduces overall time to a solution by as much a 65%-75% compared to other CFD tools.

Mentor Graphics' award-winning FloEFD CFD solution automates the most onerous CFD steps which include transferring model geometry to the CFD application, modeling internal cavities if needed, and creating a "mesh." The FloEFD CFD technology takes the geometry directly from the CAD application, automatically performs the necessary translations and cavity modeling, and generates an optimized mesh before executing analysis. This approach provides accurate analysis results quickly thus enabling designers to validate their designs early and often. It also allows the designer to explore a succession of ideas without risking project deadlines.

The new FloEFD product for Solid Edge helps companies conduct analysis earlier in the design process. Engineers can operate within their preferred and familiar MCAD interface thus reducing design cycle times by an order of magnitude compared to traditional methods and tools while increasing design quality:

- Robust 3D fluid flow and heat transfer analysis software capable of solving complex real-life engineering problems.
- Fully-embedded in Solid Edge, FloEFD technology allows users to conduct multiple design studies and evaluate how the modifications influence the design performance immediately.
- Features an intuitive user interface with built-in intelligent automation including real-time feedback and timely outputs that can be generated quickly in MS Word and Excel.
- Parametric study enables user to compare a wide range of project variations.
- Fast, automated SmartCell™ meshing technology to create realistic simulations for complex 3D models including rotating equipment and transient flow behaviors - providing unprecedented speed-up in the overall design process.

"Mentor's FloEFD frontloading CFD technology full-featured 3D analysis eliminates workflow complexity and meshing overheads compared to other available CFD software," said Roland Feldhinkel, General Manager of Mentor Graphics Mechanical Analysis Division. "We believe Solid Edge customers will reap tremendous value in using our FloEFD solution for CAD-centric CFD design and performance optimization, while reducing time and costs to meet their product delivery goals."

For more information visit: www.mentor.com/floefd

New Release:
FloMASTER™ V8.0

3D CFD Connectivity, Usability & New Physics Capabilities

FloMASTER V8 is an extremely significant release. Not only does it contain a number of powerful features aligned around the three pillars of user experience, physics and connectivity; it represents the first major step toward a completely revitalised product. John Murray, FloMASTER Product Manager: "Flowmaster has been a huge commercial success, precisely because it solved a genuine market problem and was staffed by engineers enthusiastic about doing just that. We haven't changed that, but what is significant about FloMASTER is that we're recognising that the world hasn't stayed still since V7 was released; expectations and needs have evolved and we recognise that and have adapted ourselves accordingly. This is a huge release and is the result of over 42 man years of R&D. Accuracy has always been at the heart of the FloMASTER ethos and during the development we have run ~133,000 regression network cycles and ~13,000,000 unit test runs."

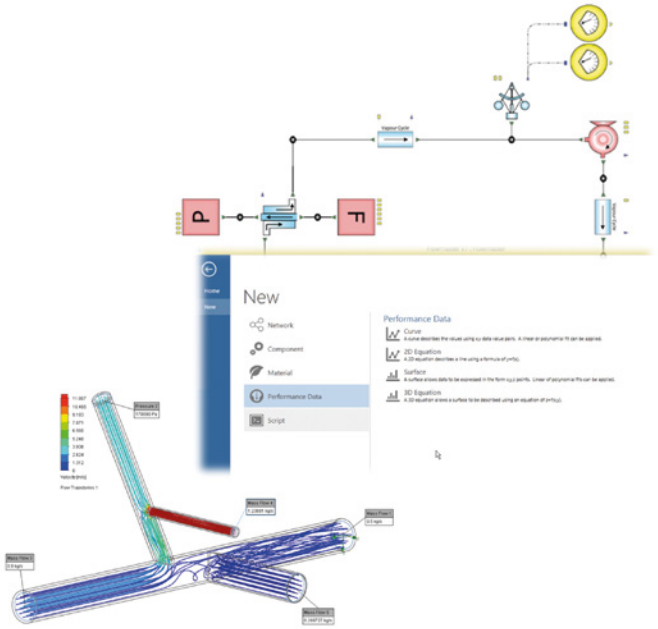

The three key areas of development are Connectivity, User Experience and Physics with the new Waste Heat Recovery functionality.

3D CFD Connectivity

At the market level, it's been about working with colleagues within the Mechanical Analysis Division to identify important trends and areas in which the Mechanical product portfolio can come together in order to deliver unique solutions. Hence, Simulation Based Characterization (SBC). Traditionally, coupling 1D and 3D CFD has always suffered from being a complex, fragile and ultimately time consuming process. However, the unique features of FloEFD – CAD embedded and speed to mesh and solve – make it ideally suited to the role of complementing system design. SBC leverages the power of FloEFD to overcome an inherent challenge in system simulation: getting component performance data for accurate System Simulation results.

FloMASTER includes built-in empirical data from Internal Flow Systems for what might be considered 'standard' geometries, e.g. bends, diffusers etc. For the increasingly common bespoke geometries made possible by modern manufacturing techniques, integration with FloEFD in order to characterize hydraulic and thermal behavior

- Significantly reduces time and cost to get essential component information;
- Does not require specialized resources or facilities; and
- Improves system level accuracy

At its core, SBC, is a technology that allows a component of up to 60 separate arms to be characterized in FloEFD using a design-of-experiments approach. The resulting performance map is packaged as a portable format (flonarm) which can be readily imported into FloMASTER where it will be applied to a NArm component for use in simulations, just as would occur with any other standard FloMASTER component.

User Experience 3.0

This development will take the form of a rolling wave of features to improve the discoverability and accessibility of the software. V8.0 is the first tranche of these User Experience (UX) improvements delivering a number of important features. One of the most prominent deliverables from this effort at V8 will be the new *Launchpad* functionality:

Launchpad is a hub for FloMASTER, helping users launch key features, access previous work and also discover the solutions the product has to offer. Recent networks are promoted and Sample Systems, complete with documentation, will be available to assist new and experienced users alike in modeling real-world fluid systems. These sample systems highlight best practise and are based on real scenarios. The new Material Workshop is intelligently configured to guide users through the creation of new fluid and solid materials.

The ability to automatically generate an Excel front end to 'drive' FloMASTER networks will help users maximise the value of the product by allowing untrained users to access the solver in a controlled fashion.

The Project Assistant functionality gives users the ability to track the database usage

"Our team will utilize FloMASTER to analyze a full simulation on our Hardware in the Loop (HIL). This innovative tool will also be used for our vehicle's complex thermal management system to optimize our vehicle's efficiency. The use of this tool and it's convenience will allow our team to spend less time on these tasks and more time on other complex facets of our vehicle."
Embry-Riddle EcoCAR 3 Team

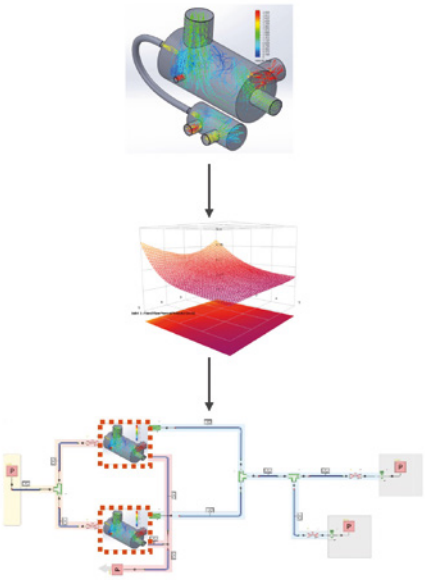

and understand and identify any projects using unexpectedly large amounts of disc space.

Finally, the extensive help system that has always underpinned the product has received a significant update at V8, reflecting both the feedback and expectations of users who are increasingly used to consuming technical support documentation in a multitude of formats.

Physics: Organic Rankine Cycle (ORC)

FloMASTER V8 also features a major new fluid modeling capability in the form of ORC, specifically targeted for Waste Heat Recovery (WHR) applications. The development team have worked closely with an experimental program run by Brunel University, allowing them to compare simulation with experiment across a range of operating points and so validate the development as it has progressed. "In many ways, we've gone back to the methods that made the original Flowmaster release such a powerful tool", says John Murray, Product Manager, "working hand in glove with an experimental program, and taking advantage of the extant literature on ORC gives us a high degree of confidence that the model we're putting together is an extremely accurate and capable one".

Product Availability

Mentor Graphics is now accepting orders for FloMASTER V8 with availability late calendar year 2016. For additional product information please visit www.mentor.com/flomaster

FloEFD Frontloading CFD Award

Mentor Graphics is pleased to announce the winners of the 2016 FloEFD Frontloading CFD Award. The award recognizes excellence in implementing frontloading CFD through award-winning FloEFD. Our 6-person panel of judges rated each entry on several criteria including clear demonstration of use of frontloading CFD and the pragmatic approach taken in the application.

The top prize was won by Ms. Aihua Wang, a thermal engineer in the automotive lighting group at Magneti Marelli. Her presentation titled "Integrating Thermal Analysis into Automotive Lighting Product Design" was delivered at the Integrated Electrical Solutions Forum (IESF) Conference in 2015. IESF is a global conference for electrical/electronic design engineers, managers and executives. Winning the top prize entitled Ms.Wang to $1,500 in cash and a trophy. Ms. Wang chose to donate the funds to her charity of choice– the American Society for the Prevention of Cruelty to Animals (ASPCA).

Our panel of judges chose "Design and Integration of Cooling Systems and Power Packs Powertrain to Meet the Next Environmental (tier IV) Regulations," by Kolio Kojouharov as one of the two runners up. Mr. Kojouharov, who at the time was working as an engineer at Liebherr-Werk Nenzing GmbH made the presentation at the October 2015 Mentor Graphics U2U in Munich.

Lastly, Mr. Georg Jäger who is an engineer at Hoval was selected as another runner-up. His whitepaper titled "From Conceptual Brainstorming to a Customized Condensing Boiler", was written for use at the FloEFD Simulation Conference which is taking place November 8 -9, 2016 in Frankfurt.

The two runners up were each entitled to $500 and a trophy. The recipients were informed of their prize via email and were scheduled to collect their awards at the FloEFD Simulation Conference in Frankfurt, Germany on November 9th.

We are very proud of the results that our customers are able to achieve with the aid of FloEFD. This award is a celebration of their achievement and we look forward to recognizing others next year.

2016 Don Miller Award Winners Highlight the Versatility of Flowmaster

Flowmaster is widely known for the variety of industries and applications that it can be used for. This is truly evident in the winning entrants of the 2016 Don Miller Award for Excellence in System Level Thermo-Fluid Design. The three papers recognized, address automotive engine cooling, two-phase refrigeration processes, and passenger comfort in rail transport. Additionally, the entrants also showed the global reach of Flowmaster with the winners coming from India, Brazil, and China. We would like to take this opportunity to recognize their excellent work.

First prize went to Soujanya C, V Sundaram, & Sathish Kumar S of Chrysler India Automotive Pvt, Ltd. for their paper **"Simulation of Split Engine Cooling System"**

The important objective of this work was to develop a Flowmaster simulation model of split engine cooling system, which was capable of predicting the coolant flow and pressure drop across different engine speeds and components. The new methodology developed to model the engine coolant jacket and two thermostats helped in achieving good correlation of simulation results with that of test.

The importance of split engine cooling system is that, the coolant flow through a block coolant jacket is stopped until the coolant reaches certain temperature. This helps the coolant reach a optimum performance temperatures quickly. For this purpose, there are two thermostats available in the system. This type of cooling system improves the efficiency of the engine by increasing the coolant temperature quickly to optimum level as soon as the engine starts.

The performance prediction through any tool depends on the input parameters which are fed to the tool. So care should be taken to get predictions near to bench test data. The authors utilized several sources of data including: CAD of the cooling system, performance details of the components, T-Stat hysteresis curves and engine performance data.

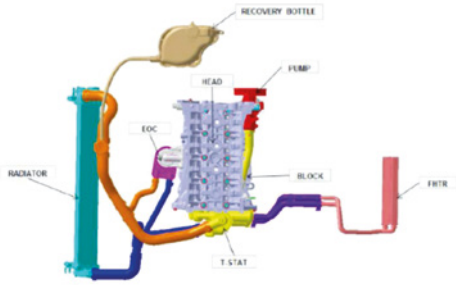

Figure 1. CAD drawing of Split Cooling System

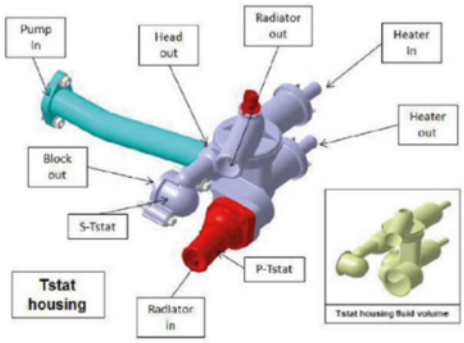

Figure 2. Detailed Thermostat Drawing

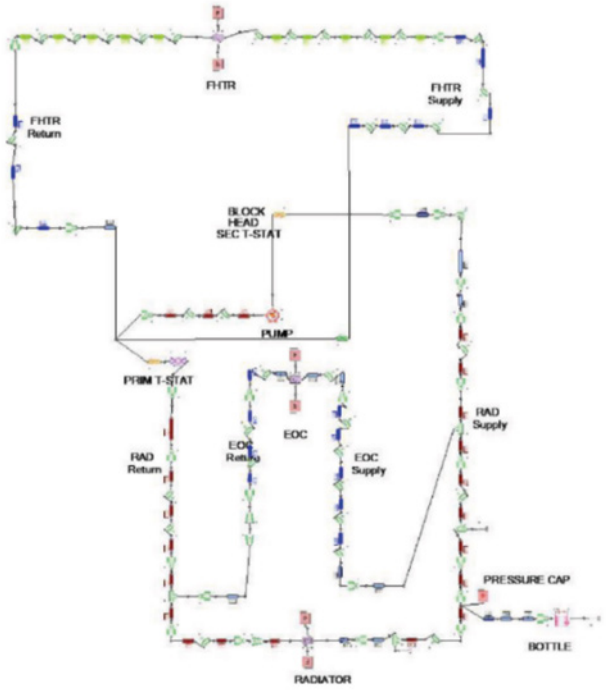

Figure 3. Flowmaster Model of Split Engine Cooling System

Internal flow geometry details like coolant pipe flow diameter, pipe length, bend angle etc. were extracted from the CAD and modeled using simple flow components available in Flowmaster and component specific data such as T-Stat hysteresis curves and pump performance curves were obtained from

manufacturer data and brought into the model. The main challenge involved in modeling split engine cooling system is the modelling of coolant jacket. Data from engine bench tests was utilized. A flow sweep test was run and the flows and pressures were obtained across different pump speeds and coolant temperatures, these results were also used in the Flowmaster model

The Flowmaster model of split engine cooling system was correlated against engine test data and the predictions are within +/– 10 % deviation.

The figures shows the comparison plots and results between bench and simulation predictions across split engine cooling system at 76°C.

This innovative approach was developed using Flowmaster which considers all the restrictions involved in a complicated cooling system like a split cooling system and resulted in correlation of simulation results with bench test data within 10% error. This kind of simulation eliminates several bench tests in analysis of engine cooling system performance. This kind of approach in engine development can reduce huge lead times and costs in system development because the simulation run time is a few seconds. The simulated model could be easily modified for different scenarios and performance criteria of the system could be easily evaluated in future vehicle development.

First runner up prize went to Thiago Rubens Vieira Ebel from the Federal University of Santa Catarina, Department of Mechanical Engineering, Brazil with his paper titled, **"Viability Analysis and Computational Simulation of a Hydraulic Circuit for a Magnetic Refrigeration System".** Truly a unique application of Flowmaster in the area of research.

Magnetic refrigeration is a cooling technology based on the magnetocaloric effect which is a magneto-thermodynamic phenomenon in which a temperature change of a refrigerant material is caused by exposing the material to a changing magnetic field. Flowmaster was used to understand the water hammer effects that can occur in one such refrigeration system.

A simplified hydraulic system of the Brazilian prototype developed by Lozano (2015) was modeled by means of Flowmaster. The transient behavior of the absolute pressures and the mass flow rate through the regenerator beds was simulated. A deep understanding of the dynamics of the circuit was gained.

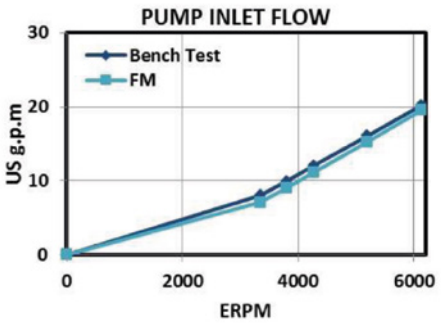

Figure 4. Pump Flow Result Comparison

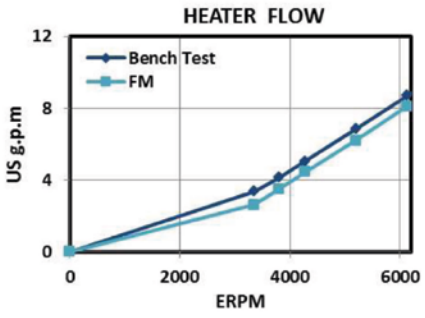

Figure 5. Heater Flow Result Comparison

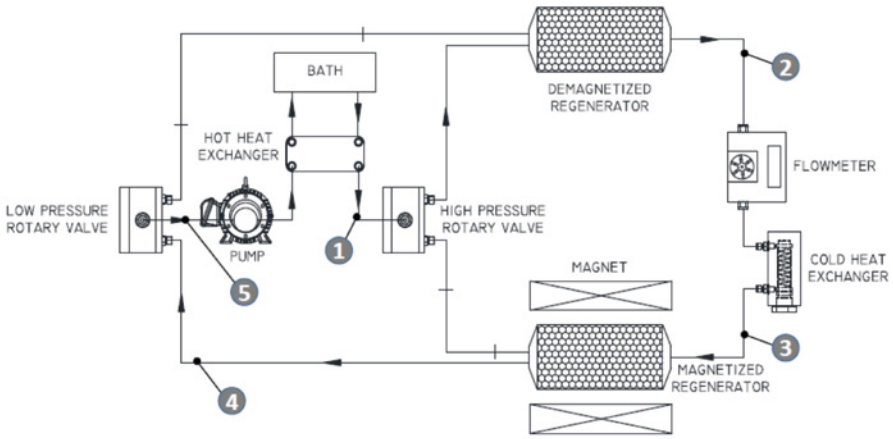

Figure 5. Schematic of Prototype Magnetic Refrigeration System

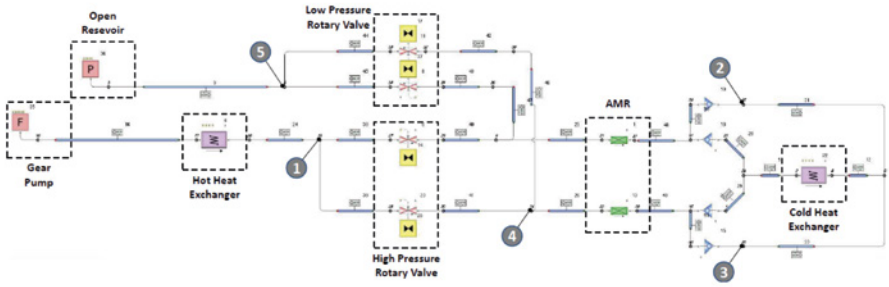

Figure 6. Initial Flowmaster Model of Prototype Magnetic Refrigeration System

The model was subjected to scenarios of different flow rates, operating frequencies and opening ramps of the valves. It was concluded that the higher the flow rates, the stronger the dynamic events such as water hammer.

The operating frequencies proved not to influence sensitivity of the hydraulic circuit. On the other hand, the variation of the duration of the opening ramps demonstrated to have a key role on the whole hydraulic circuit. By modeling a similar behavior to the former rotary valves, when having opening ramps smaller than 8° out of 360° (roughly 2% of the working period), the circuit tends to have great influence of the water hammer effect. Conversely, for opening ramps larger than 15° (roughly 4.2% of the working period) the fluid finds less resistance to bypass the regenerators during the switching time. This effect tends to waste part of the flow but also decreases the water hammer effects. Relying on the results of different scenarios, the best overall performance is found associated to opening ramps between 8° and 15°.

Through the numerical simulation results at different operating conditions, a new layout for the hydraulic circuit was proposed to improve the performance of the refrigeration system.

Based on the obtained results in this work, the most suitable solution is to include a proportional returning valve before the high pressure valves and after the low pressure valves. Such a device would be capable of absorbing the water hammer effects and to make the flow through the regenerators' beds smoother. Even though the system would require higher pumping capacity, due to flow bypass, an estimation of the novel hydraulic circuit would have a COP of 1.34 and a second law efficiency of η2nd = 9.55% (the actual system had a maximum second law efficiency of η2nd = 1.16%).

Second Runner up Award went to **"Study on the one-dimensional carriage and ventilation system of high-speed train"** from Yifei Zhu, Yugong Xu, Xiangdong Chen of the School of Mechanical Electronic and Control Engineering, Beijing Jiaotong University, Beijing, China.

Their work investigated the interaction of the outside environment and the interior airflow through the ventilation system of a high speed train during operation. In past studies, this interaction has been ignored resulting in significant inaccuracies in the results. The composition of the complex ventilation system includes: air inlet, grill, controllable dampers, ducts, air conditioning units, air orifice, return air valves, and waste discharge units. Due to the overall complexity and length vs. the hydraulic diameter of the ducts, a 1D simulation with Flowmaster was the only practical solution to the simulation problem.

Figure 9 is the 3D CAD drawing of the ventilation of the high-speed train carriage. It consists of a combination of fresh air ventilation system parts, exhaust section and return air section together.

Because the model is so complicated, a simplification process was used to reduce the complexity of the model. This included:

1. The pressure protection valve is open in normal operation, so it was ignored,
2. Air conditioning mixing box. This is just a confluence of container shaped like a Y-pipe, the drag coefficient is small, and therefore considered as a modeling point of convergence, and
3. Because the study was only interested in the airflow distribution and not temperature the components of the air conditioning and heating units were simplified to resistance elements based on local resistance.

The supply duct system lines consists mainly of long straight pipes with only a few individual bends and corners which have very small additional resistance relative to the long pipes so they were omitted as well.

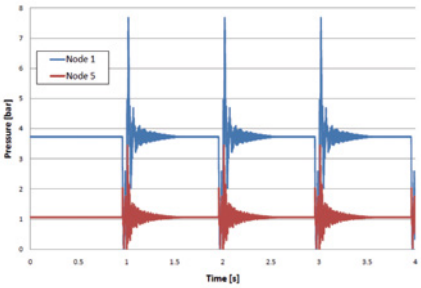

Figure 7. Typical Water Hammer results in the System

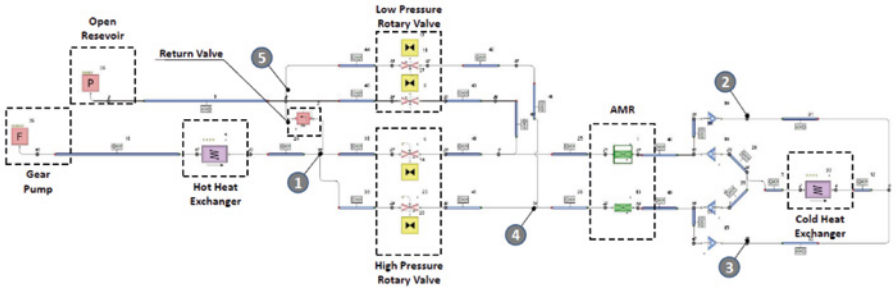

Figure 8. Flowmaster Model of Redesigned Prototype Magnetic Refrigeration System

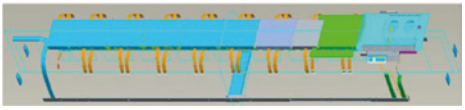

Figure 9. 3D CAD Drawing of Ventilation System of High-Speed Train Carriage

Figure 10. Flowmaster Network of Ventilation System of High-Speed Train Carriage

Parameters	Design working condition	Simulation results
Fresh air volume (m3/h)	1200	1288.08
Air inlet volume (m3/h)	4500	4605.84
Air outlet volume (m3/h)	1200	1285.56
Return air volume (m3/h)	3300	3320
Air supply velocity (m/s)	2~5	2.5912

Table 1. Comparison of Flowmaster Simulation Results Vs Actual Operating Point Values

After these simplifications were made, the Flowmaster model was constructed as shown in figure 10.

Results of the simulation showed that the new outlet flow, exhaust port flow, return airflow, and airflow rate of each branch meet design conditions and the calculation results are consistent with the actual operating point of the ventilation system, which demonstrates the rationality and accuracy of the simulation model. This modeling approach will be used to predict other environmental conditions inside the train carriage.

From these award winning papers it is easy to see the versatility of Flowmaster and how creative engineers from around the world are finding new and innovative ways to use it to solve their simulation and design problems.

References:

[1] C, S., Sundaram, V., and S, S., "Simulation of Split Engine Cooling System," SAE Technical Paper 2015-26-0196, 2015, doi:10.4271/2015-26-0196

[2] Thiago Rubens Vieira Ebel, "VIABILITY ANALYSIS AND COMPUTATIONAL SIMULATION OF A HYDRAULIC CIRCUIT FOR A MAGNETIC REFRIGERATION SYSTEM"Florianópolis - SC, February, 2016

[3] Yifei Zhu, Yugong Xu, Xiangdong Chen, " Study on the one-dimensional carriage and ventilation system of high-speed train" International Power, Electronics and Materials Engineering Conference (IPEMEC 2015)

FloEFD Technology Selected for New French Automotive Lighting Master's Degree Program

Mentor Graphics Corporation has announced its partnership of the Master's degree program on automotive Embedded Lighting Systems (ELS). Three French universities, the Institut d'Optique Graduate School, ESTACA and Strate Ecole de design, in partnership with Renault, Peugeot-Citroen, Valeo and Automotive Lighting, developed the ELS program. Mentor Graphics' leading front-loading computational fluid dynamics (CFD) FloEFD™ product has been selected as part of the curriculum.

As an industry-leading CAD-embedded solution, the FloEFD product will provide front-loaded CFD so students can evaluate thermal performance early during the design phase. As a fast, feature-rich, and easy-to-use CFD tool, students will learn how to calculate condensation, meshing technologies, radiation modeling using Monte Carlo analysis, and apply reliable physics models to their designs. "As a sponsor of this program and a user of Mentor's FloEFD product, we are pleased to be part of this much-needed master's degree program," stated Mohamed L'Baouch, Director R&D at Automotive Lighting France. "This program will help future automotive lighting systems designers understand the complexities and use the most progressive technologies to develop innovative lighting solutions, while seeding the future with new talent."

The three universities will provide specialized courses: Institut d'Optique Graduate School will offer courses on optics and photonics; ESTACA will provide transportation engineering instruction; and Strate Ecole de design will cover design. The automotive industry partners supporting this master's program recognize the importance of this specialty and the training will enable the students to master technical skills in the emerging automotive lighting market. "We are very pleased to be involved with this program since it fills a void for automotive systems education," stated Jean-Paul Ravier, ELS Chair at Institut d'Optique Graduate School. "FloEFD is uniquely positioned as a best-in-class analysis product for automotive lighting design; as a result our graduating students will be able to step in and fulfill the needs of the automotive industry immediately upon graduation."

For more information the embedded lighting Master's degree program and to apply, visit the website: http://embedded-lighting.com/formation-2/.

"We are honored to have FloEFD selected for this special automotive lighting master's degree program," stated Roland Feldhinkel, general manager, Mentor Graphics Mechanical Analysis Division. "Our market-leading FloEFD product has proven to be an invaluable technology for our automotive customers, and the students will be able to realize improved product quality, reliability and faster time-to-market when using this tool."

Mentor Graphics joins the WBG-i consortium for Power Electronics in Japan

Founded in 2013 by Professors Katsuaki Suganuma (pictured right) and Tsuyoshi Funaki of Osaka University in Japan, the WBG-i (Wide Band Gap integration) power electronics consortium seeks to pull together both academics and industrialists from Japan and across the world in harnessing the possibilities of this new technology and in dealing with its challenges.

WBG semiconductor materials such as SiC and GaN allow power electronic components to be smaller, faster, more reliable, and much more efficient than conventional silicon based power devices. All aspects of packaging and reliability in the next generation of power electronics are being addressed. Already 34 industrial companies are involved in WBG-i consortium and several work groups have been set up with regular workshops and meetings. With developing links to ECPE in Europe, and several North American and Asian partner organisations, WBG-i consortium is becoming a truly international driver for change. Speaking about the recent addition of Mentor Graphics to the consortium, Prof. Suganuma said:

"We are glad that Mentor Graphics is joining WBG-i consortium. One of the key issues for SiC and GaN based power electronics is thermal dissipation. Mentor's T3Ster™ transient thermal tester hardware is the most advanced technology in its field and can contribute to understanding what is going on in WBG semiconductors. There are standards for power LEDs already and we believe that MicReD technology in Mentor Graphics' Power Tester can help in developing power cycling standards for WBG power electronics."

Reference:

WBG-i consortium website: http://wbg-i.jp/en/

Optimizing a NASCAR Racing Machine

Voxdale collaborate to engineer a champion car using FloEFD

By Mike Gruetzmacher, Technical Marketing Engineer, Mentor Graphics

NASCAR is the most popular motorsport competition in the USA. The three largest racing-series are the Sprint Cup Series, the Xfinity Series, and the Camping World Truck Series. NASCAR sanctions over 1,500 races at over 100 tracks in 39 of the 50 US states, as well as in Canada, and its races are broadcast in over 150 countries.

Initially only modified large scale series vehicles were used for NASCAR. Today's NASCAR vehicles are racing cars with a V8 engine and up to 800 horsepower, but restricted in compliance to the applicable regulations. Only the car body silhouette resembles a series car. The cars are subjected to strict regulations, for example a limited size for the rear spoiler, the chassis material thickness or allowed production processes for the engine cylinders. It is normal practice that winning team cars are dismantled by NASCAR officials after a race to check for any irregularities. The car performances are almost equivalent. There are only a few rare opportunities to gain any technical advantage. This leads to the teams needing to find ways of making small gains wherever they can to improve their performance.

Automotive

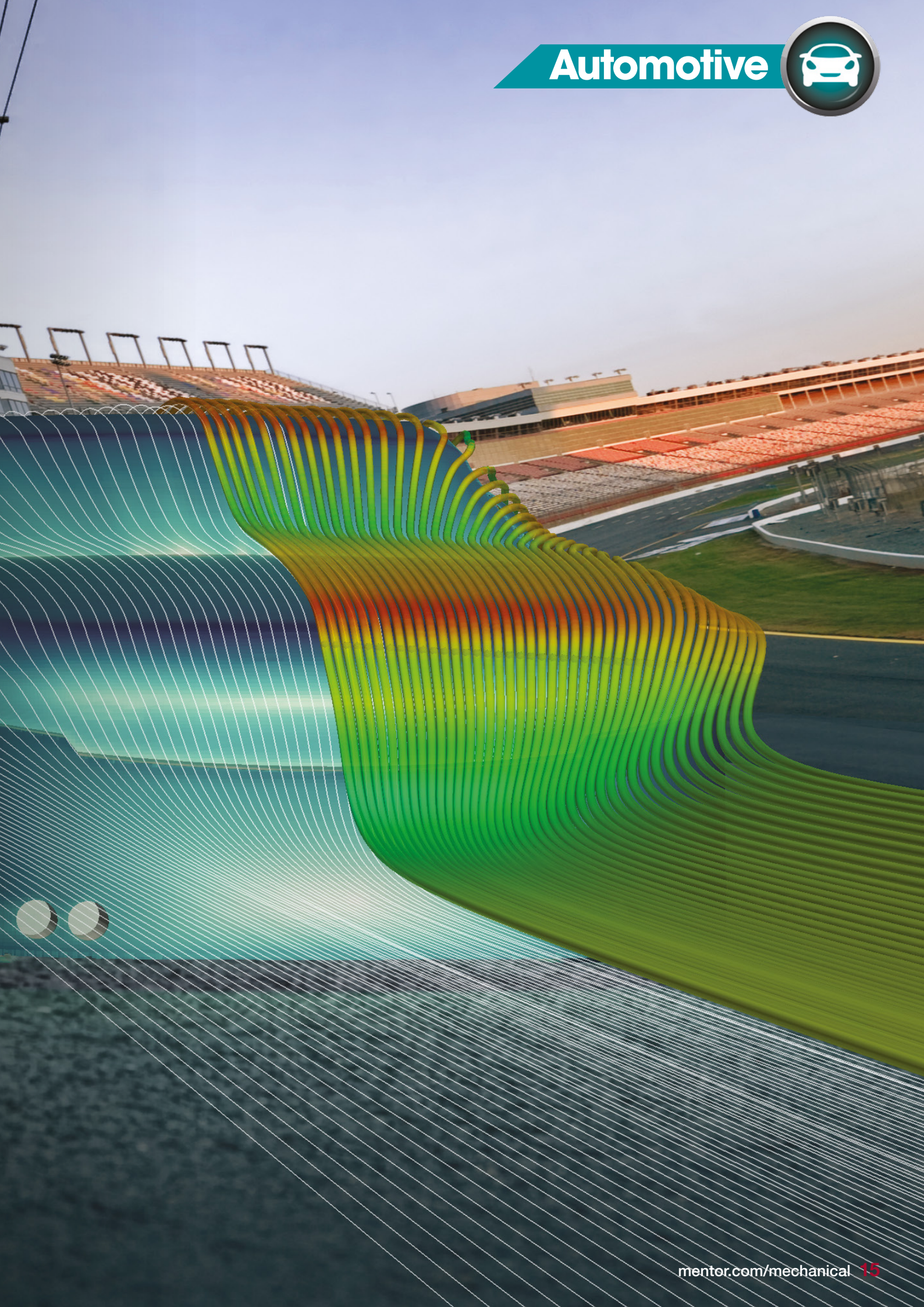

The popularity of NASCAR racing is increasing in Europe, with the NASCAR Whelen Euro Season. NASCAR rules and standards are adopted in the series but the cars are built specifically for European tracks and the horsepower is restricted to 450 hp. One of the most successful European race drivers is Anthony Kumpen from Belgium. He is the overall winner of the 2014 NASCAR Whelen Euro Series season. His huge success in Europe qualified Anthony to compete in the US NASCAR K&N Pro Series East. Today he combines the NASCAR championship in Europe with races in the USA.

We met Anthony Kumpen together with Koen Beyers, CEO of Voxdale BVBA, a successful CFD engineering consultancy, to see what CFD could do to improve their car. Voxdale collaborate to engineer Anthony's team cars using Mentor Graphics' FloEFD.

Anthony explains that there are many aspects to be considered for a racing driver, "There is the driving aspect which is one of the real interesting parts but there are also all the technical details to be optimized. I'm working with engineers and mechanics. There is a lot more than just driving fast in a car. That's what racing is all about. Being a racing driver everybody thinks I spend all the time in the car but actually I spend 80% of my time in meetings with my engineers, with my chief mechanics. Engineering is something we have to study every day in order to be a good driver."

One field Anthony and his team are particularly interested in, is aerodynamics. Since the team does not own or have access to a wind tunnel, like an F1 team would have, they had to find another way to analyze their car's performance. So they teamed up with Koen and the Voxdale team, who are experienced in racing aerodynamics. Voxdale Engineers began working on this NASCAR project by conducting CFD simulations in Mentor Graphics' FloEFD 3D Simulation software.

"The main goal of the partnership was to get insights in the behavior of the car. So when we got involved in the NASCAR project with Anthony the first thing we had to do was to look into what was actually possible to do," Koen Beyers, Voxdale CEO explains.

The NASCAR series is a closed racing series with a very tight rulebook and strict regulations. For instance, the body work could be changed nor could the manifolds or engine parts. Anthony's team and Voxdale decided to analyze the car's aero-mapping and overall behavior. They also investigated the internal flows, the flows underneath the body, and

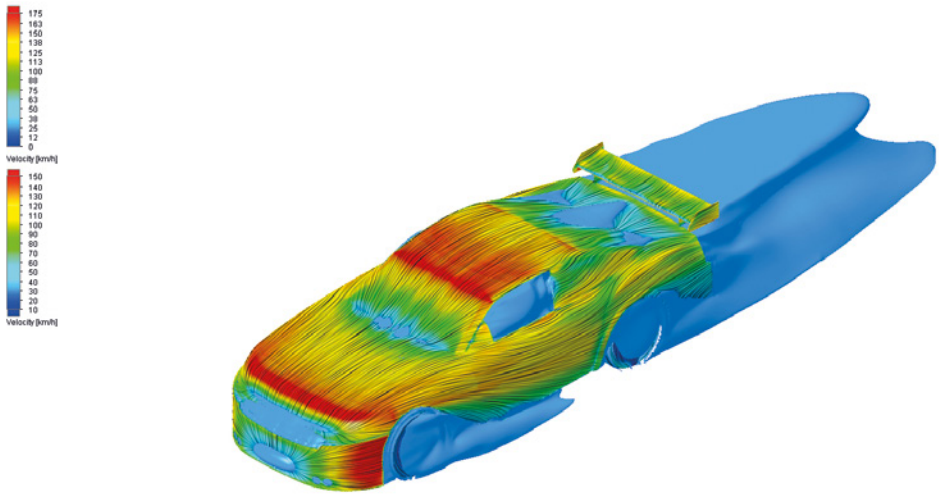

Figure 1. Velocity Streamlines on Body Surface and Isosurface around the Car Body

Figure 2. Anthony Kumpen (left) and Koen Beyers (right)

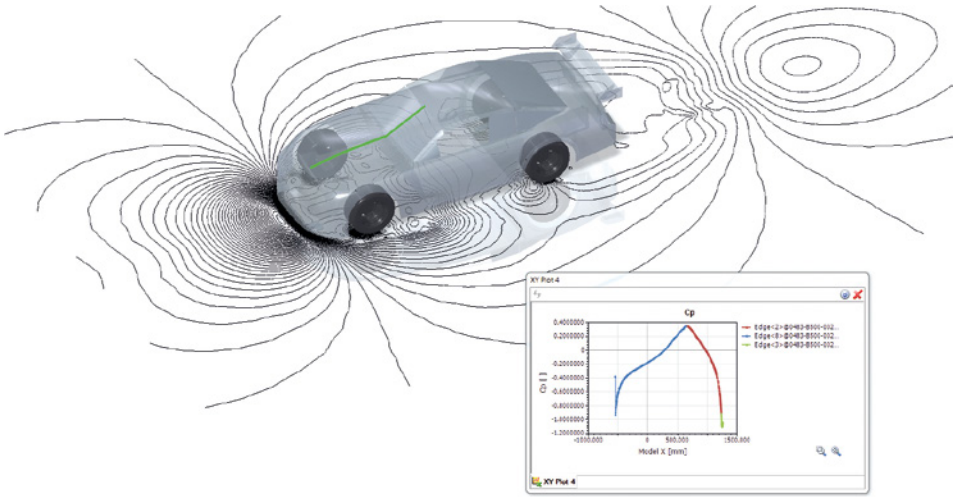

Figure 3. Pressure Coefficient Cp

the hood. Furthermore they optimized the cooling of the brakes and the exhausts. As preparation for the simulations the car model was set up in FloEFD for PTC Creo. The modeling of the geometry took around three days, the FloEFD simulation setup took about a day. The engineers conducted around ten simulations directly within the PTC Creo environment which took about two weeks including post processing. The results of these quickly prepared and evaluated simulations were used for rapid optimizations as the regulations and schedules disallow long predevelopment phases.

"At one point, we saw the effect of a specific riding height combined with an explicit rake angle resulting in a drag reduction of 0.8%. Over one lap at Brands Hatch, with this car with this power, this buys you 0.2 second. An important leap in a closed racing series", Koen illustrates.

"It is very cool to see the car racing on track, that you analyzed the car and helped the team to give an even better performance" says Patrick Vlieger, Engineer at Voxdale.

"There are a lot of different aspects on aerodynamics that are important for racing. Sometimes you want to have the maximum downforce, sometimes you want to have as little as possible downforce and make the car run really smooth. With all the data the Voxdale engineers gained Anthony's team and his engineers tried to improve the cars on the track and so far it's working really well." as Anthony confirms.

Anthony Kumpen, "With FloEFD we could do a lot of tests and improvements of the car which helped us a lot. We are winning a lot of races. It's all about the details of racing and finding the right partners and we are really happy to do this with Voxdale."

References

http://www.nascar.com

https://en.wikipedia.org/wiki/K%26N_Pro_Series_East

https://en.wikipedia.org/wiki/NASCAR

http://www.formula1-dictionary.net/map_aero.html

http://www.f1buzz.net/2009/02/17/what-is-aero-mapping/

https://www.reference.com/sports-active-lifestyle/much-horsepower-nascar-stock-car-eb5f6a334398b967#

http://auto.howstuffworks.com/auto-racing/nascar/nascar-basics/nascar-engines1.htm

http://www.racingblog.de/nascar-faq/

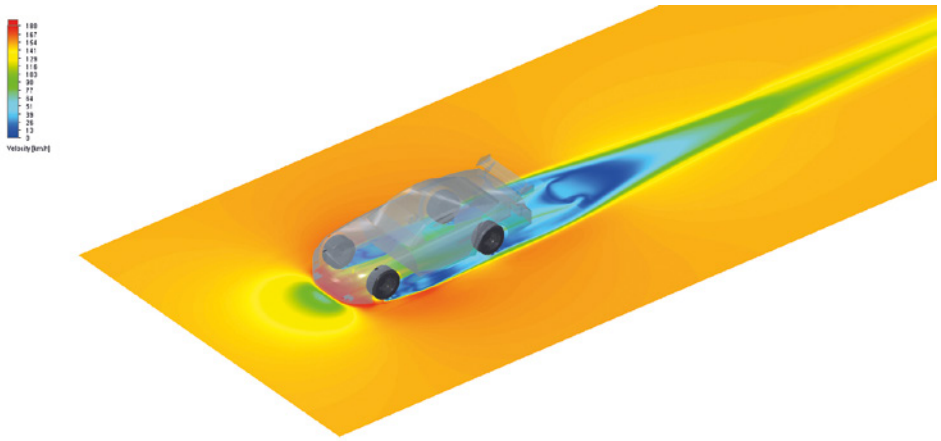

Figure 4. : Velocity Profile underneath the vehicle

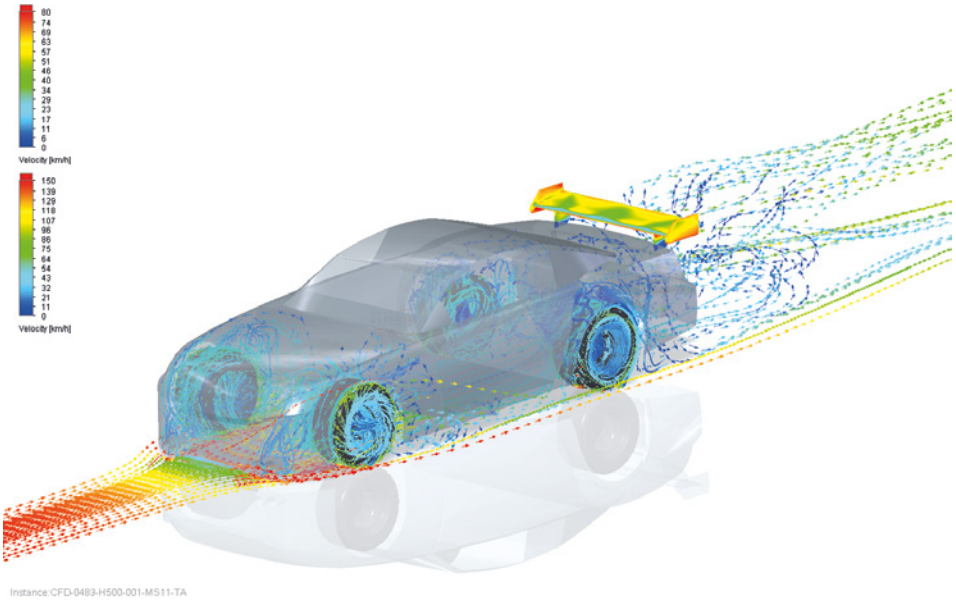

Figure 5. Velocity Profile underneath the Car Body and Wheelhouses

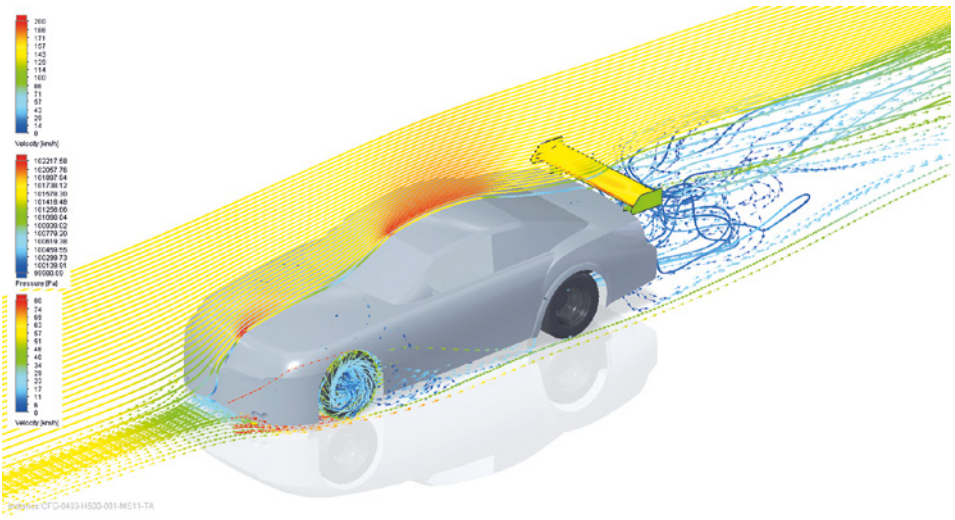

Figure 6. Velocity Profile underneath Car Body and Pressure Distribution the Spoiler

How To...

Create FloMASTER™ N-Arm Components using FloEFD™.

By Robin Bornoff, Market Development Manager, Mentor Graphics

A Simulation Based Characterization Workflow

The new FloMASTER V8 N-Arm component allows for multi-arm (up to 60) junctions to be modeled in a circuit. For applications such as automotive thermostats and pump housings, multiple inlets and outlets interact with each other to produce complex pressure drop vs. flow rate relationships. Instead of relying on the assumption that such arm pairs can be modeled as discrete parallel losses, FloEFD can be used to characterize the combined effects that each arm has on the others. The results of such a characterization are imported into FloMASTER whereupon an N-Arm component is created.

To introduce the workflow, let's consider a simple five arm pipe junction. This is modeled in FloEFD by applying boundary conditions to five faces. A combination of flow and pressure boundary conditions can be set. However (at least) one face needs to have a pressure boundary condition, this face will be considered the reference arm in the subsequent calculation of pressure drops. The working fluid is set as water and the model meshed using default settings.

A new 'characterization' parametric mode has been added to FloEFD solely for the ability to create N-Arm components for FloMASTER. Ranges over which the geometry is to be characterized is first set for all non-reference arm boundary conditions. These might be mass flow, volume flow, velocity or pressure ranges.

A user defined number of computational experiments are then created that set random, but equally spaced, combinations of the boundary condition values, throughout the characterization space. Each experiment is shown as a column in the Scenario tab. These models can then be solved, either on the local machine, or concurrently utilising a network.

When solved, FloEFD automatically extracts a dimensionless mass flow value for each arm (akin to the Reynolds number) and a dimensionless pressure drop between an arm and the reference arm (akin to a loss-coefficient). Non-dimensionality

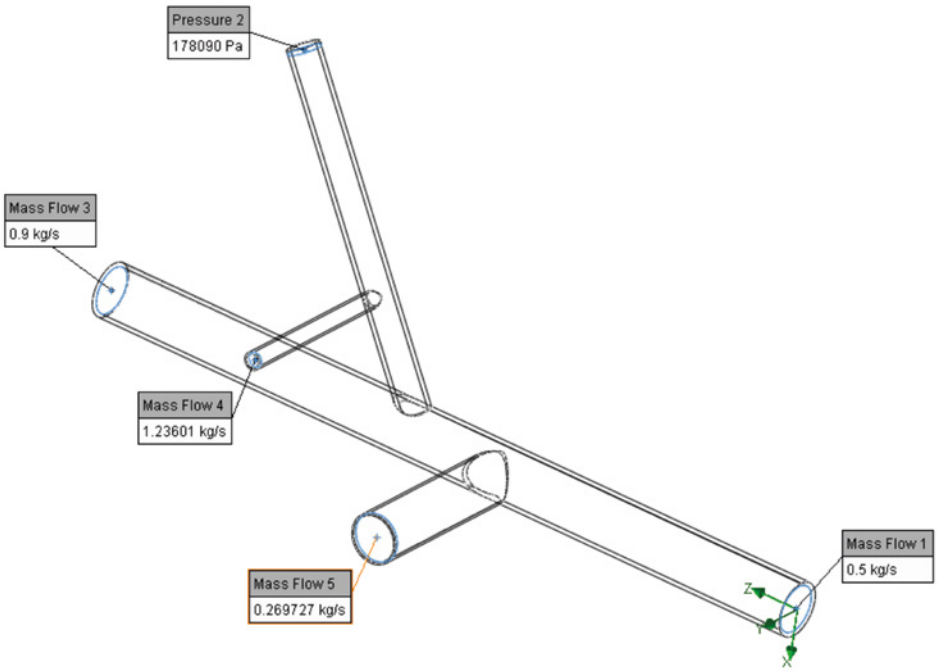

Figure 1. FloEFD five Arm Geometry Showing Boundary Conditions

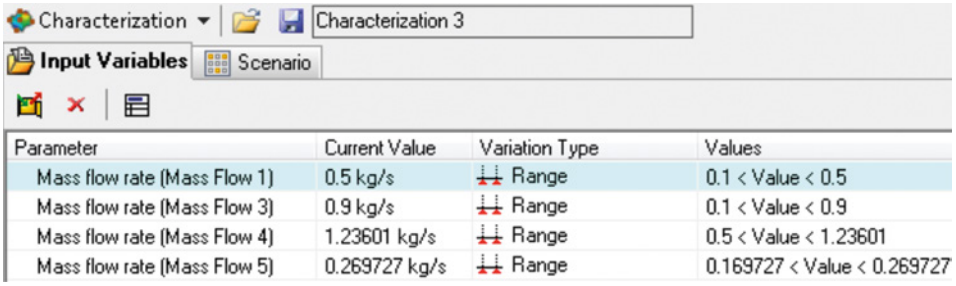

Parameter	Current Value	Variation Type	Values
Mass flow rate (Mass Flow 1)	0.5 kg/s	Range	0.1 < Value < 0.5
Mass flow rate (Mass Flow 3)	0.9 kg/s	Range	0.1 < Value < 0.9
Mass flow rate (Mass Flow 4)	1.23601 kg/s	Range	0.5 < Value < 1.23601
Mass flow rate (Mass Flow 5)	0.269727 kg/s	Range	0.169727 < Value < 0.269727

Figure 2. Characterization Range Extents

ensures that the characterization will be fluid independent, i.e. the fluid used in FloEFD need not be the same fluid used in FloMASTER.

To consider the effects that all arms have on the pressure drop between an arm and the reference arm, the following relationship has to be determined:

$$\text{Dimensionless Pressure Drop}_{\text{Arm i-Ref Arm}} = f(\text{Dimensionless Mass Flow}_{\text{Arm 1}}, \text{Dimensionless Mass Flow}_{\text{Arm 2}} \ldots \text{Dimensionless Mass Flow}_{\text{Arm N-1}})$$

This is done using response surfaces. For each dimensionless pressure drop, an N-1 dimensional response surface is created. The error showing how well, on average, the response surface fits the solved points is shown in the scenario table.

The response surfaces may be visualised; 2D plane response surface sections are shown. Slider bars can be used to alter the parameters of the dimensions not included on the displayed axis. This provides a graphical indication of the relationship between the pressure drop (between an arm and the reference arm) and the flow rates in all the arms.

Should the error of the response surface fit be considered too large, additional experiments can be created and solved and the response surface regenerated, until such time as the error falls below acceptable levels.

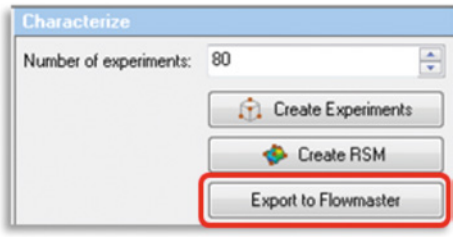

The response surface models, together with a 3D interactive view of the geometry, are then exported to the file system in a .flonarm file. This file is imported into FloMASTER whereupon an N-Arm component is created. The N arms are then connected to the FloMASTER circuit and solved in the usual way.

Summary

This simulation based characterization workflow enables FloEFD to be used to capture all complex interacting 3D flow effects, incorporated into the behavior description of the N-Arm component. For multi-arm geometries that are complex to extend where errors may be introduced using collections of existing FloMASTER components, or to extend the operational range of existing FloMASTER components, FloEFD used together with FloMASTER provides unique opportunities.

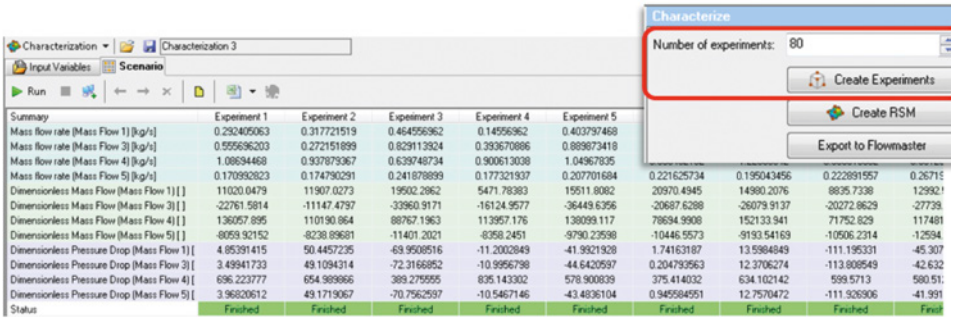

Figure 3. Scenario of Solved 'Computational' Experiments

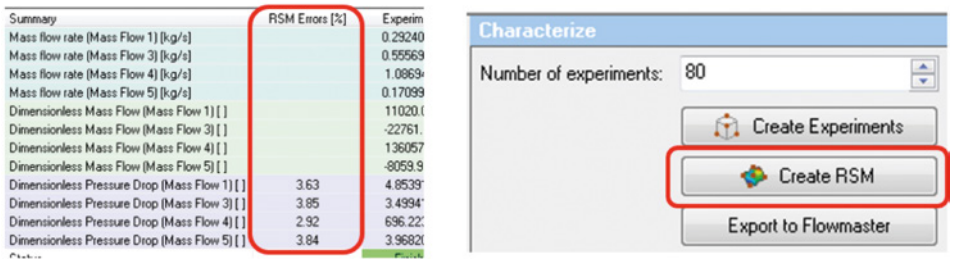

Figure 4. Dimensionless Press Drop Response Surface Creation

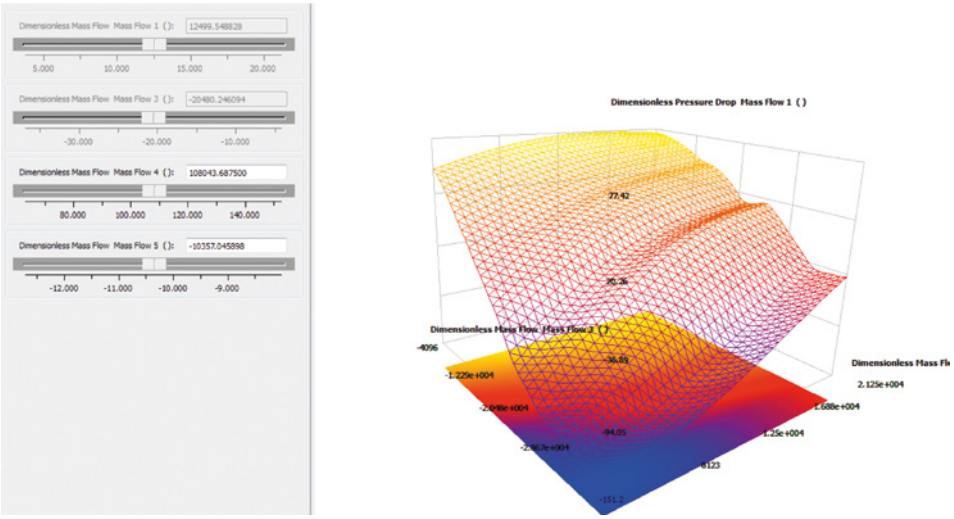

Figure 5. Response Surface Visualization

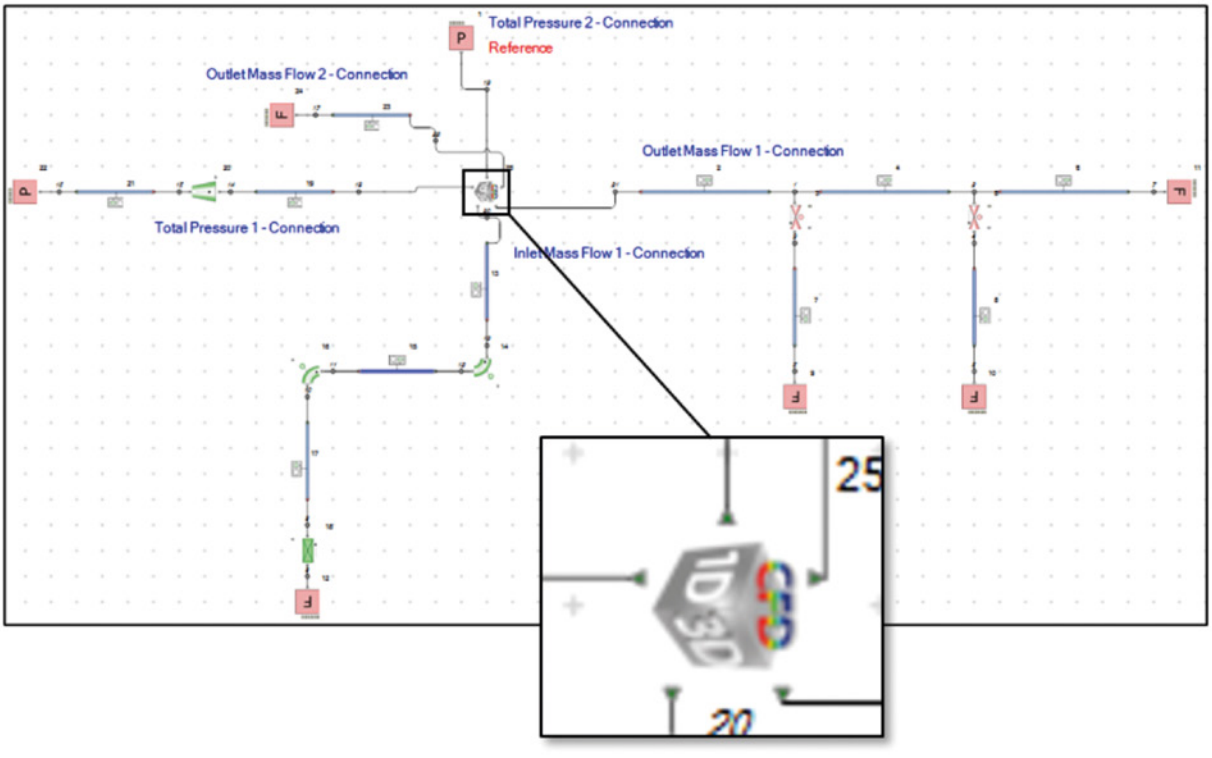

Figure 6. N-Arm Component in a FloMASTER Circuit

Air Dynamics Simulation of the Tamturbo Oil-Free Air Turbo Compressor

By Timo Pulkki, Mihail Lopatin, Tamturbo Oy, Tampere, Finland & Alexandr Nikulin, Axis Engineering (Mentor Graphics distributor), Saint Petersburg, Russia & Tatiana Trebunskikh, Mentor Graphics, Moscow, Russia

Nowadays to be competitive in the air turbo compressor industry, the company must provide high performing hardware with the lowest life cycle cost. In most cases to achieve such characteristics the company has to use a range of innovative technologies. Tamturbo Oy, was founded in 2010 in the Tampere region, the birthplace of several compressor innovations, has achieved their goal of transforming their view of oil free technology into a worldwide success story. They are fully committed to delivering solutions that bring the highest life cycle value to their customers.

Figure 1. The Tamturbo compressor

Performance prediction of the prototypes of air turbo compressors is one of critical questions during the design process. As soon as such predictions are available, the design engineers are able to optimize the device, taking into account a number of factors like the cooling of the compressor stages or cooling of the electrical engine driving the compressor. Moreover all issues with new design should be discovered as soon as possible before hardware testing, to reduce development time and cost. The required changes can be minor or major for larger parts. Without dependency on the scale of the changes, a deeper understanding is required into processes inside the particular parts as well as the whole device. This is the reason Computer-Aided Engineering (CAE) software and Computational Fluid Dynamics (CFD) software in particular are so popular in the modern industrial world. CFD in particular is more effective in investigating directly, during the product design process as an integral part of the product lifecycle management (PLM) in the early development stages. There are several approaches in CFD including traditional and frontloading. In addition to relying on the vast knowledge and experience in CFD, the traditional approach usually requires transferring geometry from a CAD system to CFD software, via different exchange formats, where some issues with geometry can occur. Issues such as cleaning and healing geometry to make it suitable for mesh creation and manual mesh generation with focus on boundary layers. Investigations

of a wide range of designs using such an approach is very time-consuming and as a result only a few particular cases are examined by CFD experts after all changes are made by the design engineer.

The frontloading approach presented in Mentor Graphics' FloEFD™ tool, is intended for use in the early design development stages by design engineers. There are two main principals in FloEFD: direct use of native CAD as the source of geometry information, and a combination of full three-dimensional CFD modeling solving Favre-averaged Navier-Stokes equations with simpler engineering methods in the cases where the mesh resolution is insufficient for direct simulation.

To overcome a traditional CFD code restriction of having a very fine mesh density near walls in a calculation domain, FloEFD describes boundary layer, with the "Two-Scale Wall Functions" method including the near wall functions and the sub-grid model of the boundary layer.

For the simulation of the compressor, the rotation model should be used. There are two local rotation models in FloEFD – circumferential averaging and sliding. The circumferential averaging approach is employed for calculating transient or steady-state flows in regions surrounding rotating solids, which are not bodies of revolution (e.g. impellers, mixers, propellers, etc). To connect solutions obtained within the rotating regions and in the non-rotating part of the computational domain, special internal boundary conditions are set automatically at the fluid boundaries of the rotating regions. The rotating region's boundaries are sliced into rings of equal width and the values of flow parameters, transferred as boundary conditions from the adjacent fluid regions are averaged circumferentially over each of these rings.

The sliding rotation model produces a time-accurate unsteady solution of the flow fields, where the rotor-stator interaction is strong. The sliding technique takes into account the relative motion between stationary and rotating regions. Rotor and stator control volume (CV) zones are connected with each other through "sliding interface". During the calculation, zones linked through "sliding interface" remain in contact with each other. The sliding interface has CVs on both sides and as a consequence each face of the sliding interface has two sides belonging to both rotor and stator zones. All these techniques allow FloEFD to be used for the calculation of air turbo compressors.

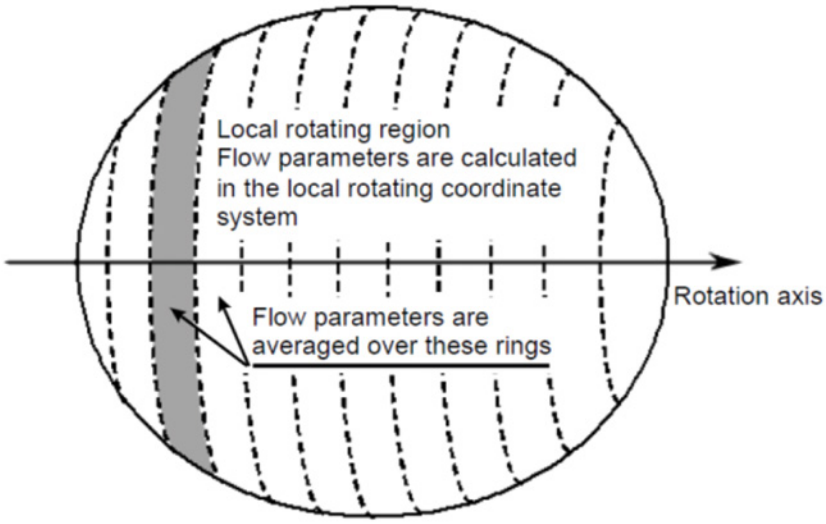

Figure 2. Ring creation in the Circumferential Averaging Rotation Approach

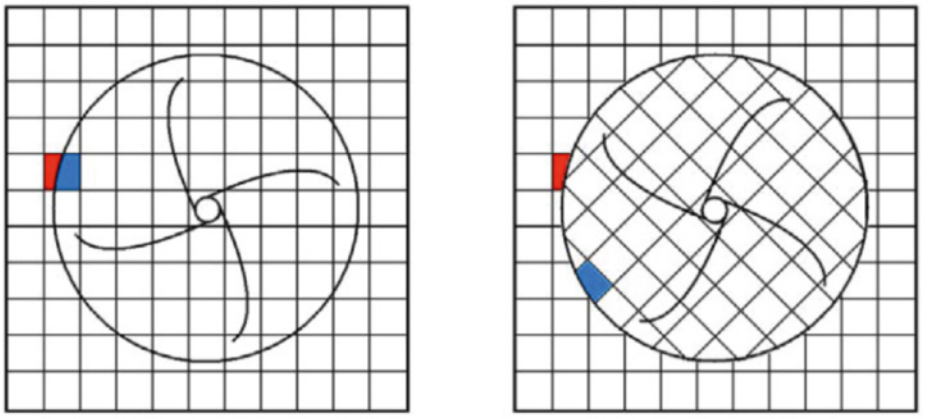

Figure 3. Sliding Rotation Approach

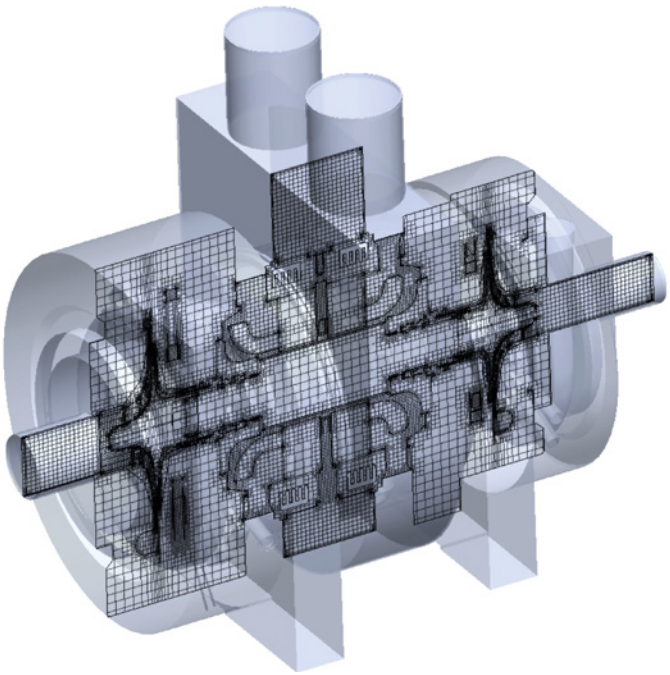

Figure 4. The Mesh of the Compressor Model

This article shows a great example of the two stages of oil free compressor investigation, completed by Tamturbo Oy with support from Axis Engineering.

For analysis, the full assembly of the compressor was used, the construction of which includes several contours: compressor flow area, and several cooling contours. Each contour includes components manufactured from different materials, such as titanium steel or aluminum, which were chosen based on the results of the preliminary calculations of thermal loads and strengths of the various parts of the compressor.

The geometry of flow area has been determined by required compressor characteristics and has a very complex internal structure. The CFD analysis of the compressor, where final pressure rise ratio was calculated, allows for the assessment of air temperature rise. To decrease the temperature of the compressor's body, Tamturbo engineers added the cooling system for the compressor with a complex internal structure.

All geometry features of the compressor, presence of the rotating parts and special requirements for temperature in some critical places like bearings, volutes, shaft and so on, predetermined mathematical models which were needed for the analysis.

The turbulence model used in the analysis can detect a flow regime and switch the mode between laminar and turbulent automatically. This solver is unique and allows an engineer to obtain a solution inside narrow channels even on a coarse grid. The calculation was made taking into account conjugated heat transfer, where heat transfer equations were solved in solid bodies. The radiation model has been disabled due to relatively low temperatures.

In the analysis of the flow, to consider the rotation of the impellers, special rotating model "sliding" was used, which helps to predict characteristics of any type of turbomachines with better quality.

As boundary conditions for the airflow inside the compressor were specified so were the conditions for pressure at the volutes outlets, mass flow rate at their inlets, and shaft rotating speed. For cooling paths, pressure difference between inlet and outlet boundaries was determined. To simplify the thermal analysis of the engine and the shaft, a heat emission process was simulated by adding heat sources with constant power

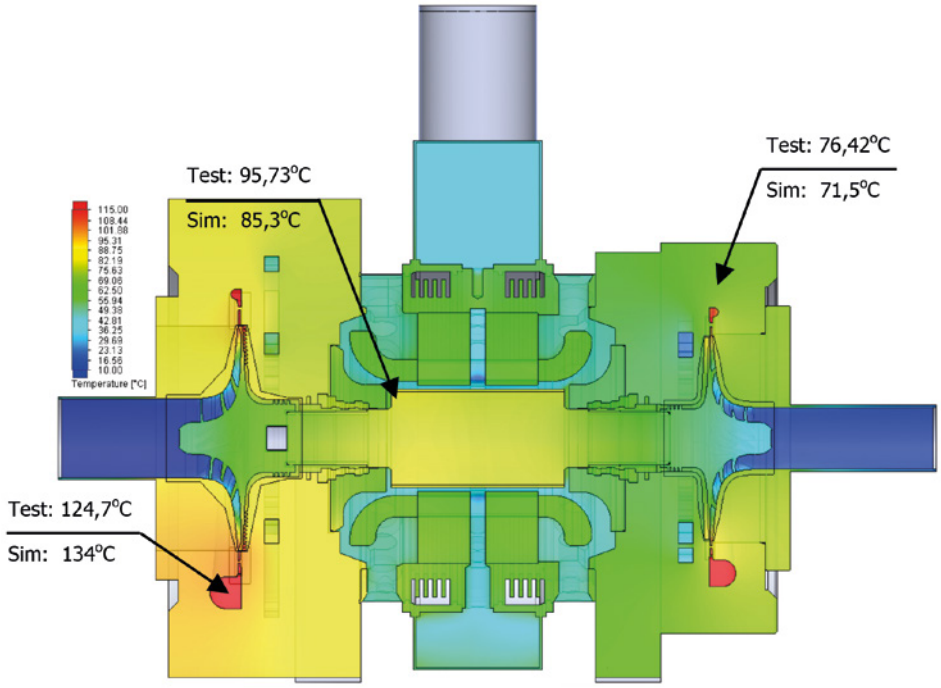

Figure 5. Temperature Distribution in the Longitudinal Section of the Compressor

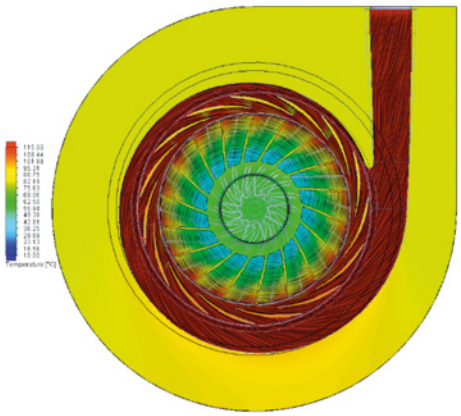

Figure 6. Stage 1. Temperature Distribution in the Cross Section of the Compressor with Streamlines

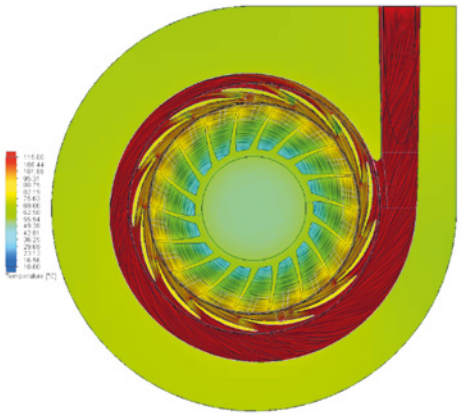

Figure 7. Stage 2. Temperature Distribution in the Cross Section of the Compressor with Streamlines

values instead of using the FloEFD feature emulating a real Joule heating process.

Simulation of conjugate heat transfer process for all zones and units of the compressor, allowed for the investigation of their mutual influence and predicting the thermal state of the compressor components.

The most important parameters under investigation were air temperature before the bearings the volute and the shaft temperature. Mainly bearings work properly when their temperature is lower than 100-120°C, but on the other hand the temperature of the compressed air can be higher than 200°C. And of course every calculation has to predict the compressor pressure rise ratio for the required mass flow rate range.

Initially homogeneous structured mesh was created on the entire geometry, where the number of cells along the main axis of the compressor did not exceed 90. The number of cells for the other axis was chosen in the way that the final size of the basic cells was similar in all three dimensions. After creating the basic mesh, some local regions for better mesh resolution around compressor impellers and in the bearing's area were added. Additionally mesh generator settings were specified to allow for automatic detection of the narrow channels and further splitting mesh in these areas. As a result the total number of cells in the entire two-stage machine was approximately 4.9 million.

The analysis was run in the transient regime on the usual workstation for CFD calculation:

two CPU with frequency 3.1 GHz and only 8GB RAM were used for the task. As a result the simulation of 30 seconds of physical time took only 1.5 days of computer time.

According to the calculation results, the additional seals have been designed and the optimal mass flow rate of the cooling agents were chosen. The temperature in the bearings, was in the range of 60-80 degrees in the calculation results. Tests showed the temperature rise in the nodes close to the bearings up 7-12 degrees.

The difference between pressure values of simulation results and natural tests of the real equipment was not more than 3-5%.

Tamturbo Oy uses FloEFD for a wide range of other tasks, from the turbo compressors developing area, closing all questions of aero and thermal calculations. The quality of the results was proved by the series of experiments which were provided by Tamturbo Oy and a number of completed projects. The software has several direct interfaces with other codes which are used in the company, and as a result of this fact and due to the unique solver technology as well as all other features mentioned above, the development product lifecycle and its costs were significantly reduced without compromising the quality of the results.

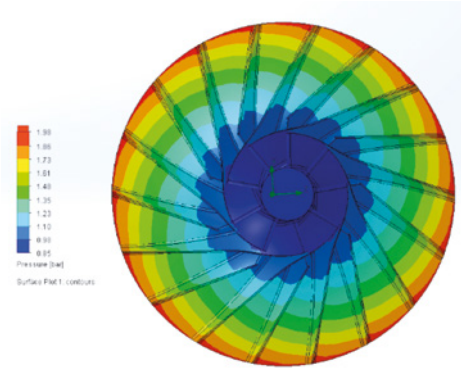

Figure 8. Stage1 impeller. Static pressure distribution on the surfaces at normalized mass flow rate 0.8, normalized rotational speed 0.943. Pressure rise ratio - from simulation 1,9718/ from test 1,9723

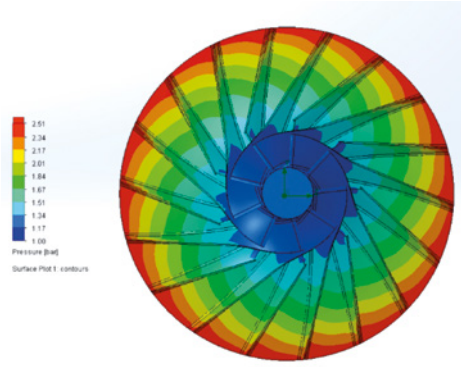

Figure 9. Stage1 impeller. Static pressure distribution on the surfaces at normalized mass flow rate 1.5, normalized rotational speed 0.943. Pressure rise ratio - from simulation 1,9585/ from test 1,9589

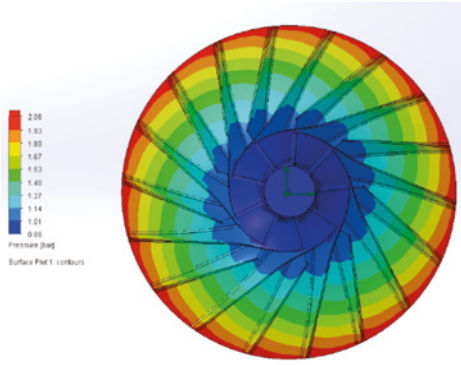

Figure 10. Stage1 impeller. Static pressure distribution on the surfaces at normalized mass flow rate 0.9, normalized rotational speed 0.97. Pressure rise ratio - from simulation 2,0391/ from test 2,0302

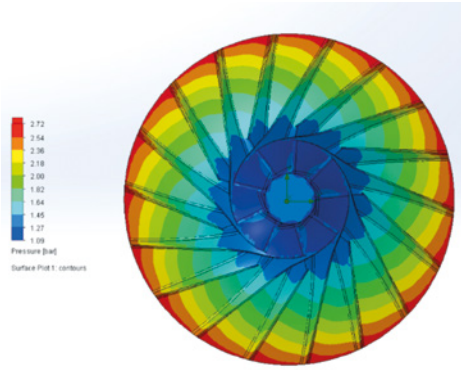

Figure 11. Stage1 impeller. Static pressure distribution on the surfaces at normalized mass flow rate 1.6, normalized rotational speed 0.97. Pressure rise ratio - from simulation 2,0083/ from test 2,0057

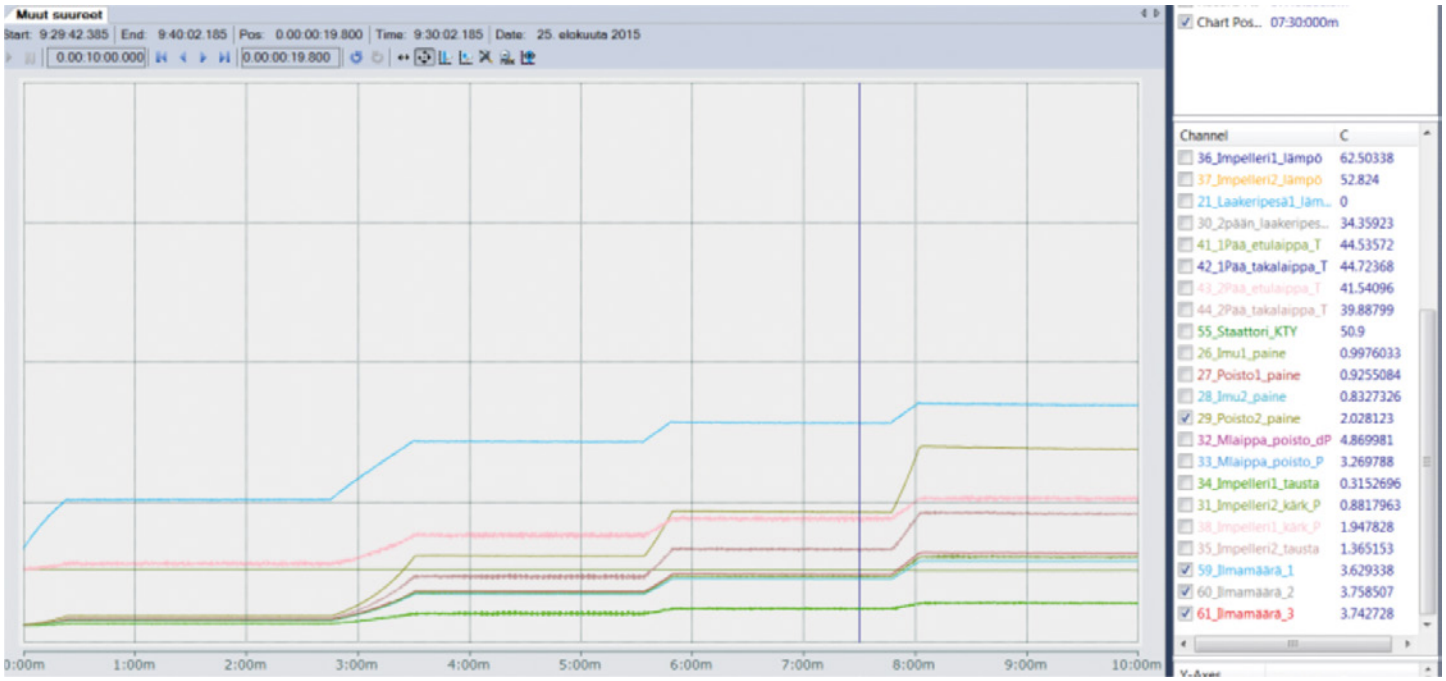

Figure 12. Dynamics of different parameters from the final compressor test.

Fujifilm Frontloads Camera Design with FloTHERM®

By Kazuya Mayumi, Optical Device and Electronic Video Product Development Center, Fujifilm Holdings Corporation

FUJIFILM

Our department focuses on the development of cameras with high performance and high quality, to preserve the culture of photography and to develop imaging technology. The team I belong to develops the elemental technology of such cameras and lenses and supports the business by running simulations. I have been involved in thermal design by predicting temperature with simulation tools ever since the first "X-100" of Fujifilm's X digital camera series. Now simulation technologies are essential for product development today.

Modern digital cameras, like Fujifilm's X-Pro 2 are developed to dissipate the minimum amount of heat as form factors shrink. Excessive heat can increase the size and weight of the cooling solution, preventing miniaturization. It is associated with the concept of poor design by the consumer, as the design can appear to have "regressed" back to an earlier bulkier form factor. It also requires the use of higher-cost parts, adding cost to the product, further reducing its competitiveness.

Heat generated within the camera has to be managed for many diverse reasons, such as the tendency for elevated temperatures to reduce image quality through noise in the Complementary Metal–Oxide–Semiconductor (CMOS) circuitry. The temperature of the chassis must also be limited to avoid the risk of a low temperature burn for the user. For cost reasons, sheet metal parts within the camera can't be replaced with alternatives that spread the heat better if a problem is found in late design or prototyping.

For these reasons considerable care must be taken prior to prototyping. Fujifilm do this by undertaking the following work from the start of development:

- Present an optimal solution for the structure, as an outcome of thermal simulations on several different design variations,
- Predict the maximum temperature without using any correlations, and
- Complete the study by defining what parts, including their size and number, are needed for the heat dissipating structure.

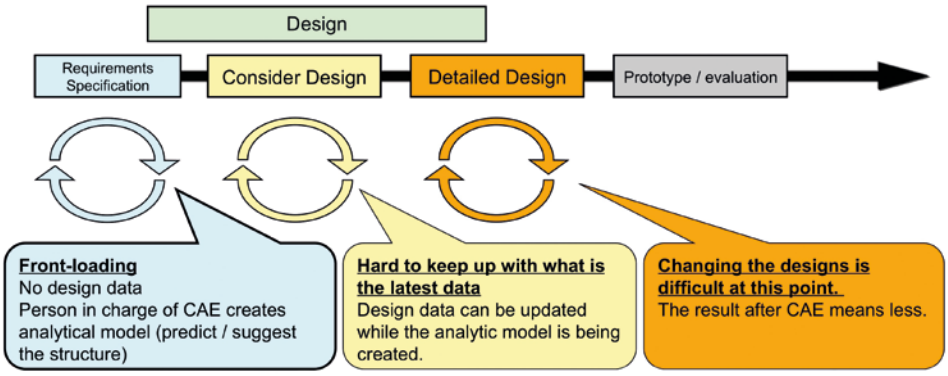

Figure 1. Fujifilm Camera Design Process

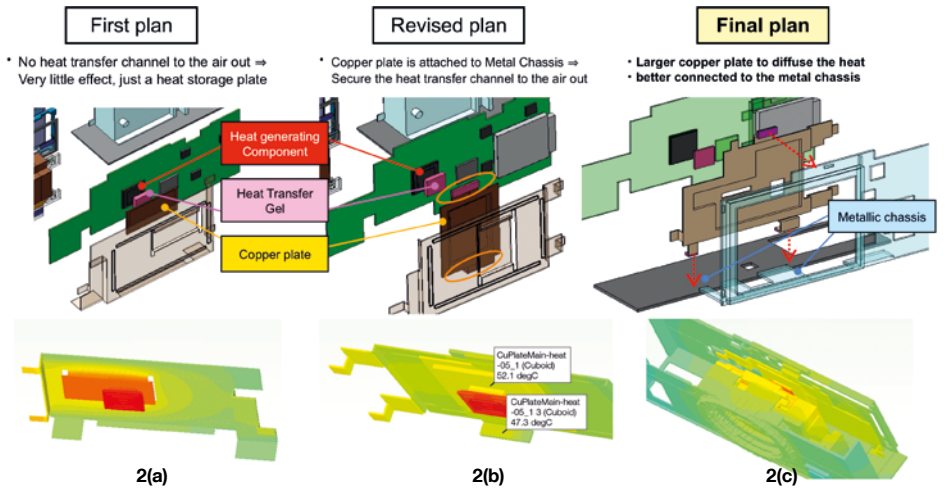

Figure 2. Initial, Intermediate and Final Frontloaded cooling solutions (pre-CAD)

The process is shown in figure 1: It starts with a simple analysis model built in Mentor Graphics' FloTHERM Electronic Thermal Analysis software. It uses geometry simplified from the CAD model – the exact details of the process Fujifilm considers proprietary.

"We use FloTHERM to frontload our thermal design. FloTHERM enables us to explore design alternatives early on, design the optimal solution for removing the heat, and provides very good accuracy against the final test results we get for chip, component, and touch temperature on the case."

Kazuya Mayumi, Optical Device and Electronic Video Product Development Center, Fujifilm Holdings Corporation

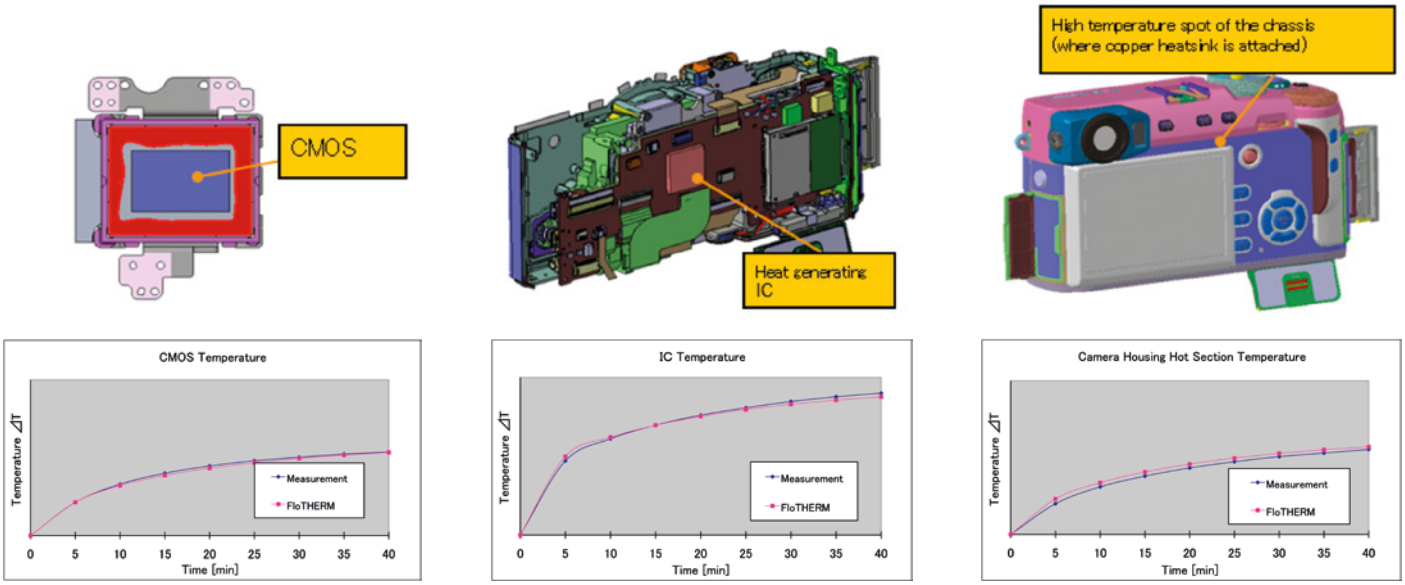

Figure 3. FloTHERM model agreement with test results at different packaging levels.

By keeping this analytical model updated, the effects of changes can be fed back into the design process immediately, frontloading simulation in the development process.

As a case in point, Fujifilm needed to improve thermal performance, introducing a copper heatsink and thermal gel into the product for the first time. In the initial design, shown in figure 2a, along with the FloTHERM result, the copper heatsink just acted as a heat storage device, as there was no heat flow channel to get the heat out. The revised design shown in figure 2b, attached the copper heatsink to the chassis, ensuring that the heat could be transmitted to the air. However, the temperatures were still too high. A final design iteration, shown in figure 2c, increased the size of the copper plate to better diffuse the heat, and additional connections were added to improve heat transport to the chassis.

Using this approach, Fujifilm are able to get highly accurate temperature predictions during the early part of the design process, and use the results of improvements made to the design using FloTHERM to update the CAD model. The predictive accuracy of this analysis model is checked towards the end of the development process once a physical prototype becomes available. The detailed CAD geometry available at this stage is shown in figure 3 for the CMOS chip generating the heat, the component housing the chip, and the hot spot on the camera housing, resulting from this heat source, together with the comparison between measurement on the prototype and the FloTHERM model, which shows excellent agreement at all of these packaging levels.

Using CAD data directly in FloTHERM gives results which are very similar to those shown in figure 3, for the model based on a simplified geometry for the analysis. The import of the CAD geometry is also acceptably fast for use in the design, however this approach is not favored for the simple reason that CAD geometry is not available at the start of the process, so this approach would have the effect of delaying the CFD work until later in the design, when the business benefits of using CFD are less. Whereas the requirements for the cooling solution must be addressed and different options investigated at the outset.

Critical to the design effort is the ability to predict accurate temperature values, not just trends or relative differences. This is because of the thermal limits both on the component's operating temperature, and also the maximum permissible touch temperature of the case. Consequently, it is the responsibility of the CAE engineer to investigate any differences between the simulation result and test data. One source of this discrepancy can be the power values used for the heat sources. It is quite common for electrical engineers to provide power values during design that are conservative, i.e. they over-estimate the likely actual power by say 20% to ensure that the cooling solution will be adequate. However, this makes it impossible to match simulation results to test results, so Fujifilm now ensure that the power estimates that the electrical design team share with the thermal design team are as accurate as possible.

More broadly, Fujifilm consider the ideal role for a CAE engineer is to remain in the background. However, they should be proactive, working to reduce the workload of the designer, and thereby speed the design. CAE engineers should present the results of design optimization and an improved design back to the designer, rather than just reporting back the results of the design iteration they were asked to simulate. Only by optimizing the design process in this way is it possible to perfect the design of the product.

Continental

Dr. Uwe Lautenschlager
Senior Technical Expert - Simulation

Q. Tell us about Continental AG
A. Continental can look back on a successful history for 145 years, founded in 1871, when the company started manufacturing soft rubber and rubberized fabrics. Although most consumers recognize Continental for its tire division, we are a leading diversified German automotive manufacturing company specialized in brake systems, automotive safety, powertrain and chassis components, as well as instrumentation or driver HMI, connectivity, infotainment, access systems and many more. Today, Continental has sales above €39 Billion with around 215000 employees worldwide. My place is inside the "Infotainment & Connectivity" Business Unit's Mechanical Engineering team within the Interior Division. We are located here in Wetzlar, Germany, a town known for optical and fine-mechanics industry.

Q. Tell us about what you do in your role at Continental?
A. I started my career at our Wetzlar site in 1999 as a structural analysis specialist. However, the task quickly extended into the electronics cooling and thermal simulation area. Today I manage our BU's mechanical simulation team which is based at several sites around the world. It covers optical, structural, EMC, molding and thermal simulation of our products. My team role is to innovate the simulation processes by setting the simulation methodology, tools and knowledge sharing and targeting the same level at all sites. Nevertheless, I'm always passionate about developing models and doing simulations by myself. Besides my work in the simulation team, I'm also fortunate because Continental supports me to be an "ambassador" at the nearby University of Siegen where I have been giving lectures on "Modeling and Simulation" since 2009. The students love the close connection to Industry they can get from my hands-on course.

Q. What are the products that you and your team are involved with?
A. Speaking about our Business Unit, our product portfolio includes radios, which have evolved from simple tuners and amplifiers to proper entertainment hubs, multimedia systems, and telematics modules. Connectivity

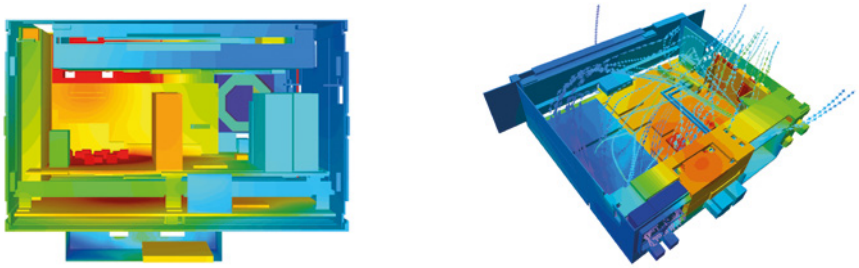

Figure 1. Thermal analysis of an infotainment system with multiple components and devices.

devices allow the communication between the vehicle and the internet and, in future, increasingly to other peers as part of the Vehicle-to-X (V2X) trend. A permanent exchange of data from the vehicle is aimed in our "Always On" vision. Infotainment is a fast growing part of the automotive industry and is rapidly changing from year to year in both car connectivity and car communications. Our products have to deliver new answers for future mobility and intelligent technologies, they are networked together by taking on more driving tasks.

Q. Do you work mostly within your Business Unit or does your work stretch to other Continental Business Units in Germany or even Worldwide?
A. We have two aspects here, one being the integration of products across our division in the future. The second aspect is our simulation network. Not only do we have our experienced and agile simulation team, we have established a close simulation network and User and Working Groups across Continental for several disciplines. For example, I'm the speaker and organizer of our FloTHERM® User Group. We meet regularly with all international users in varying locations and support each other across all divisions if necessary and possible. Our BU's simulation team itself is positioned worldwide like in Singapore, France, Germany, Romania etc. so it really is a worldwide working group. Our team has the desire to serve our customer's, (internal and external) needs quickly and reliably; we have a high documentation standard in order to provide the same high quality in all our simulation results.

Q. How different are the requirements or thermal limits of your products and how different are the environmental boundary conditions for them?
A. Thermal limits become increasingly obvious as package dimensions shrink, power dissipation increases locally or globally and packages have lower temperature specifications, e.g. from consumer electronics. Boundary conditions as part of the requirements are given by the OEM and can therefore vary according to the standards they specify. The ambient temperatures vary, the requirements on housing temperatures and the thermal management options differ and are dependent on the location of where the product is installed (roof, dashboard etc.). Since our infotainment systems can be found in trucks, we have to fulfil a higher lifetime expectation (25,000 hours) for them compared to cars (with around 10,000 hours being more normal). Hence, the overall variation is more between the OEM or vehicle type and we try to re-use the platforms across OEMs to keep the costs for development to a minimum. There are many parallel thermal challenges nowadays, not "only" designing a good amplifier heatsink as maybe in the past.

Q. When you use FloTHERM in your work, how many simulations do you run on one product on average until the design has matured?
A. In 2000 we chose FloTHERM as our thermal simulation tool, convinced primarily by its quality and robust solution capabilities. We use FloTHERM to run thermal simulation very quickly and it is deeply integrated into our design process. It allows us to do lots of variant simulations very fast. If my boss says "we need something today", I can get a satisfactory answer quickly. Productivity is important but it depends on what type of answer is needed, or how much detail and data to include. In the very early phase of a product's design, such as the quotation phase, the simulation detail is secondary as the product cannot be defined as accurate as compared to the final product development stages. So it is not a number, it is a level of confidence that can be achieved rather quickly.

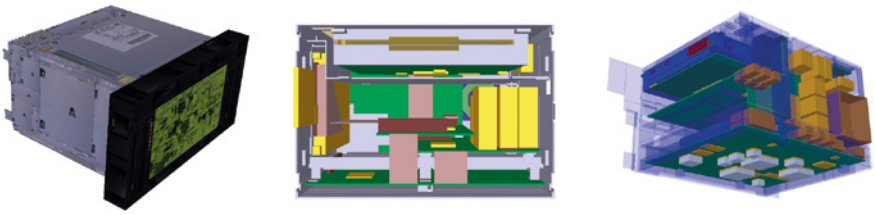

Figure 2. A FloTHERM model with texture map and the internal view of an assembly with its components and modules.

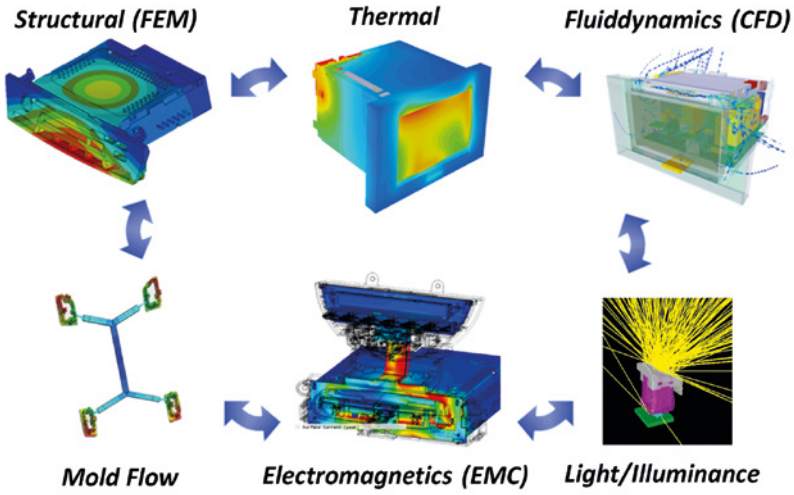

Figure 3. The overall connectivity of various simulation disciplines in multimedia system simulations.

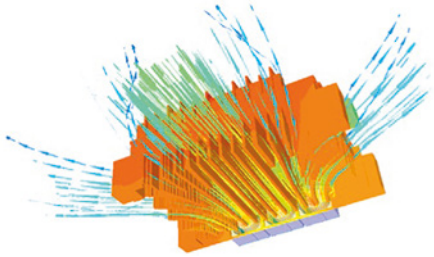

Figure 4. Thermal analysis of an infotainment system with multiple components and devices.

Q. Do you think the products you develop today would be realizable without simulations?
A. We always need to understand our products - that's where simulation tools come in. Of course, developing a product on time and to cost was a goal when there was not much virtual analysis done 20 years ago. Often the products were overdesigned and we had many prototypes and samples created. Today, however, we can design the products closer to their limits as we understand the physics behind them better through simulation. The development cycle we have today could not be done without simulation. Our first shot has to be correct. A good simulation is also not only about being correct, but it also helps to understand the product. The design of our automotive multimedia systems has to fulfill requirements from mechanical stability and thermal management to electromagnetic compliance, hence a multi-disciplinary design and optimization problem. Conflicting objectives among these disciplines require a concurrent design approach with different modeling levels, parameter variation (e.g. DOE techniques), optimization techniques and the consideration of uncertainties and changes within the design process. Such up-front simulations enable us to test and modify system and components as virtual prototypes before performing physical tests and building real prototypes.

Q. How important is it to interact with the other simulation groups from electrical and circuitry design teams and how often do you need to communicate the changes and the results?
A. Extremely important! Every change with a thermal benefit can greatly impact the structural behavior or Electromagnetic Compatibility (EMC) and electrical circuitry aspects. A larger heat sink in the back of the system could increase the vibration and cause rattling for instance; or moving a processor closer to a colder zone for better cooling, but also closer to a high frequency zone near an antenna for example can cause EMI issues. As said before, we have a multi-disciplinary design problem.

Q. Where do you see electronics thermal simulation in the future? Will there still be physical testing or will it be all virtual testing through simulation?
A. We typically skip the A-Sample that we had in the past and almost directly go into the tools as we expect already a good sample from the simulation. Potential design risks are typically identified by simulation early enough and eliminated. This is besides the many tests we put our devices under with physical laboratory stress tests from long term use of buttons, shock and random vibration to environmental tests in climate chambers. For us the testing will not be replaced in any foreseeable future; final qualification testing will always be done on the matured design in a laboratory. However, the number of prototypes is reduced and the risk of failure should be at a minimum.

Q. When thinking about the future, where do you see the biggest challenges in your work with the future technology developments that will go into your products?
A. Several years back CPUs generated 1-2 W of heat in a car; now they are more in the range of 10W. We are also seeing the trend towards bigger touch-screen displays and multimedia systems are getting more and more condensed into smaller spaces of non-rectangular shape. Those are some of the technical challenges we face, additionally we must put a big focus on developing the skills of our simulation team to be able to understand and handle new technologies and simulation tool features accordingly. I always see the resource aspect as we will never have enough simulation people to do everything that could be done, but we do everything that's necessary.

Q. Do you have any goals over the coming years to increase your simulation productivity?
A. Our daily work is changing faster than ever. Improving the post processing and documentation of simulation tools and results will help us to communicate answers more efficiently to our customers. We try to reduce the time for modeling and documentation and spend more time for creativity and solutions. We want to implement highly efficient workflows with the right tool landscape. Continental is on the way to being a digital company for sure.

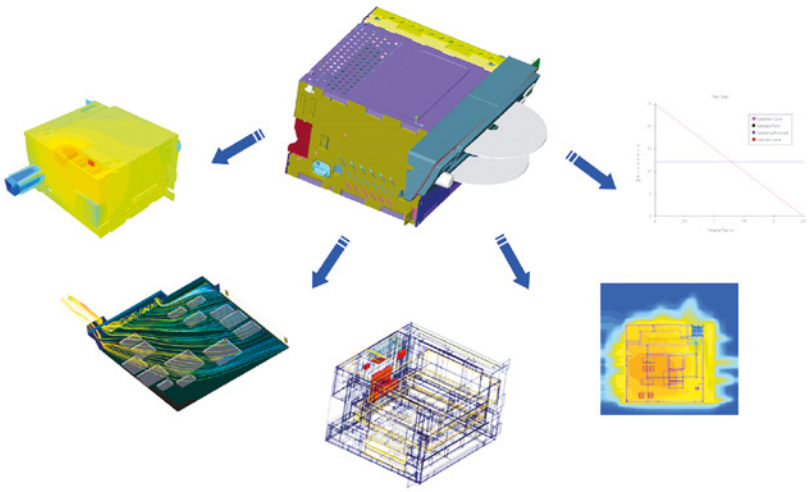

Figure 5. Showing a range of simulation tasks and result evaluations in an infotainment thermal simulation.

Using FloEFD™ to design Liquid-Cooled Nozzles for Cutting Tools

By Hidebumi Takahashi, Mitsubishi Materials Corporation, Advanced Materials & Tools Company, Machining Technology Center

MITSUBISHI
MITSUBISHI MATERIALS

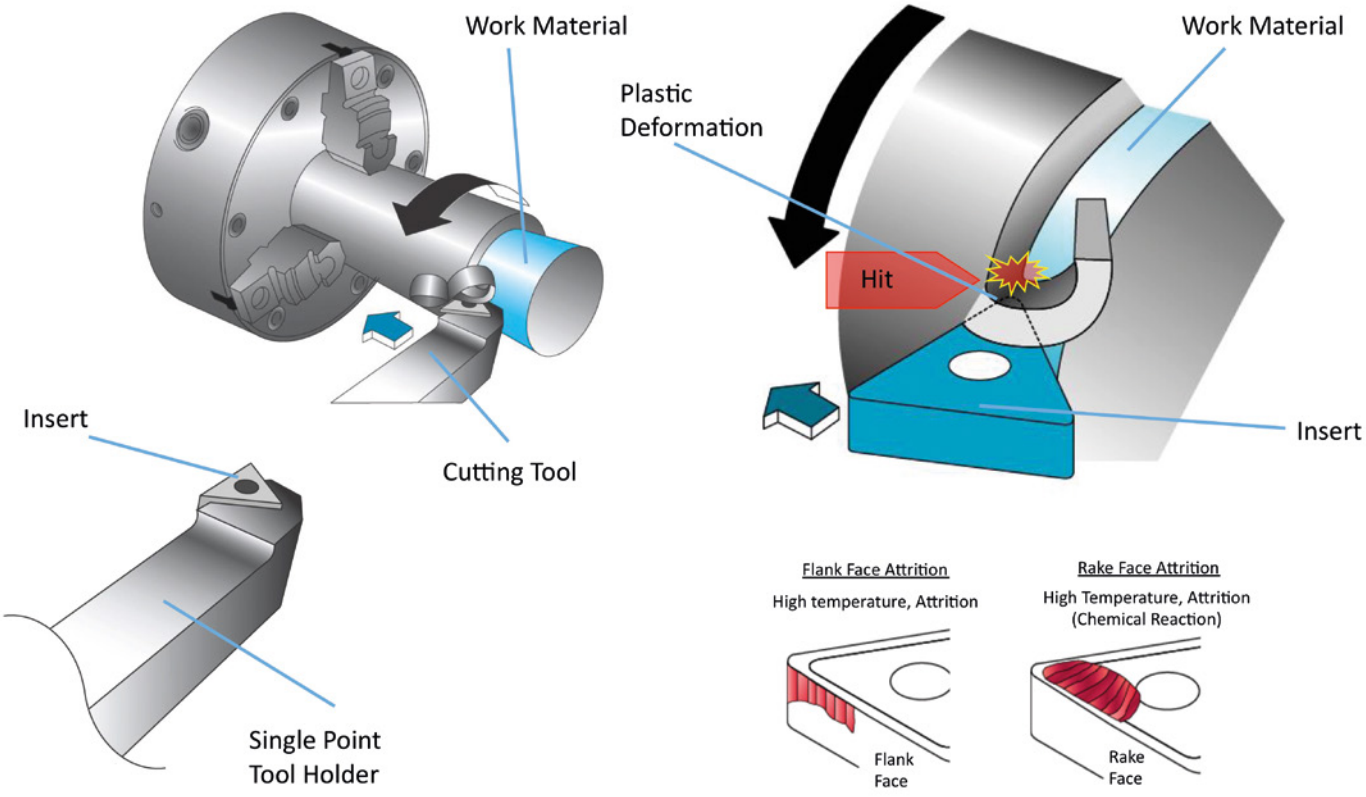

Figure 1. Typical Cutting Bits used in Lathe Turning and the wear issues they face

The Mitsubishi Group is a huge Japanese industrial conglomerate and Mitsubishi Materials Corporation is one of the subsidiary companies of Mitsubishi Mining Company Ltd. and has been in existence for approximately 100 years. Its Advanced Materials & Tools Company and its consolidated subsidiary companies employ approximately 6,800 people worldwide, making and delivering a wide range of machine cutting tools based on tungsten carbide. A subset of these tools is in rotating lathe applications (Figure 1) that tend to generate surface temperatures of 600 – 700 degrees at the contact cutting point (at the rake and flank faces) and the cutting tool's lifespan can consequently be low. Tungsten Carbide triangular tool inserts are typically used on all six of their corners before they are disposed. They therefore experience several thermo-mechanical effects that damages them and affect their lifetime – attritional wear on the rake and flank faces of the tool, frictional heating effects, mechanical separation due to the extreme forces involved in the cutting, and even chemical reactions.

Traditional cooling systems for such cutting tools have used a single circular nozzle cooling hole near the insert. The tungsten carbide insert can last for 20 minutes per corner edge whereas better cooling could

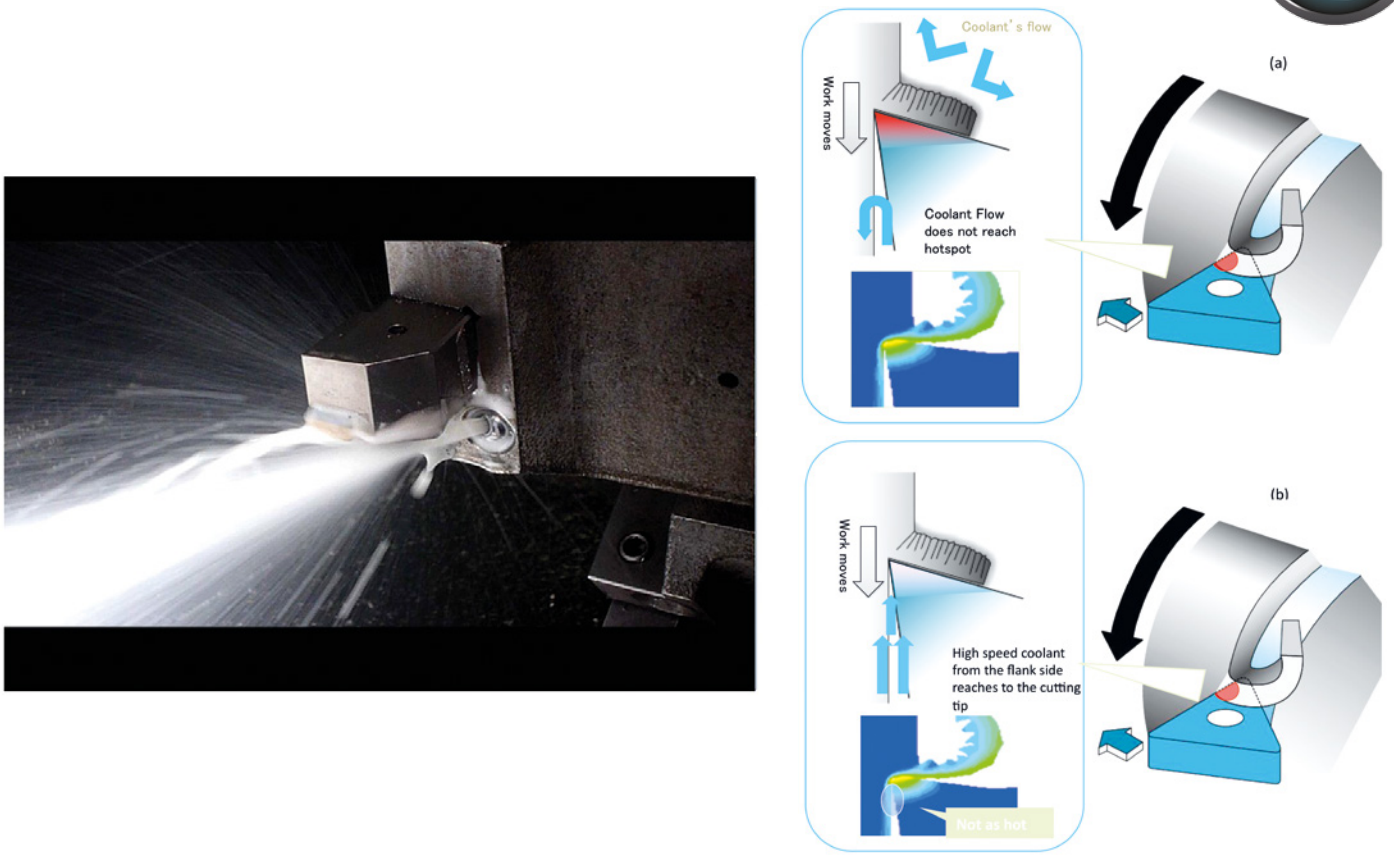

Figure 2. Typical Cutting Bits Coolant Spray and good hot spot cooling (b) versus bad (a)

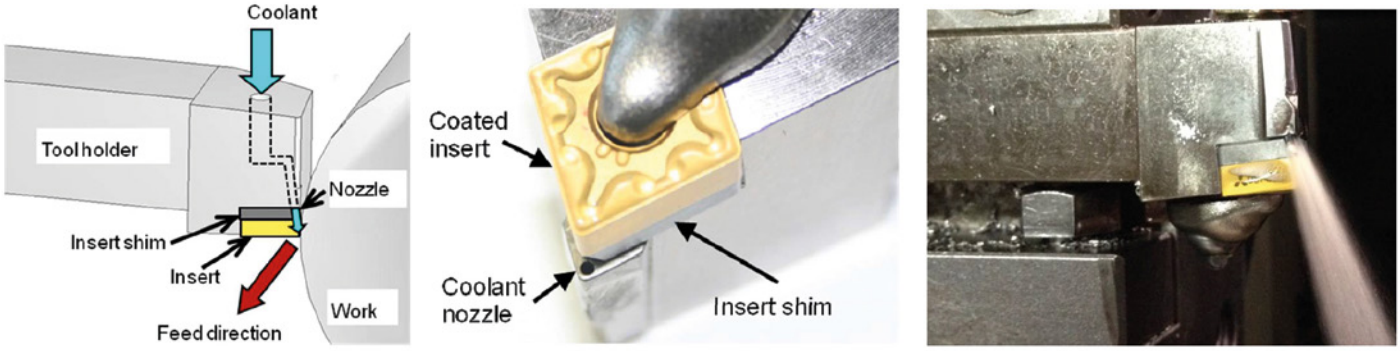

Figure 3. JC Technology's laboratory concept for a Tool Bit Cooling Jet (with circular nozzle)

increase the insert's lifetime by 40%, to 28-30 minutes per corner edge. Such well-cooled tool holder's lifetime performance is an advantage to productivity for cutting tool users.

Mitsubishi turned to Prof Obikawa of the Institute of Industrial Science at Tokyo University and established an academic-industrial partnership to extend the life of their tools. He came up with ideas for new cooling technology for the Mitsubishi tool holder that needed to be tested. The goal of the new cooling technology was to reduce extreme frictional heat generated while cutting (Figure 2), which in turn has the adverse effect of reducing product lifetimes. Prof Obikawa's "Jet Coolant Tech" (JC Technology) came out of the collaboration.

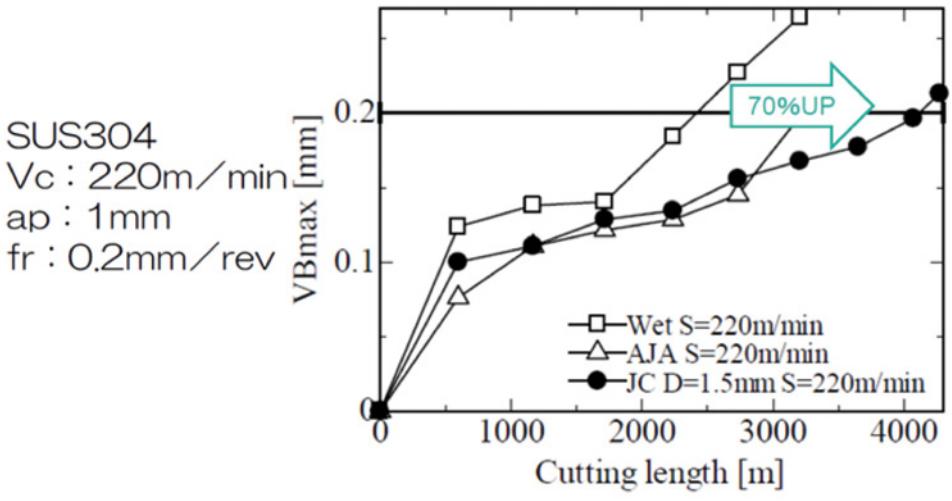

Figure 4. JC Technology's results in a Cutting test - Jet Coolant effect is proved by the basic lab study

Usually it is hard to make the nozzle coolant liquid reach the hottest point on the tool, thereby cooling is not working effectively, (Figure 2a), versus the ideal scenario of coolant getting to the hot spot (Figure 2b). Making the coolant spray reach the heat source by applying high speed targeted jets from the flank face in particular is key.

The crucial idea from JC Technology was to apply the liquid coolant as a "high speed jet" spray from the bottom part of the insert sheet, cooling it down directly, and thus extending the insert's lifetime (Figure 3). At SUS304 laboratory test, JC Technology was able to show significant improvements (70%) in the laboratory, in cutting length for the coolant jet configuration employed (Figure 4).

Mitsubishi worked with JC Technology to come up with an "L" Shaped nozzle that they believed would perform better than a circular nozzle in terms of jet performance in cooling (Figure 5) within their laboratory tests.

Mitsubishi needed a methodology to simulate the cooling and mechanical effects of its new nozzle. Would it produce enough cooling? Would the nozzle component be durable enough? As such engineers and designers assembled an array of computer-aided engineering tools to virtually test the new design (Figure 6). With regard to fluid flow and heat transfer analysis, they decided to use FloEFD™ from Mentor Graphics and Particleworks™ from Prometech Inc. They only used the standard functions of FloEFD (Figure 7) and Particleworks (Figure 8) software in their coupled simulations with no user subroutines required.

The coolant used in the holder itself was 5-10% diluted water but regular water was used in the CFD simulations. The main goal of the simulations was to optimize the liquid cooling channel opening geometry for enhanced cooling purposes with as few prototypes as possible. Hence, the best cooling geometry was sought for the system. FloEFD showed that for the same pressure drop, the "L" shaped nozzle allowed 11% more liquid flowrate and produced 57% higher peak velocities than the round nozzle. Liquid flow rates and pressures were extracted from the FloEFD CFD simulation as inputs into the Particleworks simulation tool. It simulated the way droplets emerged from the nozzles and where they ended up on the Holder for cooling purposes (Figure 8). Commenting on how Mitsubishi used FloEFD, Hidebumi Takahashi said, "We like

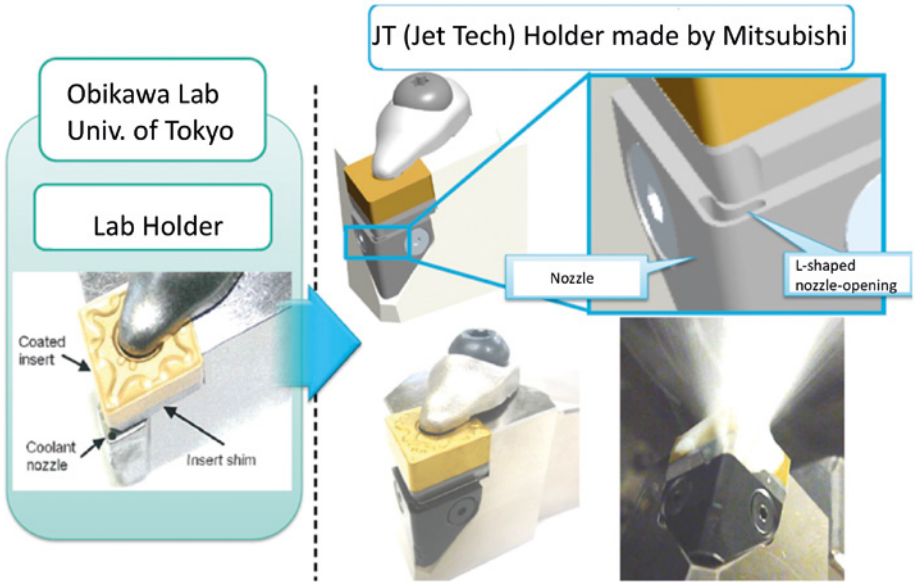

Figure 5. Mitsubishi's Jet Tech Holder configuration and associated CAD model

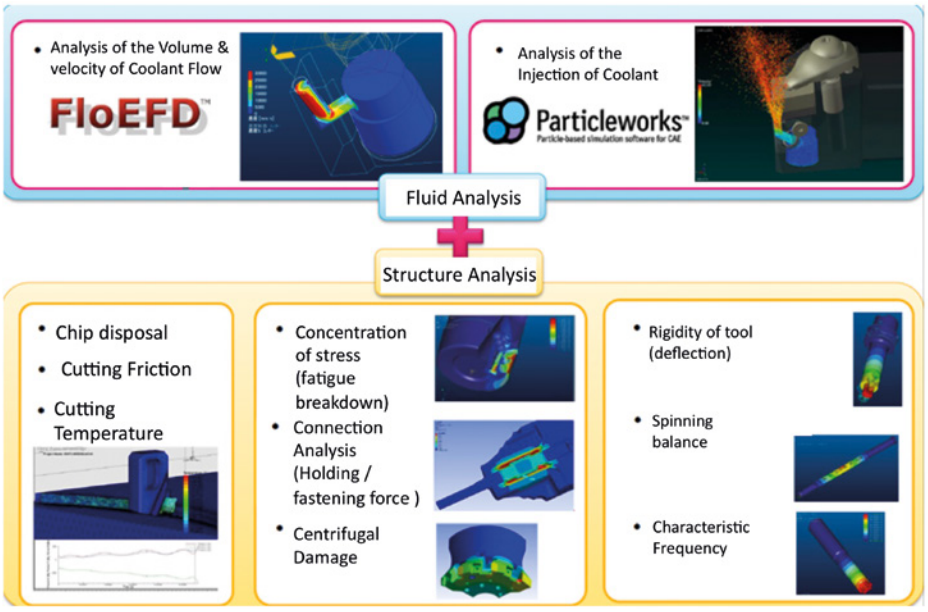

Figure 6. Mitsubishi's Coolant Nozzle Computer Aided Engineering Design Process Methodology

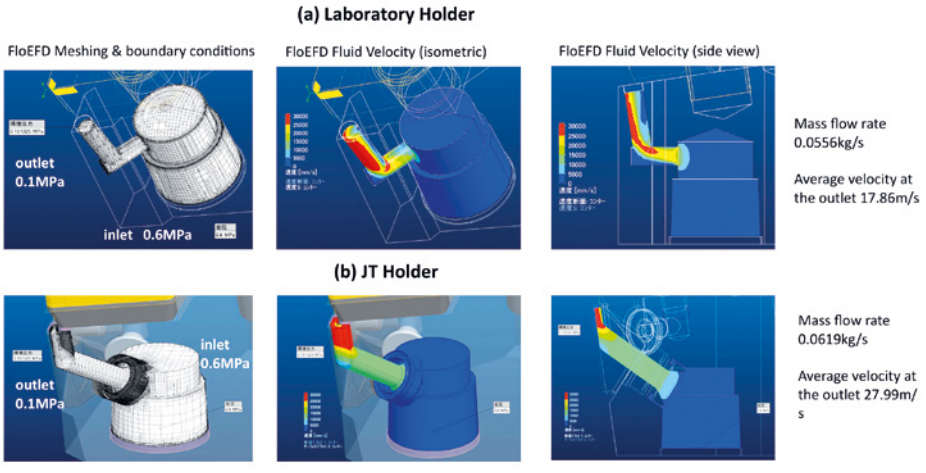

Figure 7. CFD Analysis inside FloEFD of the Laboratory Holder (a) & JT Holder (b) Volume Flow Rate and Velocity of Coolant Flow

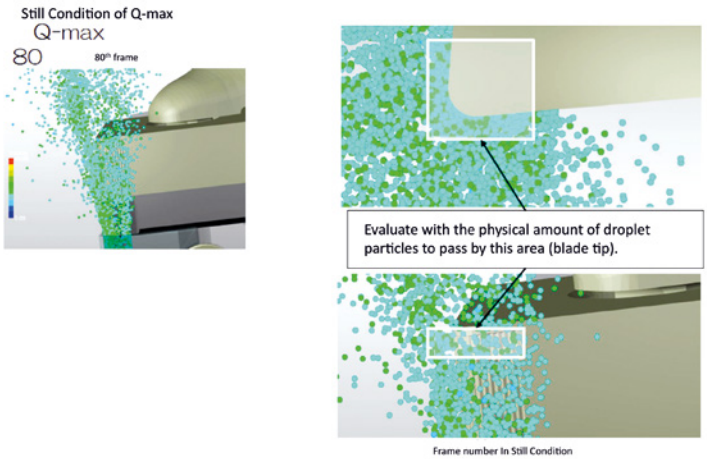

Figure 8. Spray Analysis of the JT Holder in Particleworks™

Figure 9. Final JT Holder Nozzle Spray Configuration

FloEFD because it is fast in calculation for steady analysis. Since we have no specialist CFD experts, our designers take care of simulation analysis. FloEFD is the best for CFD because of its simplified auto-meshing setting inside our preferred CAD package, PTC Creo. We found the cut cell CFD function to be very valuable."

Subsequent experimental test measurements of the JT Holder system prototype created by this approach proved to be very satisfactory in thermal performance as was structural simulation analysis of the rigidity and durability of the nozzle. The methodology devised by Mitsubishi allowed them to patent the JT Tech nozzle (Figure 9) they devised and can be used to create other Holder nozzle configurations relatively quickly. In future Mitsubishi would like to see a closer coupling of the two fluid simulation software tools for similar analyses.

Cutting Test Results

Figure 10 shows the damage of the wear after cutting test and figure 11 shows the line graph of frank wear. In figure 10, the level of wear describes the wear distance from the cutting edge, and the end of the life time is based on when the amount of frank wear reaches to 0.2mm. As seen in figures 10 and 11, with conventional coolant, the edge is worn out with 0.5mm of the frank wear in 14 minutes of cutting, when the remarkable attrition can be seen on the cutting edge, in the meanwhile, with JT holder, the frank wear is only 0.15mm at the time of 14 minutes and it finally became worn out with 0.2 mm of frank wear, in 20 minutes of cutting time. The JT holder performs 40% better in lifetime extension compared with the case of conventional coolant.

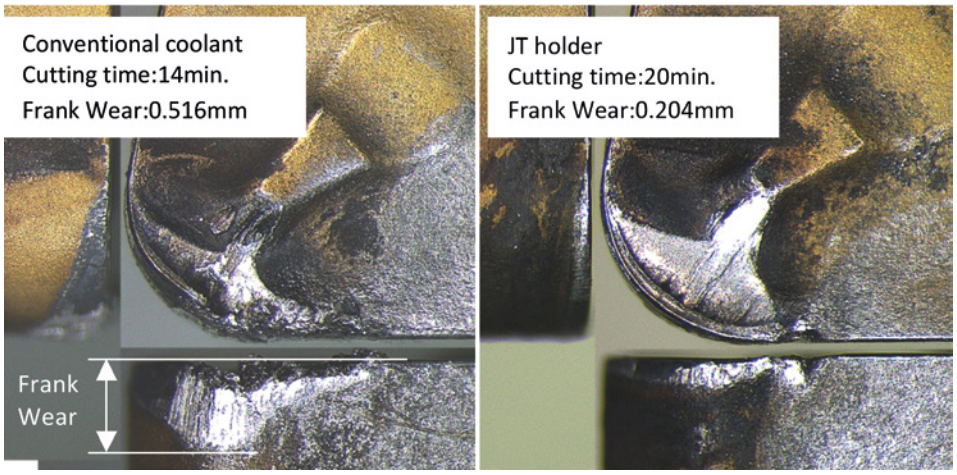

Figure 10. Wear apparatus after cutting test.

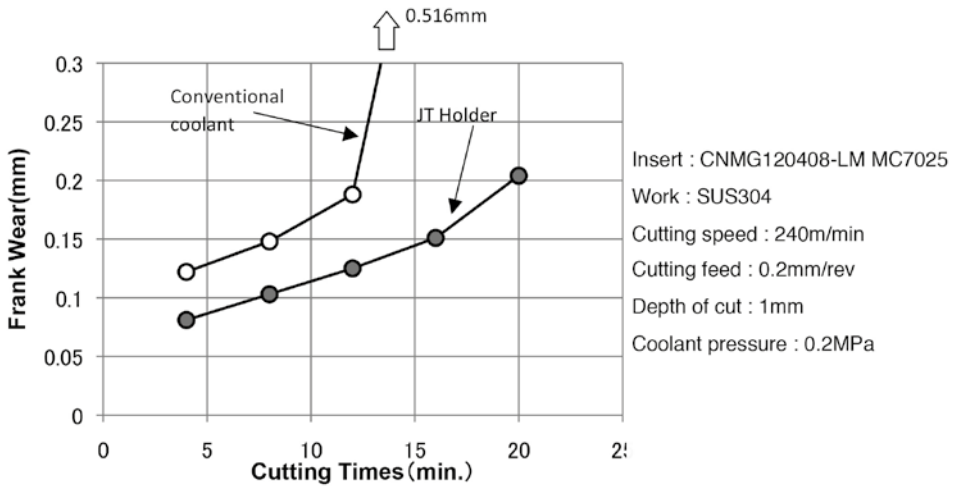

Figure 11. Frank wear of JT holder compared with Conventional coolant.

Mitsubishi Material succeeded in applying the lab testing result to the design process and achieved their target of extending the lifetime of the cutting tools, with an efficient cooling method. The fluid analysis tool, FloEFD, is an extremely efficient tool for product development.

Thermal Testing of an Automotive LED Fog Light using MicReD T3Ster™ & TeraLED™

By Gang Wang, Application Engineer, Mentor Graphics, Beijing, China

Automotive lighting is an essential feature of a car's safety system. All drivers will at some point face deteriorating light or weather conditions that require good head and tail lights. Such lights are used regularly and should be checked often for optimal performance. Fog lamps, on the other hand, are used much less often and when required are safety critical because reliability is paramount. One of the biggest sources of failure in automotive lighting are thermal issues. Thermal design is therefore critical to LEDs in automotive lighting. Poor thermal management in automotive LED lights will lead to a drop in the emitted luminous flux of a bulb because of high junction temperatures. Besides the drop in luminous flux, there will also be a shift in forward voltage when the junction temperature changes and the peak wavelength of the emitted light's spectrum can also be impacted. High LED junction temperatures will also impact the lifetime of the LEDs. Hence, poor thermal management is an issue for reliability, thus making it also an issue for safety. Unlike conventional, incandescent bulbs, LEDs convert up to 30% of their electrical energy into light and 70% into heat. A conventional light bulb emits up to 85% of its energy as heat that is dissipated as infrared radiation unlike the heat from LEDs which dissipates mainly by conduction, providing design engineers with a different thermal challenge in complex LED assemblies (Figure 1 overleaf).

Designing Automotive LED Lighting Systems

Many automotive engineers will adopt the principle of a design flow to optimize their lighting design. The initial boundary conditions would be considered first, like LED size, lighting flux, power, weight, lifetime, cost, ambient temperature and maximum junction temperature. After considering these boundary conditions, the maximum thermal resistance is calculated and it obviously has to be larger than the real thermal resistance. The real thermal resistance is then measured and if the requirement is not fulfilled, the boundary conditions would need to be changed and the exercise repeated until thermal demands are satisfied. These standard design steps to create good thermal management of a LED light can be summarised as follows:

- Define maximum Junction to Ambient thermal resistance, R_{j-a}, based on the worst system boundary conditions: Tj,max (Datasheet), Ta,max (Application), Pthermal (Vf Bin, WPE) – see figure 2;
- Set up thermal resistance network model and calculate the Rheatsink;
- Estimate the shape and the size of the heatsink by the selection of the material, the area and the position of the heatsink etc;
- Simulate and analyze by thermal simulation (CFD) software;
- Create a LED Light prototype and conduct thermal measurement; and
- Iterate on optimization if necessary.

But how do we define the maximum R_{j-a} ?

Automotive Lighting Engineers can use software to help solve these lighting thermal design issues either by a generic spreadsheet or by dedicated thermal simulation software (CFD). Whilst the former is considerably cheaper and more readily available, it will only provide a rough calculation and the result will not be accurate enough as soon as the system gets more complex. Commercially available thermal simulation software are more dedicated to delivering precise and detailed analysis even in highly complex systems. However, they are dependent on good measured material properties of the LED's in-situ performance in an assembly which are frequently not available. Hence, temperature measurements can complement CFD simulations by, for instance, the use of a thermocouple,

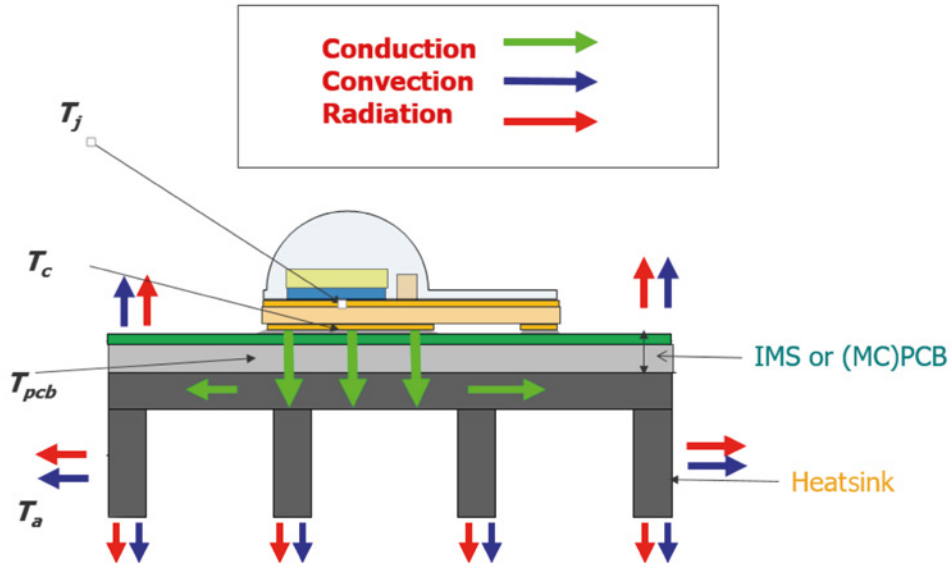

Figure 1. Heat Transfer Mechanisms in an LED Lighting system

$$T_j = T_a + R_{j-a} P_{Thermal}$$

$$R_{j-a} \le \frac{T_j^{\max} - T_a^{\max}}{P_{thermal}}$$

$$T_j \le T_j^{\max}$$

T_j = Junction temperature
T_a = Ambient temperature
$P_{thermal}$ = Power dissipated by the LED into the environment
R_{j-a} = Total Thermal Resistance from Junction to Ambient

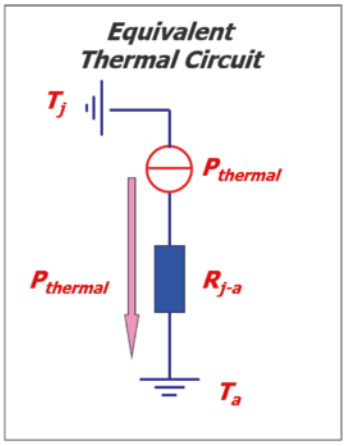

Figure 2. Thermal Analysis – representation of the maximum Rj-a

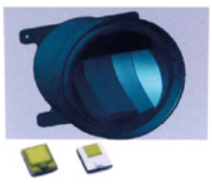

Single LED FF

•Cost effective
•Diameter Φ=75-80mm
•ECE R19 class B or F3
•Most efficient: 2-3W only

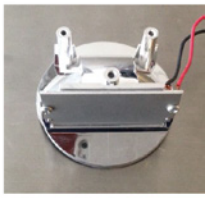

Figure 3. LED Fog Light sample used in the study

although such temperature measurements are not entirely accurate and can be easily impacted by the ambient temperature as well as the very presence of the probe itself in the system. Thermocouples also cannot usually be used in some restricted areas (like inside an automotive lighting assembly) such that the junction temperature is therefore not easily measureable. An IR camera can be used instead, but again it is easily impacted by the ambient temperature and it also does not measure the actual LED junction temperature. Increasingly it is being recognised that LED junction temperature and thermal resistance can be measured best by thermal transient measurement, in for example the Mentor Graphics T3Ster™ hardware equipment and TeraLED™ for optical and thermal measurements. The MicReD Structure Function approach to showing thermal flow paths in LEDs (based on T3Ster measurements) can be derived from this method and it in turn can help in finding faulty LED packages or assemblies as well as being utilized to determine degradation over the LED's lifetime because it is non-destructive and non-invasive.

For this particular study, an Automotive Fog Light was purchased off-the-shelf and dismantled (Figure 3) in order to be thermally tested inside the MicReD T3Ster/TeraLED suite of hardware from Mentor Graphics (Figure 4). To measure the LED package the LED was first placed with thermal grease onto a surface of a temperature-controlled heatsink (that is, a cold plate) and connected to the T3Ster testing system. The T3Ster thermal transient tester then measured and calibrated the K-factor of the LED package and a thermal response curve was measured by T3Ster which gave the junction temperature of the package, and finally a R-C Structure Function was then generated within the T3Ster-Master software.

In this study the LED was mounted on the heatsink both with and without the grease (Figure 6) in order to determine the separation point in the Structure Functions plots to see where the LED ends and the rest of the thermal path starts. The first T3Ster measurement was taken during the cooling phase after the LED was switched on and a heating current of 1A applied. Once the hot steady state was reached (after 120 seconds in this case), the LED was switched to a 5mA measurement current and the LED was cooled down to 25°C by the temperature controlled heatsink, during which the voltage change of the LED was measured over another 120s (until the steady state temperature

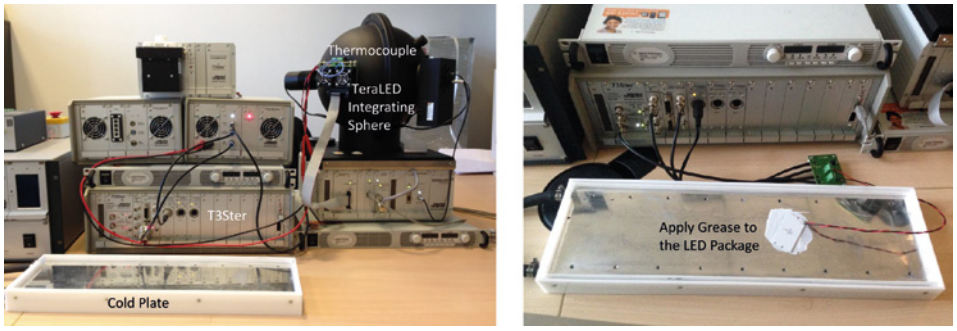

Figure 4. LED light T3Ster & TeraLED Test Facility used in the Study

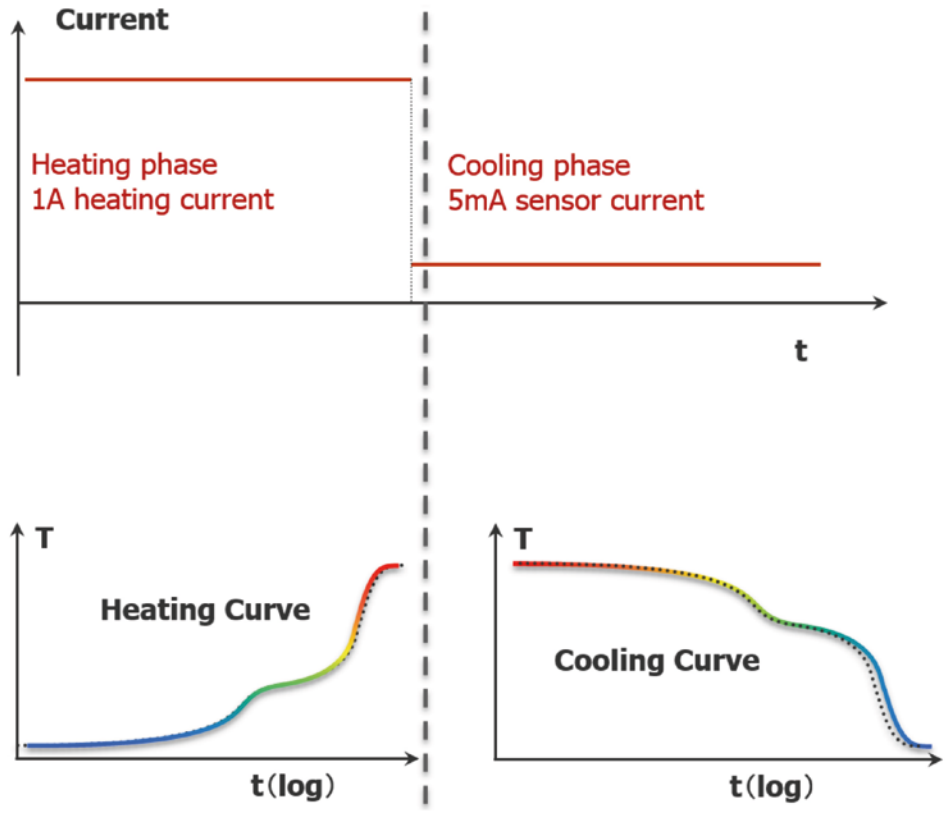

Figure 5. Schematic Fog Light LED Test Heating and Cooling Graphs under T3Ster testing

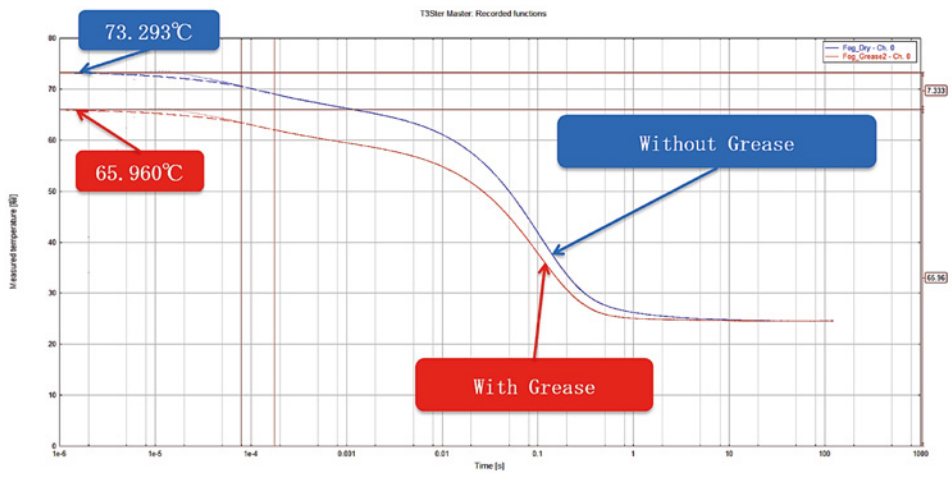

Figure 6. T3Ster Master thermal response graphs for the Fog Light under test with and without thermal grease in the cold plate

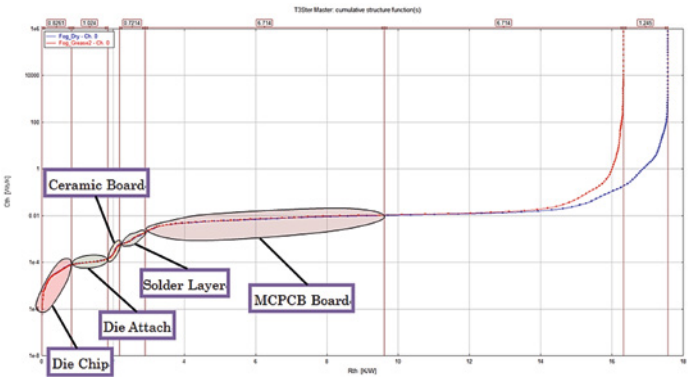

Figure 7. T3Ster cumulative Structure Function Graph showing the component parts of the Fog light package under test with and without grease

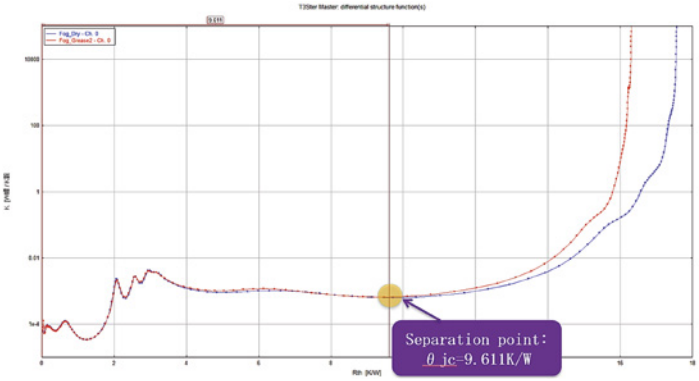

Figure 8. T3Ster differential Structure Function Graph showing the component parts of the Fog light package under test with and without grease

of 25°C was reached) – figure 5. In this test the LED Package K-factor test and calibration results produced a figure of 2.218mV / °c

The T3Ster Master temperature-time curves shown in figure 6 were derived from the test suite and show the transient thermal measurement responses; the red curve for the LED measured with a grease layer and the blue curve without a grease layer. It can clearly be seen that without grease the LED reaches a higher junction temperature of around 73°C while the LED with grease reaches only around 66°C due to the lower thermal resistance between the Metal Core PCB (MCPCB) and the heatsink.

T3Ster Master Software was then used to process the data from the test suite according to the JEDEC standard JESD51-14 (Reference 1) yielding T3Ster Structure Functions such that every layer of the LED's structure can be seen in graphical form up to the point where the MCPCB ends and the separation point of the two mounting methods (with and without grease) can be determined. This can be seen in figure 7 where the LED assembly without the grease has a thermal resistance increase of around 1.25 K/W. The Structure Function graph shows the thermal capacitance on the vertical axis and the thermal resistance on the horizontal axis.

In a derivative differential T3Ster Structure Function graph (Figure 8), the separation point for the tests with and without grease can be seen even clearer. If the two LEDs tested had any difference in their structure either by manufacturing or due to lifetime degradation, the effect would show on both Structure Functions by vertical and horizontal shifts in the graphs. The location of the shifts can therefore point to the layer in which the difference occurs.

This T3Ster measurement process can also be conducted for a fully assembled

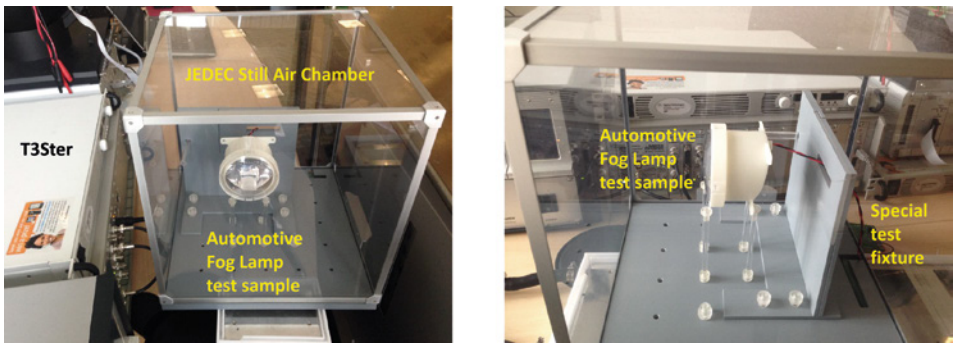

Figure 9. T3Ster Still Air Chamber test arrangement for the Fog Light under test

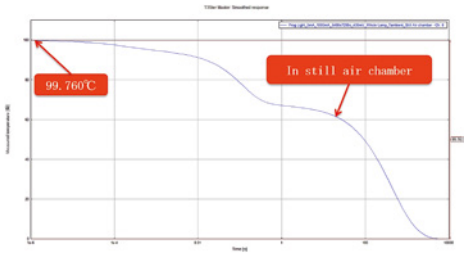

Figure 10. T3Ster Thermal Response Graph for the Fog Light under test in the Still Air Chamber

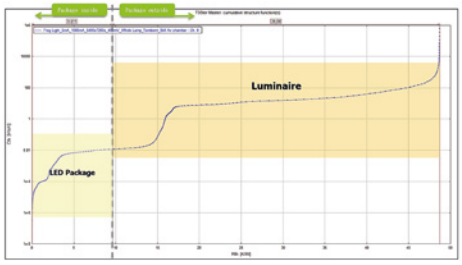

Figure 11. T3Ster Structure Function for the Fog Light under test in the Still Air Chamber

fog light as well as head lights or tail lights if necessary, although the measurement time the LED needs to cool down from the hot to the cold steady state condition can take considerably longer without a temperature controlled heatsink. However, such a measurement in the case of a fog light can be completed in a suitable JEDEC still air chamber (Figure 9) and in this test we can see the full heat flow path plot of the assembly including the luminaire (Figures 10 and 11) under natural convection conditions.

In order to also get radiometric properties of the LED fog light it can also be measured with the help of TeraLED, an integrating sphere, coupled to T3Ster (see test arrangement in Figure 4) that measures both thermal as well as radiometric properties of the LED in one combined measurement. This facility provides automotive lighting engineers with information on temperature and current dependent parameters such as the radiant flux, luminous flux, color coordinates, color temperature and many more related parameters in graphical or tabular forms (Figure 12).

The test measurement of the fog light under test in the still air chamber showed a junction temperature of 99.76°C above the environment temperature (Figure 10). Hence, with 50°C as a typical design environment temperature, the LED junction temperature would just reach a maximum junction temperature of 150°C and the luminous flux would be below 200lm whereas the design goal would be 200lm or more. This test points to the fact that some design improvements are therefore necessary for the fog light assembly such as a heatsink inside the luminaire, or a better thermal conductive luminaire material

to reduce the LED junction temperature and increase the luminous flux, while at the same time increasing the lifetime expectancy of the fog light.

Summary

This MicReD T3Ster/TeraLED thermal characterization testing process can be conducted at various stages of an automotive fog light's development from the initial LED selection process from different vendors, to its lifetime tests, up to the point where the LEDs are mounted on the PCB, or even in a full fog light assembly to validate the quality of the assembly. A combination of thermal transient measurement data from T3Ster coupled to thermal simulation with a CAD-embedded 3D CFD code like FloEFD (Figure 13) can then be used to provide highly accurate simulations this predicting LED assembly thermal performance, and ultimately helping to ensure fog light reliability over its lifetime.

Reference

[1] JEDEC, "JESD51-14 Transient Dual Interface Test Method for the Measurement of the Thermal Resistance Junction to Case of Semiconductor Devices with Heat Flow Through a Single Path," vol. JESD51-14, ed. http://www.jedec.org/standards-documents/results/51-14: Joint Electron Device Engineering Council, November 2012, p. 4

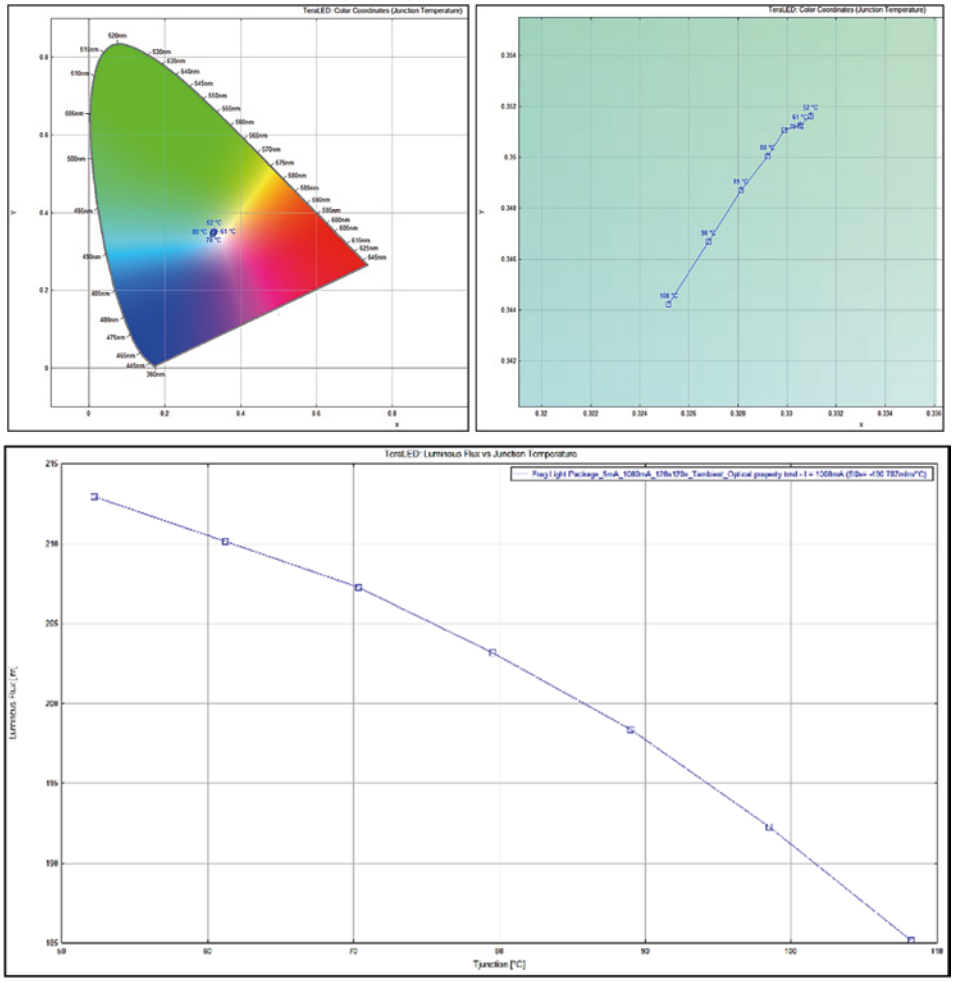

Figure 12. TeraLED output variables for the Fog Light under test

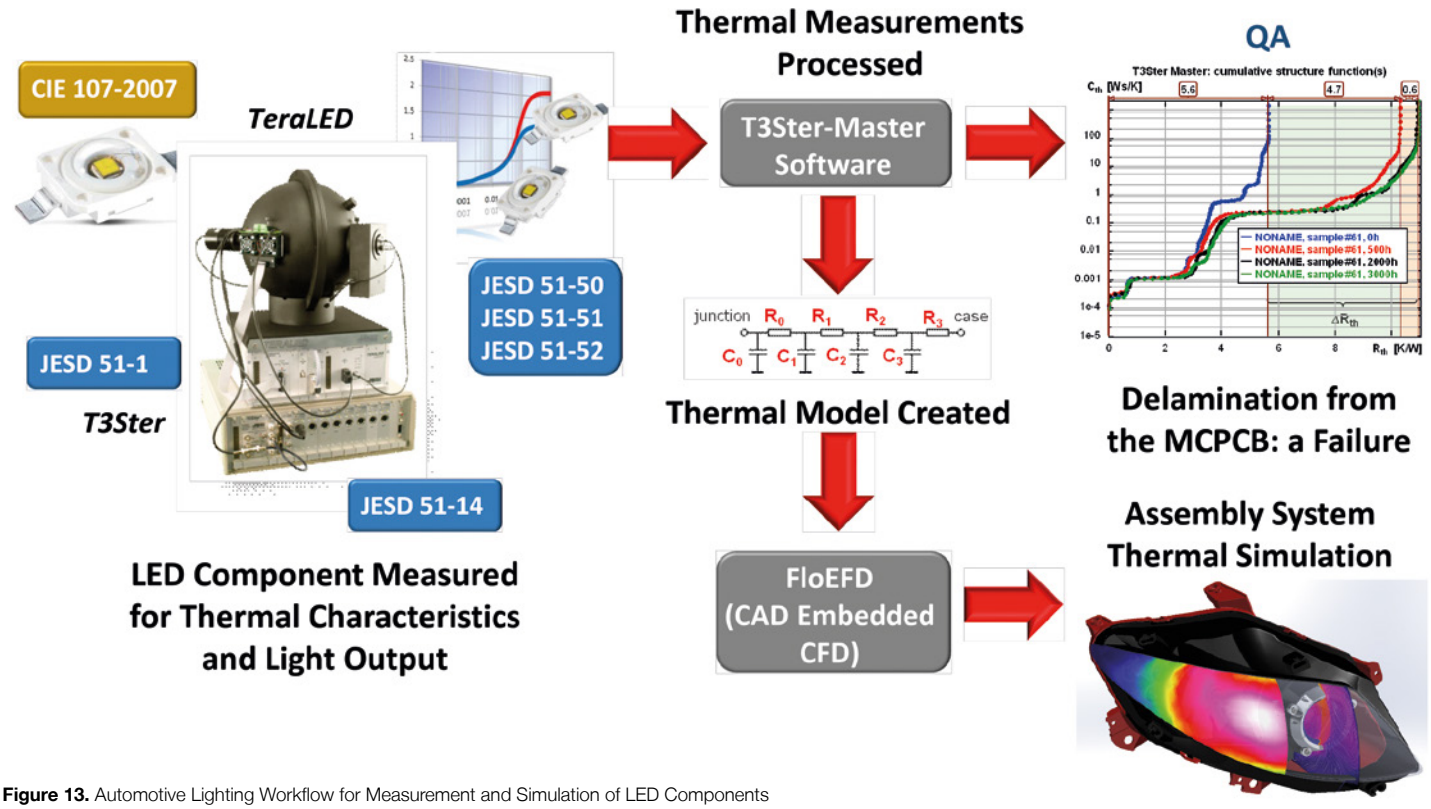

Figure 13. Automotive Lighting Workflow for Measurement and Simulation of LED Components

Robert Bosch India Drives ECU Temperatures Down

BOSCH
Invented for life

By Ritwik Alok Pattnayak & Dr. Laxmidhar Biswal, PhD, FIE, CEng,
Robert Bosch Engineering and Business Solutions, India

Modern cars can contain upwards of 100 Electronic Control Units (ECUs) so the reliability of these units is critical to the reliability of the vehicle. ECUs can be found throughout a vehicle, often in hot, harsh environments, yet component temperatures must be kept within acceptable limits even when the ambient temperature is high, making optimizing their thermal performance a key element of the design challenge.

For this, Robert Bosch Engineering and Business Solutions needed a fast, accurate and robust simulation tool they could depend on, to explore different design options quickly and effectively, including the transient response to a time-varying power load, so they turned to Mentor Graphics' FloTHERM.

A product recently developed by the team was an ECU with various functions within the vehicle which result in a different thermal load on the unit. The ECU consists of PCB, components, thermal interface material, and metal housing. There are both active components (e.g. transistors, diodes etc.) and passive components (e.g. resistors, inductors, capacitor etc.) on the board in the ECU that generate heat during the operation. There must be a good conductive path (Figure 1) for heat to flow from components to the housing. Automotive components often contain a thermal slug, to spread the heat internally within the component. These can either be between the die and the top of the component (slug up), to assist heat removal from the top of the component, or between the die and the bottom of the component (slug down), to assist heat transfer into the PCB. Heat entering the housing by either route is dissipated to the external ambient by convection and radiation. The top cover is anodized to improve radiative heat transfer to the environment. Thermal simulation is used to predict the temperature of components and determine their thermal criticality.

The FloTHERM model of the ECU is shown in figure 2, with the housing acting as a

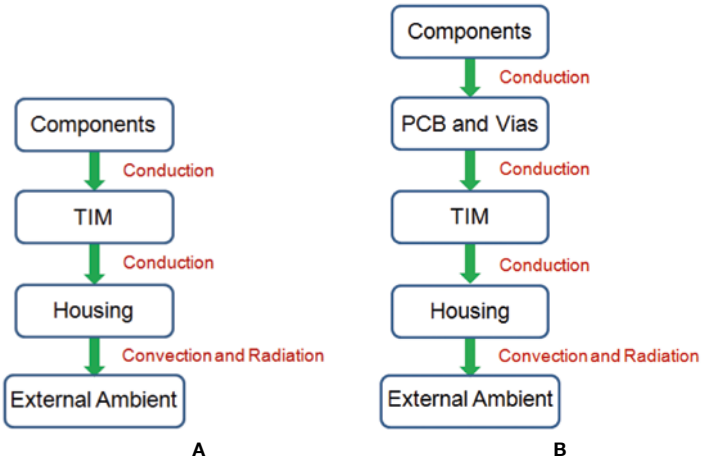

Figure 1. Heat Transfer Paths for (a) Slug-up and (b) Slug-down components

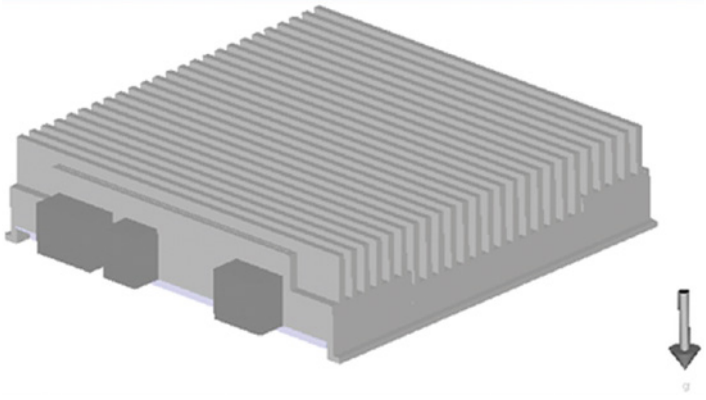

Figure 2. FloTHERM Model of ECU showing Finned Housing

heatsink to the surrounding air. The ECU is designed to be mounted either inside or outside of the vehicle, and the design has to operate under the worst case ambient condition.

The 3D thermal simulation in FloTHERM includes conduction, convection and radiation. The active components (transistors, diodes, etc.) are modeled in detail (with die, die-attach, die-pad/slug etc.), whereas the passive components that generate heat (resistors, inductors and capacitors) are modeled as lumped cuboids, unless the detailed model is available. The PCB is a multi-layer board constructed from copper and FR4. Each copper layer is modeled as a lumped cuboid with orthotropic thermal conductivity based on the percentage of copper coverage separated by FR4 layers. Appropriate surface emissivity is assigned to the components, PCB and housing to address radiative heat transfer. For the transient simulation the load profile vs. time is needed (Figure 3), where 100% thermal load corresponds to 43.0W. The FloTHERM simulation for the unit in natural convection showed that the maximum component temperature reached 162°C, well beyond the acceptable limits specified in vendor datasheets.

In the baseline design, the PCB does not have a contact with the bottom housing. Hence, heat transfer from the PCB to bottom of the housing is hampered by the absence of a proper thermal conduction path. Convection and radiation from the components and PCB to the housing is not as effective as direct thermal conduction. Bridging the gap between the bottom of the PCB and the housing without requiring a structural change is a challenge, making the thermal design harder.

To address this, Bosch's engineers, Ritwik Pattnayak and Dr. Laxmidhar Biswal, decided to make two changes to the design. The first was to add a metal heat spreader on the underside of the PCB, with a thin layer of thermal interface material in between, to spread the heat and pull down the maximum component temperature. A second change was to add a much thicker section of thermal interface material between the metal heat spreader and the bottom to provide more effective conduction heat transfer.

With the first improvement, the maximum junction temperature of the hottest component is 133°C (Figure 5a), a reduction of 31°C compared to the baseline design. The second modification reduced the maximum junction temperature of the component by a further 5°C to 127°C (Fig. 5b), giving

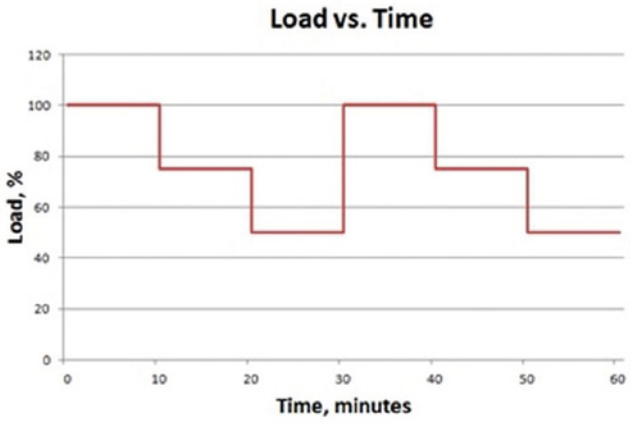

Figure 3. Power Load Profile for the ECU

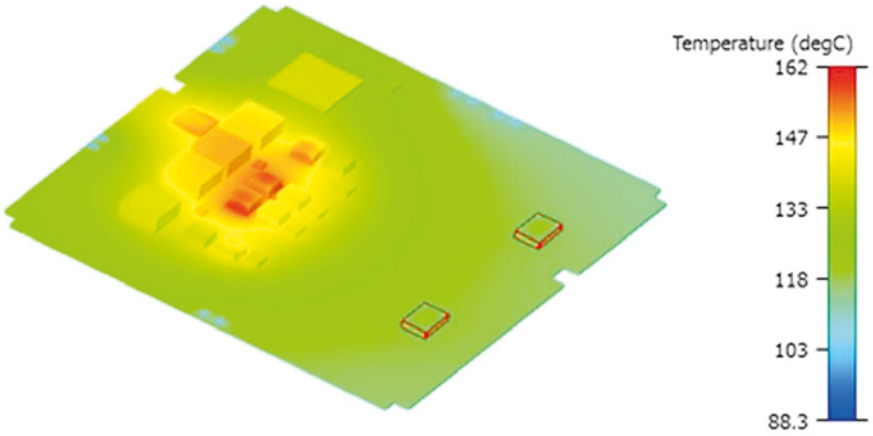

Figure 4. Temperatures of Components in Baseline model.

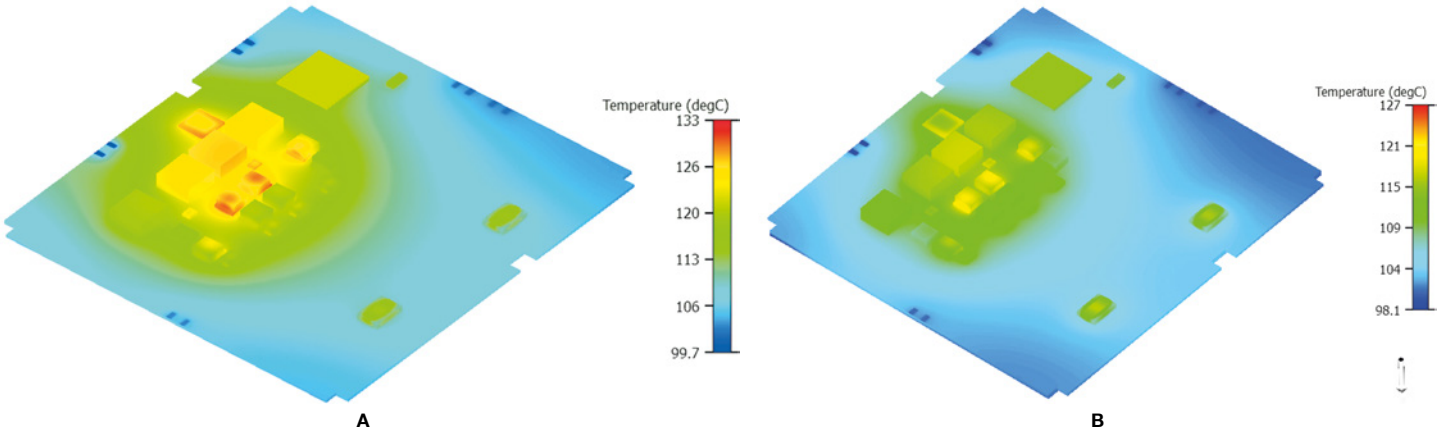

Figure 5. Temperature of Components and PCB for optimization # 1 & optimization # 2.

a total reduction of 35°C is achieved in comparison to the baseline design.

To account for the variation in load power for the system, the sensitivity of the response of individual components to different power levels was tested. Two components were chosen for this, D1600 and V1907. The D1600 component is a slug up design and interfaced with the top finned housing via thermal interface material. Because of lower thermal impedance of the thermal interface material and finned top housing, junction-to-ambient thermal impedance is relatively low, below 5K/W. V1907 is a slug-down component and interfaced with bottom housing via PCB, Thermal Vias, TIM, Heat Spreader and TIM. Due to several layers of materials between the component, bottom housing and associated thermal impedance, junction-to-ambient thermal impedance of 'V1907' is relatively very high in comparison to the slug-up component 'D1600'. This latter component was simulated in FloTHERM to obtain its transient response at 100%, 75%, and 50% power loads. Plotting these temperature responses normalized the applied power to give a graph of dynamic thermal impedance, Zth, the data almost mirror each other as shown in figure 6.

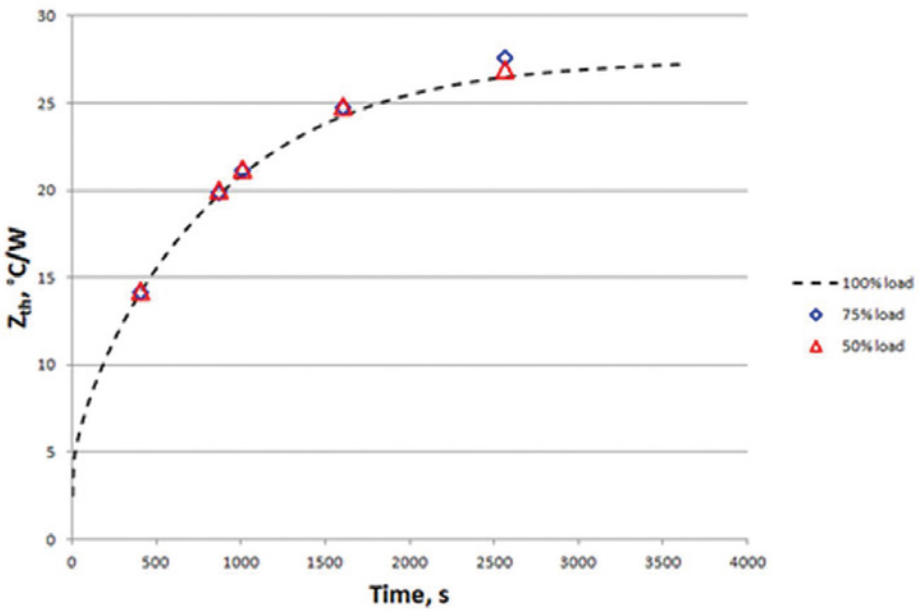

Figure 6. Comparison of dynamic thermal impedance (Zth) of 'V1907' for different loads

As the data line almost mirror one another, engineers at Bosch were able to derive an analytical model for dynamics thermal resistance (Zth,j-a) of all heat dissipating components from the FloTHERM simulation. This model could then be used to predict the temperature of the components for different power dissipations and external ambient, without having to run a full 3D thermal simulation for each scenario.

The results of the design optimizations were checked with a prototype using a thermal chamber, shown in figure 7. The experiment was conducted for the specified ambient, and at an air speed of 0.6ms-1, with the velocity of the airflow over the ECU measured with an anemometer. Thermocouples were placed on the components of interest to measure their temperature.

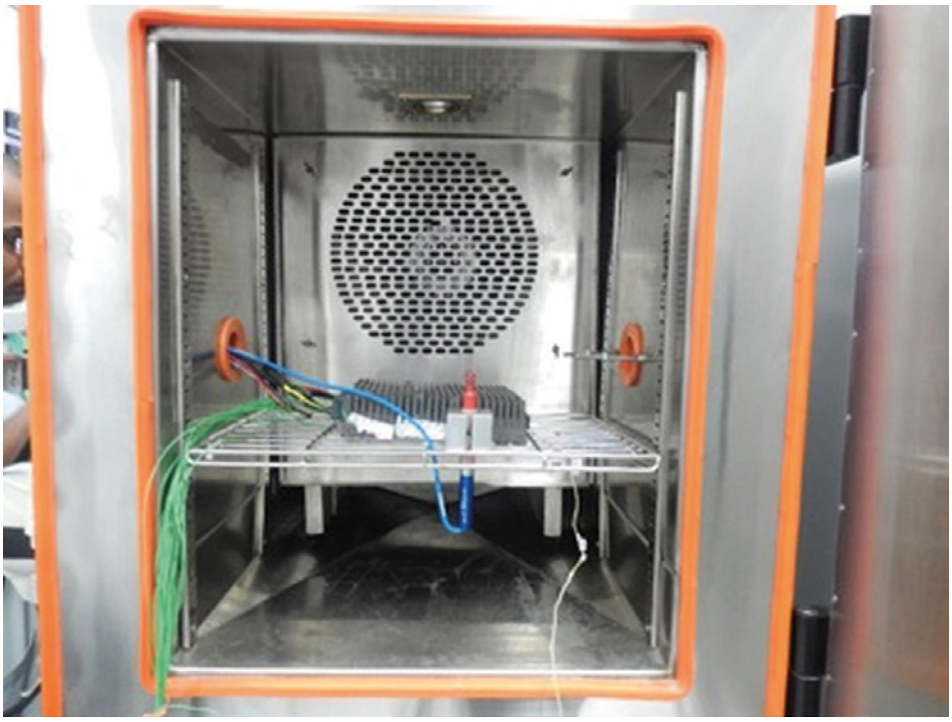

Figure 7. Thermocoupled ECU and Anemometer in the Thermal Chamber

The comparison of the simulated temperatures against the experimental measurements showed a good correlation, confirming the robustness and reliability of the FloTHERM model. The outcome of this work was that the design optimizations in FloTHERM overcame the thermal bottleneck and reduced component temperatures by 35°C from the baseline design, resulting in an acceptable operating temperature of components. Using analytical models derived from FloTHERM results, Robert Bosch Engineering and Business Solutions have been able to predict junction temperature of component at any load for a given design and time duration or operational time duration of the ECU for the desired junction temperature. This has delivered a significant saving in time.

Acknowledgement:

This work "Thermal design and analysis for high power automotive electronic product" by Ritwik Alok Pattnayak & Dr. Laxmidhar Biswal, PhD, FIE, CEng (Robert Bosch Engineering and Business Solutions, India), was first published at NAFEMS' World Congress in San Diego, 21-24 June 2015, www.nafems.org

NAFEMS

Ask The GSS Expert

Gas Turbine Secondary Airflow

By Sergio Antioquia, Application Engineer, Mentor Graphics

Traditionally, Computational Fluid Dynamics (CFD) software can be divided in two basic types. The most widely spread is the three dimensional (3D) approach, sometimes simplified as 2D. 3D codes generally calculate the flow and temperature field by solving the Navier-Stokes equations; this is achieved by dividing the geometry and fluid volume in small subdivisions (the mesh) and using a finite volume/element iterative method applied to the equations in their derivative form.

The other basic kind is the one dimensional (1D) approach. The idea behind these codes is that, for big systems, many components can be modeled by using correlations, empirical data or representative equations. Then the components are set in the form of a network and the whole system is solved iteratively for pressure, pressure and temperature, or pressure and enthalpy as appropriate.

Whilst full 3D simulation can provide very accurate solutions of the flow field in every point of space, it requires a large amount of computational power and time to solve. Therefore, it's also not really suitable to solve very big networks, where many components might be repeated. 1D on the other hand, by capturing 3D effects in the empirical data-set or through assumptions built into the algorithms, sacrifices 3D detail and focuses on the dominant flows.

Flowmaster is a code that can be used to solve some gas turbine subsystems with its 1D capabilities and the wide range of components compiled in the library. Normal 1D applications include systems such as the fuel and injection, the oil and lubrication, or blade cooling conducts. But due to its unique capabilities, Flowmaster is not limited to usual 1D systems in gas turbines. The Secondary Air module uses a hybrid 2D/1D method to solve the flow in rotor-stator cavities. Whilst this airflow would require 3D approach, Flowmaster can provide good accuracy in a much shorter time.

Using either regular capabilities or Secondary Airflow, Flowmaster can solve a wide range of applications suitable for Gas Turbine design, operation and maintenance.

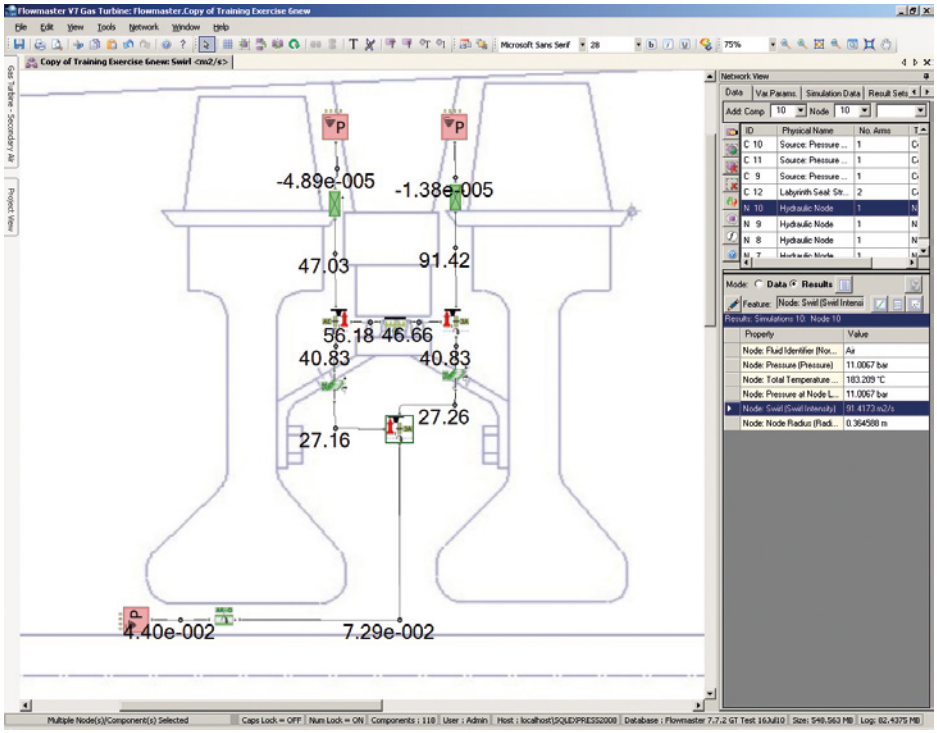

Figure 1. Example of three cavities between two rotor disks and a stator. It also shows rotating passages and labyrinth seals.

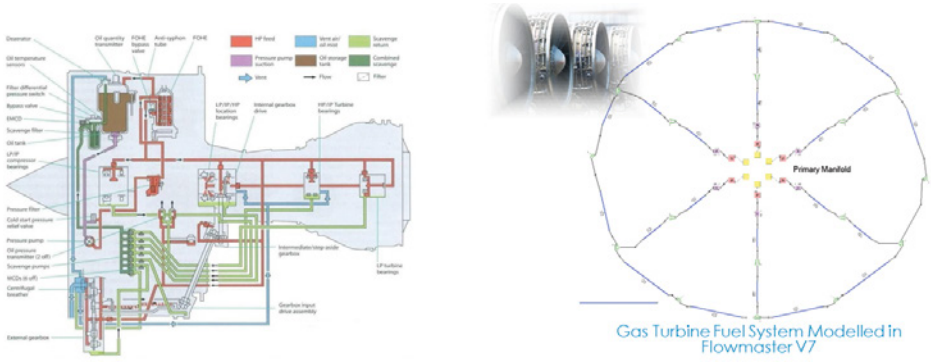

Figure 2. Lubrication network (left). Fuel injection network (right).

Lubrication and Fuel systems.

The previous example was extremely simplified, just to explain quickly the basic operation of Flowmaster. The same philosophy can be followed to create any other kind of network. For example, to connect an oil tank to pumps and bearings in the case of an oil system, or to connect the fuel tanks together through orifices, then through pipes and pumps to the fuel injectors. Transient analysis is available and serves for different applications.

Blade cooling

Blade cooling applications do not represent a bigger challenge to the already mentioned methods when the cooling is applied to stator vanes, because they don't rotate. So starting from a pressure source, representing the bleeding from the compressor, the airflow can be connected to a set of pipes and nozzles that represent all the passages and cooling holes in the vane.

The challenge is, however, a bit harder in turbine blades, as they rotate, and then centrifugal forces have to be taken into account. Different specific component have been developed to take into account these forces, so instead of regular pipes, rotating passages can be used.

The procedure is then very similar for either vanes or blades, with compressible analysis of the network.

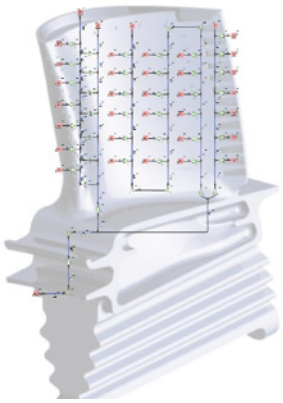

Figure 3. Blade Cooling Example

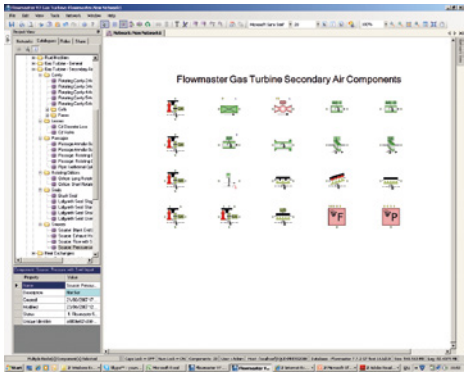

Figure 4. Gas turbine secondary air module example of components.

Other systems

Whereas the two main applications of Flowmaster to gas turbine subsystems would be the already mentioned Oil and Fuel, and Blade Cooling, it can be used to any other subsystem that is suitable to be modeled using a one dimensional approach. This would include for example:

- Bleeds from the compressor (or any other purges). This can be coupled with the air conditioning capabilities for the cabin in planes.
- Water injection, mainly for power generation.
- Intercoolers and heat exchangers.
- De-icing systems.
- Combustion liner cooling systems.

FloMASTER V8 capabilities include direct and live coupling of 1D networks with 3D components, so the user can obtain the best of both worlds, saving time and resources and having a dynamic and more accurate information of the node conditions.

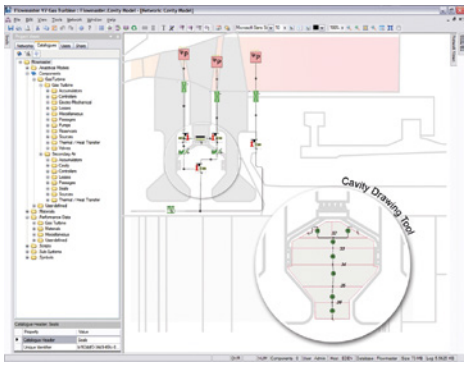

Figure 5. Network (left) and cavity (right zoom) levels.

Secondary Air Module

As a system that works in high pressure, alternating rotating and steady components, a gas turbine cannot be fully sealed. In every transition from steady to rotating component (or vice-versa), there will be an open gap. These gaps often connect the main airflow with the cavities that are left between rotor and stator discs, shafts, etc. These cavities are big, and interconnected through orifices in the discs. This airflow can represent a relatively big loss in overall efficiency. One of the hardest challenges for gas turbine design and operation involve the reduction of the clearance between components and the design and maintenance of seals. Being able to reduce the secondary airflow losses to a minimum can represent a significant increase in efficiency. The secondary airflow is often used to drive flow from compressor stages to combustor and turbine, for cooling purposes.

One of the biggest strengths of Flowmaster in the gas turbine field is the proprietary technology that combines 2D and 1D methodologies to solve this secondary airflow inside cavities.

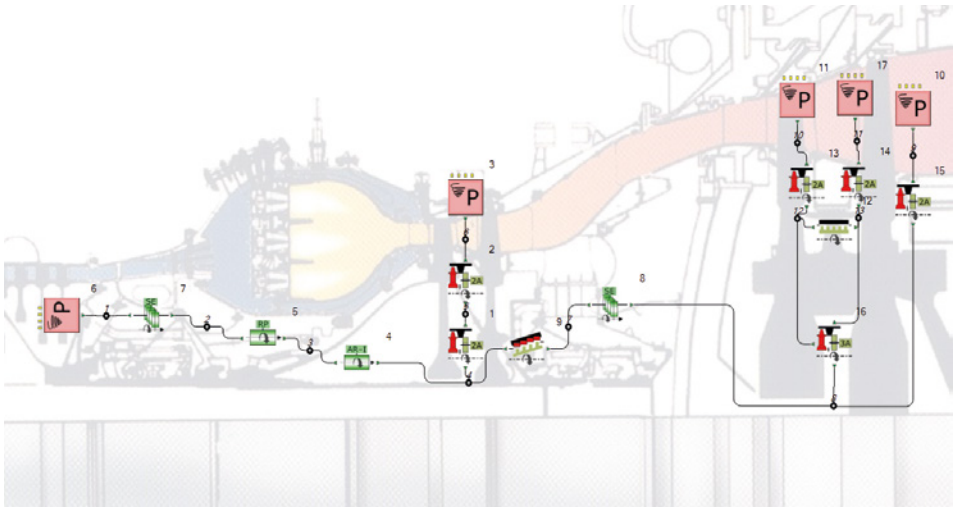

Figure 6. Example of a gas turbine secondary airflow system showing multiple cavities, seals and connections.

The secondary air study is a dual system. First, a main network with pressure or flow sources, rotating passages, orifices, seals and cavities. Then the cavities themselves: they are subnetworks within the main network but are formed only by cells.

The main network is not restricted to one cavity, as can be seen in figure 6. Many cavities of different sizes and shapes can be interconnected through seals, rotating passages, orifices or clearances, among them or to pressure/flow sources; creating then a quite complex network that can represent the whole secondary airflow of a gas turbine.

Running the simulation is as usual, the user selects the kind of simulation that is desired, steady state and compressible, and after convergence is achieved the results can be studied. They are not restricted to the main view, but they can be studied, of course, inside the cavities as well.

The Secondary airflow calculator can be used in design or analysis level. The ability to quickly represent parts of, or even the whole secondary air network, by the selection of representative components and cavities, allows the study of any variations in either design or operation. This process can also be automated by the use of parametric studies, which can run a whole range of values for different parameters. Making it even easier and faster to study the results.

HYUNDAI
HEAVY INDUSTRIES CO.,LTD.

Force Analysis Due to Pressure Surge in an Offshore Floating Production Unit using Flowmaster

By Sangmin Park, Senior Researcher, Hoon Choi, Lead Researcher, and Woo-Young Byun, Lead Process Engineer, Hyundai Heavy Industries

As countries continue to develop their natural resources to drive the economies of the world, the need to find and make productive additional deposits of hydrocarbons continues to grow. This has really been seen over the last three decades in the large increase in the number offshore oil reservoirs that have become productive around the world. While oil has been produced offshore since the 1940s, this was done using platforms that sat directly on the seabed. With the move to deeper waters starting in the 1970s a shift to Floating Product Units (FPUs) allowed for these more challenging deposits to be reached.

There are four general type of FPUs, and Hyundai Heavy Industries has decades of experience in projects relating to types of design.

- Semi-submersible Floating Production systems (FPS)
- Floating Production, Storage, and Offloading systems (FPSO)
- Tension Leg Platforms (TLP)
- Spar platforms

Photo: Offshore & Engineering Division of Hyundai Heavy Industries (Ulsan in Korea)

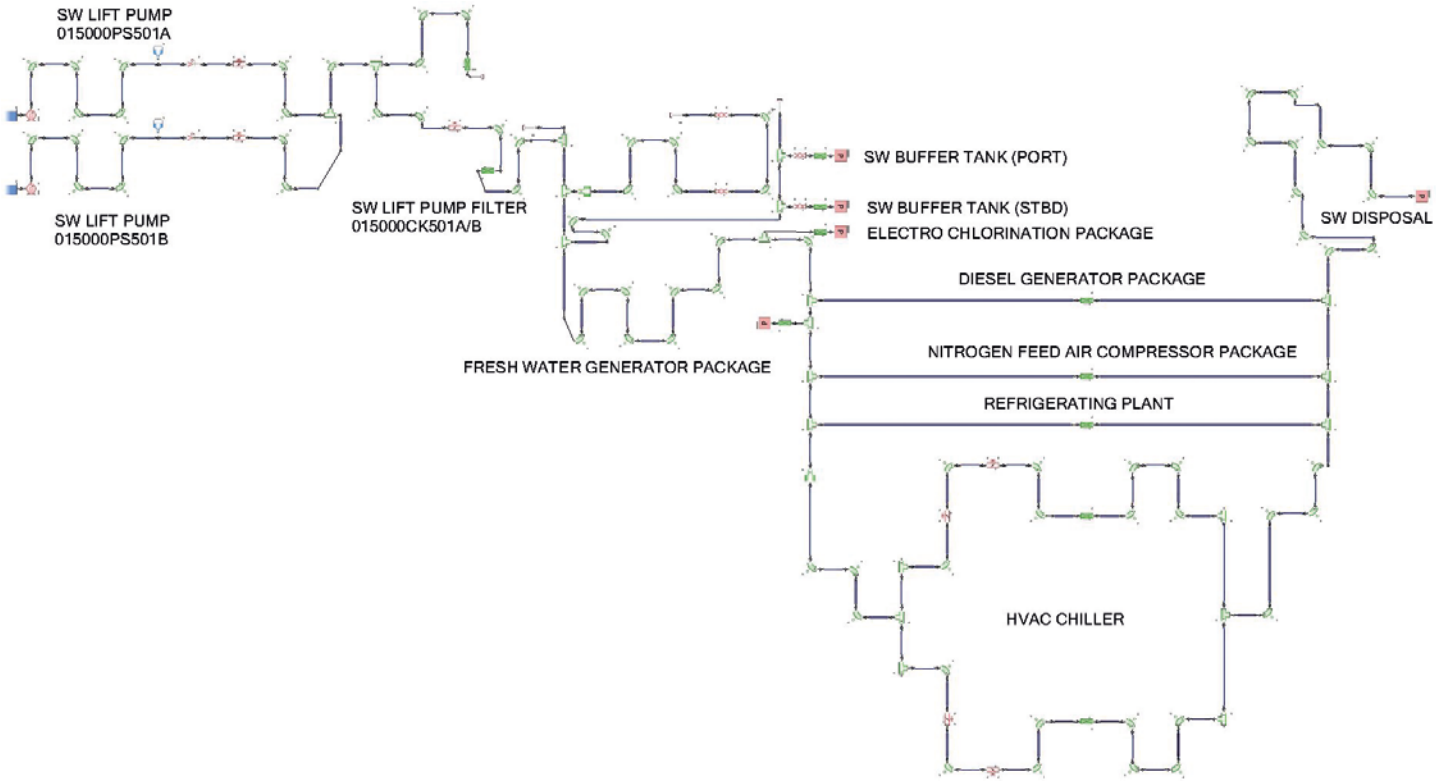

Figure 1. Full Hyundai Heavy Industries Seawater System Modeled in Flowmaster

While each type of platform has its own unique characteristics, they also have many similarities especially for the engineering systems design perspective. This article discusses analysis of a very important system that all of these FPU types have, a seawater system.

While often very isolated, FPUs usually have one thing around them in abundance at all times and that is sea water. As a result many systems on a FPU are designed to use sea water either as a working or cooling fluid, as well as for a source of water desalinization for fresh water.

This means the seawater system needs to be designed for safe use over a wide range of operating conditions. While designing a system for expected pressures, temperatures, and flow rates is generally a straightforward process with steady state analysis, often the most dangerous situations arise as a result of a change in the system that hasn't been accounted for.

To analyze the potential effects on the system that was being designed Hyundai Heavy Industries constructed the detailed piping system in Flowmaster. The goal was to determine the maximum occasional force that the seawater system would experience at selected locations under different operating conditions as a result of pressure

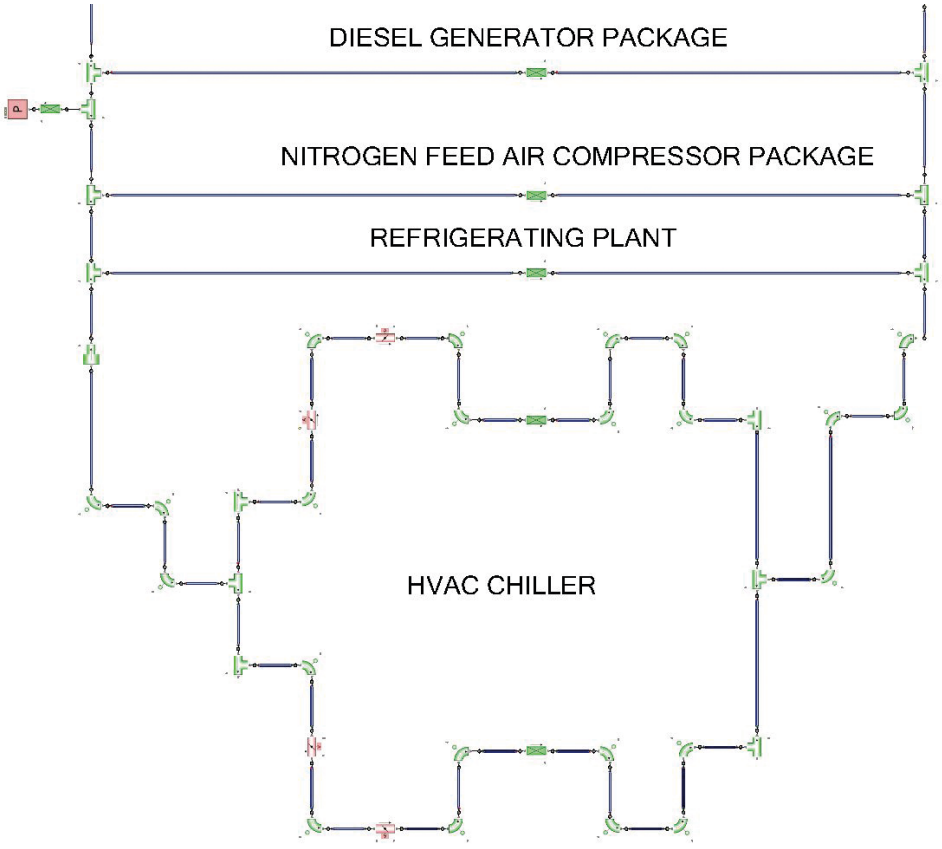

Figure 2. Seawater Piping System for the Mechanical Sections of the FPU

surge. The forces would then be compared against the maximum allowable forces for the pipes or fittings where the force occurred.

With the model constructed, eight different operation scenarios were outlined for analysis:

- CASE 1-A: Closure of MOV-521(HVAC System) when a SW lift pump is running;
- CASE 1-B: Closure of FV-501(min. flow line) when a SW lift pump is running;
- CASE 2-A: A SW lift Pump starts when FV-501 and RF-501 are open;
- CASE 2-B: A SW lift Pump starts when FV-501 is opened and RF-501 is close;
- CASE 2-C: A SW lift Pump starts when FV-501 and RF-501 are close;
- CASE 2-D: Two SW lift Pumps start when FV-501 and RF-501 are open;
- CASE 3: A SW lift Pump starts when other pump is running; and
- CASE 4: A SW lift pump trips due to power failure.

For each of these scenarios, a transient analysis was conducted using Flowmaster to calculate the pressures through the system. As expected the actions of opening or closing valves and starting or tripping pumps were the main drivers for pressure surge in the system. The maximum pressures as a result of these pressure surges were recorded at the thirteen locations engineers deemed most susceptible to failure.

These values were then automatically extracted from Flowmaster using VBA scripting in Microsoft Excel, where the net force on each section of pipe was calculated. As seen above, all of the forces at each location for each scenario were tabulated (table 1) with the maximum force experienced at each location highlighted at the bottom. For this design, all of the predicted occasional forces due to pressure surge were below the tolerance of the piping material so the design could be approved. The ability to accurately calculate the surge pressures as a result of operational scenarios in Flowmaster was key to early stage design.

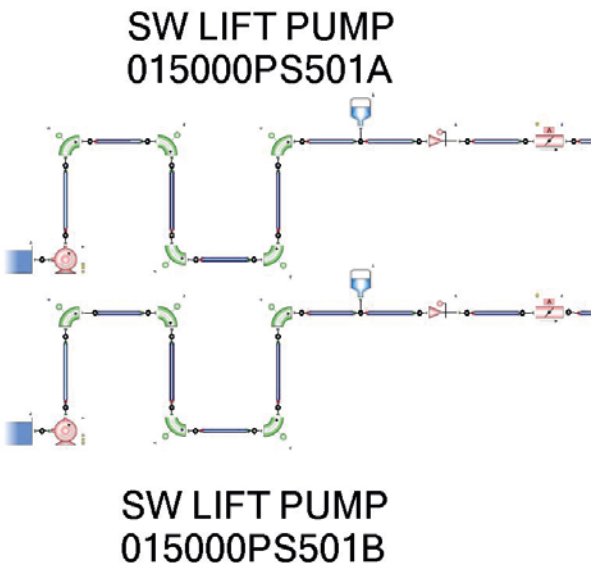

Figure 3. Seawater Lift Pumps, Flow Valves, and Relief Valves Used for Simulation

CASE	Maximum Surge Force (kN)												
	S	S-1	A	A-1	B	C	D	E	F	G	H	I	J
1-A	1.18	0.03	0.15	0.00	0.04	0.00	0.00	0.15	0.09	0.55	0.66	1.57	2.37
1-B	0.62	0.03	0.05	0.00	0.03	0.00	0.17	0.10	0.03	0.19	0.06	0.01	0.15
2-A	8.16	0.03	0.75	0.00	0.23	0.00	0.23	0.39	0.15	0.92	0.33	0.07	0.81
2-B	6.18	0.03	0.57	0.00	0.15	0.00	0.32	0.03	0.00	0.01	0.00	0.00	0.01
2-C	15.59	0.03	1.03	0.00	0.37	0.02	0.21	0.55	0.01	0.03	0.00	0.00	0.02
2-0	8.09	0.03	0.74	0.00	0.23	0.00	0.23	0.38	0.16	0.93	0.33	0.07	0.82
3	3.56	4.59	0.30	0.46	0.08	0.15	0.00	0.29	0.09	0.40	0.15	0.03	0.41
4	2.29	0.03	0.21	0.00	0.06	0.00	0.00	0.24	0.08	0.46	0.11	0.02	0.31
Max. Surge Force	**15.59**	**4.59**	**1.03**	**0.46**	**0.37**	**0.15**	**0.32**	**0.55**	**0.16**	**4:93**	**0.66**	**1.57**	**2.37**

Table 1. Maximum Surge Forces for each Scenario at 13 Critical Locations of the System

Liquid Cooling Technology

Leveraging FloTHERM to design a Compact Liquid Cooling System for High Power Microelectronic Devices

By Gongyue Tang, Yong Han, Boon Long Lau, Xiaowu Zhang, and Daniel Min Woo Rhee, Institute of Microelectronics, Agency for Science, Technology and Research, Singapore

Air cooling can provide a simple, low cost, effective, and reliable cooling solution for microelectronic devices. However, with the increase in heat flux dissipation, current air cooling technology is not sufficient for new high power devices. When the heat flux goes beyond 100 W/cm2, air cooling methods become inadequate for most applications. Therefore liquid cooling technology for microelectronic devices with high power chips is required.

There are two major modes of liquid cooling technology; single-phase cooling and two-phase cooling.

Considering the higher pressure drop and complexity of a two-phase liquid cooling system, utilizing the single-phase liquid cooling technology for high-heat-flux microprocessors is an attractive option. For a single-phase liquid cooling technology, both microchannel and microjet heat sinks can dissipate high heat fluxes found in high-power electronic devices. Compared with the impinging microjets, microchannel cooling has a lower averaged heat transfer coefficient but the coolant in microchannels can exchange energy with a larger effective surface area with multiple walls within each of the channels. Combining these approaches into a hybrid microcooler would be the ideal approach.

The proposed liquid cooling system includes three major components:

1. A silicon-based hybrid microcooler with multiple drainage microtrenches (MDMTs);
2. A customized compact liquid-to liquid heat exchanger; and
3. A commercial micropump.

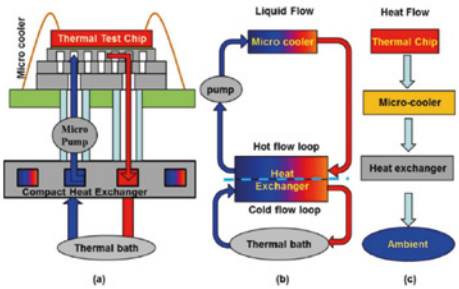

Figure 1. Schematic of the compact liquid cooling system. (a) Concept design of the system. (b) Liquid flow loops in the system. (c) Heat flow path in the system.

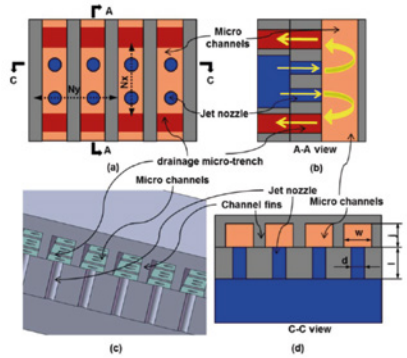

Figure 2. Schematic of the proposed hybrid microcooler with MDMTs design. (a) Pattern of the microchannels, jet nozzles, and MDMTs. (b) Side view of the A—A cross section. (c) 3-D isometric view. (d) C—C cross-sectional view.

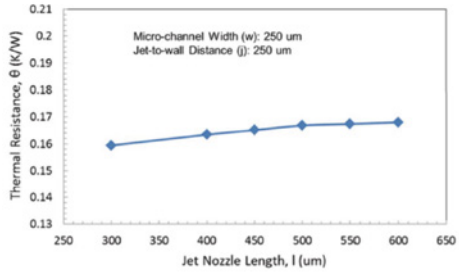

Figure 3. Variation of junction to microcooler thermal resistance with jet nozzle length.

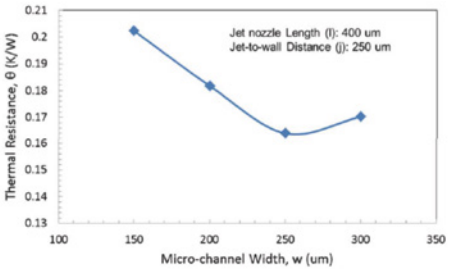

Figure 4. Variation of junction to microcooler thermal resistance with microchannel width.

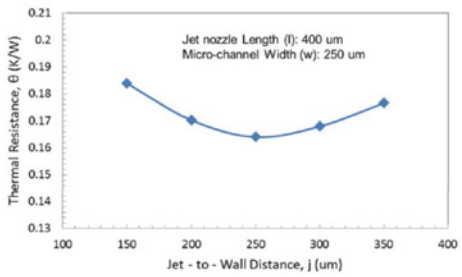

Figure 5. Variation of junction to microcooler thermal resistance with JTW distance.

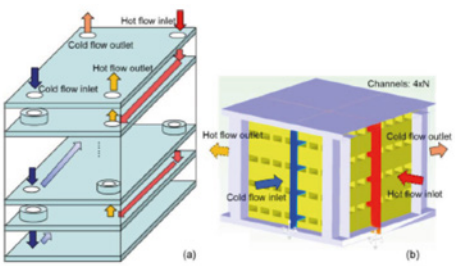

Figure 6. Schematic configurations of the heat exchangers investigated in this paper for (a) counter-flow configuration of commercial heat exchanger A (Hex-A) and (b) cross-flow configuration of customized heat exchanger B (Hex-B).

A compact liquid cooling system for a microelectronic chip is shown in figure 1(a). It mainly consists of a microcooler to remove the heat from the high performance chip, a commercial micropump to drive the liquid flow, and transport the heat from the chip to an external heat exchanger, where the heat is transferred to the secondary fluid and then rejected to the ambient.

To maximize the performance of the system, the following design criteria should be considered in the design of the proposed liquid cooling system:

1. Avoid large pressure drop the flow rate in the loop at chip cooling side should be maintained at a low level;
2. The heat exchanger should be compact with high heat exchange efficiency, or heat transfer density; and
3. It must maintain the thermal resistance and pressure drop of the heat exchanger at a level obviously lower than that of the microcooler.

A silicon-based microcooler, combining the merits of both microchannels and jet impingement, has been developed to dissipate the heat flux for the high-power IC chip. Figure 2 shows the conceptual design of the hybrid silicon microcooler for the pattern of the microchannels, jet nozzles, and MDMTs. As shown in figure 2(a), there are two nozzles between each of the two trenches in the proposed MDMTs design. The jet flow from the microjet nozzle impinges on the top wall, is constrained to flow along the microchannel, and then exits through the nearby drainage microtrenches.

For this work, the CFD modeling and simulation is conducted using FloTHERM® for the microcooler design optimization. For the chip of size 7 × 7 mm^2, the microjet array is designed to cover an area of 8 × 8 mm^2 for the cooling. The jet nozzle diameter is fixed at 100 µm. The nozzle length, microchannel width, and jet to wall distance are varied in the modeling to evaluate their effects on the thermal performance of the microcooler. Other parameters include nine drainage trenches with a width of 150 µm, 16 nozzles along the microchannel direction and 21 jet nozzles along the drainage trench direction. The coolant in the microcooler is water with an inlet temperature of 25°C. A heat source of 175 W is set for the thermal chip, and a gauge pressure of 20 kPa is set at inlet of the microcooler. A mesh of one million cells is generated, and a grid independence study is conducted. The mesh number is sufficient to obtain accuracy within around 1% for

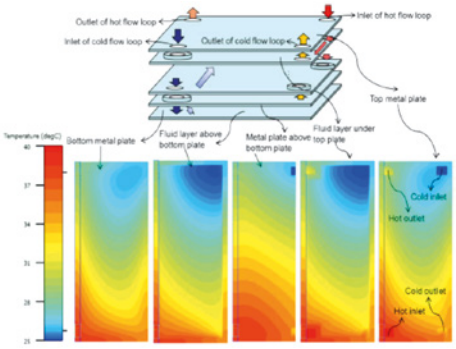

Figure 7. Simulation results of the temperature profiles in the commercial heat exchanger A.

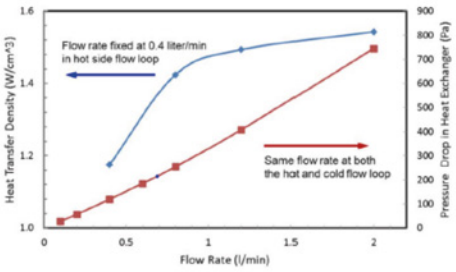

Figure 8. Variation of the heat transfer density, and pressure drop with the rate in Hex-A at the specified conditions.

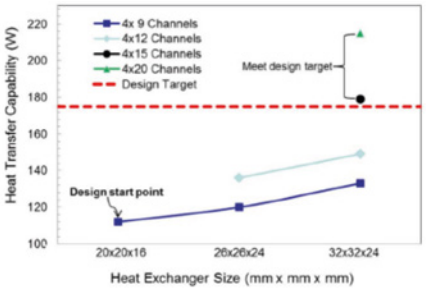

Figure 9. Variation of the heat transfer capability with the channel number's and footprint size of Hex-B at the specified conditions,

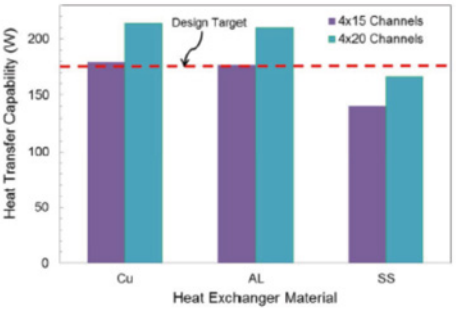

Figure 10. Effect of the material on the heat transfer capability of Hex-B at specified conditions.

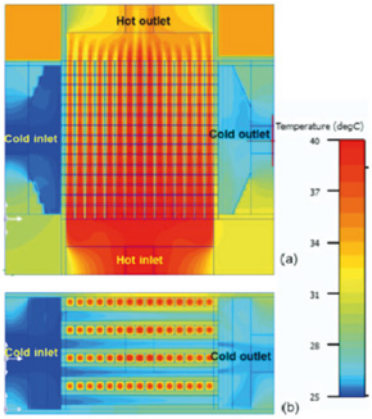

Figure 11. Simulation results of temperature profile for Hex-B with the final design at the specified condition. (a) Top plane view. (b) Side plane view.

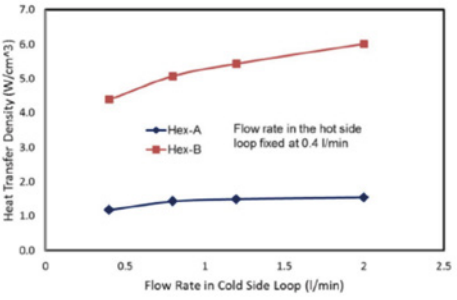

Figure 12. Comparison of heat transfer density for Hex-A and Hex-B at the specified conditions.

hydraulic and thermal performance. The effects of the nozzle length, microchannel width, and JTW distance on the thermal performance of the microcooler are, respectively, presented in figures 3–5.

A liquid–to-liquid heat exchanger was chosen because it has the advantage of higher heat exchange efficiency, smaller size, and centralized management of the secondary liquid flow through facility cooling, such as a coolant distributed unit.

Two liquid-to-liquid heat exchanger configurations are investigated in the present case. The first heat exchanger (Hex-A) is commercially available with a counter-flow configurations, and it is used as a benchmark to design and optimize the second heat exchanger (Hex-B). Hex-B is a customized compact heat exchanger, which represents the cross-flow configuration, consisting of mini-channel layers alternatively stacked for both the hot and cold fluid flows. Hex-A is with the counter-flow configuration, as shown in figure 6(a); the hot fluid and cold fluid layers are stacked alternatively, separated with metal plates. There are a total of 11 stainless steel (SS) layers, including the top and bottom

cover plates with a thickness of 1.1 mm for each layer.

These metal layers form ten layers of liquid channels, which include five layers for the cold liquid and five layers for the hot liquid. The overall size of Hex-A is of 204 mm long by 74 mm wide by 25 mm high. Hex-B is designed with cross-flow configuration, as shown in figure 6(b), in which the hot fluid and cold fluids are stacked, with the two types of flow channels arranged at an angle of 90°.u. Hex-B is targeted to have similar performance as Hex-A while have smaller footprint size than that of the Hex-A. FloTHERM is utilized to simulate the thermal and flow profiles in the heat exchangers.

The inlet flow rate is varied from 0.4 to 2 L/ min with a fixed temperature of 25°C for the cold flow loop of the heat exchangers, whereas the flow rate is fixed to 0.4 L/min for the hot flow loop. The inlet flow temperature in the hot flow loop of the heat exchanger is fixed to 40°C for case study.

Due to the relatively small Reynolds number, the laminar flow is assumed. A mesh of 530 K is generated and the grid independence study is conducted. The fields of flow, pressure, and temperature are obtained through the modeling and simulation; as such the liquid temperature at different locations can be captured through the obtained temperature profiles. The performance of Hex-A is used to benchmark the performance of optimized Hex-B. Figure 7 shows the simulation results of the temperature profile in Hex-A. In this case, the flow rate is 0.4 L/min in both the cold flow loop and the hot flow loop; the inlet fluid temperature is of 25°C in cold flow loop and 40°C in the hot flow loop of the heat exchanger.

The heat transfer density is extracted to evaluate the thermal effectiveness of the heat exchangers. The variation of the heat transfer density with liquid flow rate for Hex-A is shown in figure 8. The flow rate in the hot flow loop is fixed at 0.4 L/min. The inlet fluid temperature is 25°C for the cold flow loop and 40°C for the hot flow loop. The heat transfer density is sensitive to flow rate when the flow rate is low (e.g., less than 1 L/min), and less sensitive to the flow rate when the flow rate is high. The pressure drop in the heat exchanger is also important to the cooling system. The variation of the pressure drop with the flow rate for Hex-A is also shown in figure 8. The flow rates in the hot flow loop and cold flow loop remain the same. As expected, the pressure drop in the heat exchanger increases with an increase in the flow rate.

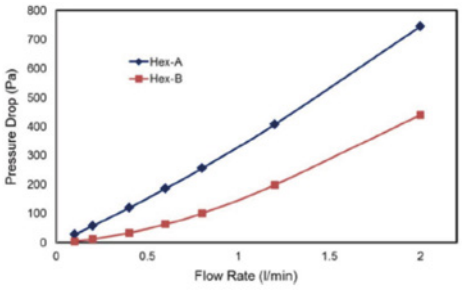

Figure 13. Comparison of pressure drop for Hex-A and Hex -B at the specified conditions.

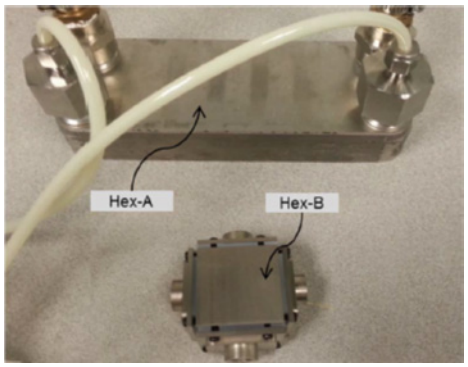

Figure 14. Comparison of the footprint size between the commercial Hex-A and the customized Hex -B

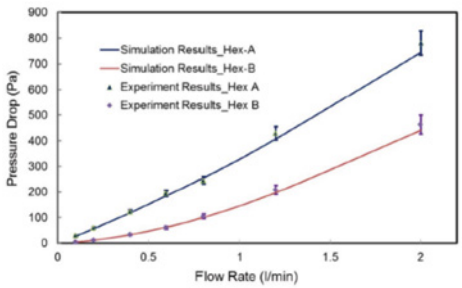

Figure 15. Pressure drop in commercial heat exchanger (Hex-A) and customized compact heat. exchanger (Hex-B).

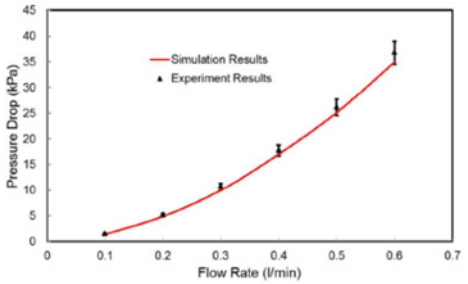

Figure 16. Pressure drop in Microcooler

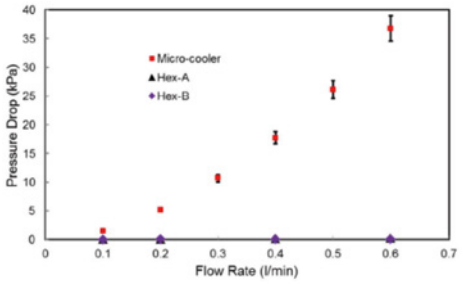

Figure 17. Comparison of the measured pressure drop in microcooler and heat exchangers.

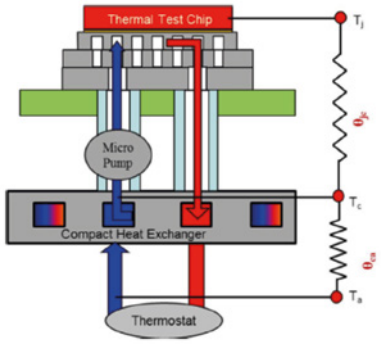

Figure 18. Schematic of the system thermal resistance analysis.

To design the compact Hex-B, the simulation model is first built with 4 × 9 channels in each fluid side with a footprint size of 20 × 20 mm as the design start point. The 6 × 6 cells are assigned in each channel cross section to ensure the computational accuracy, and the grid independent solution is obtained with a mesh number of 1.2 million cells. The simulation results are shown in figure 9. Hex-B with initial configuration, only provides about 110 W heat transfer capability under the specified conditions, which is too low for system design target. Therefore, the design is further optimized to increase the power dissipation capability.

The optimization for Hex-B includes: an increase in channel numbers, an increase in the footprint size and a different the material with higher thermal conductivity. Figure 9 shows the effect of channel numbers and footprint size on thermal performance of the Hex-B. The thermal performance increases as the channel number and footprint size increase. For the heat exchangers with a footprint area of 32 × 32 mm and a channel number of ≥15, their heat transfer capability exceeds the design power of 175W, meeting the design target. The effect of heat exchanger material type is shown in Figure 10. The SS, with a thermal conductivity of 16 W/mK, would have unfavorable thermal performance below the design target, which is not preferred material for Hex-B. Additionally, the aluminum heat exchanger has similar thermal performance as that for the copper heat exchanger. Hence, the aluminum heat exchanger is suggested for practical fabrication due to the light weight.

Based on the above analysis, the optimized heat exchanger has a footprint area of 32 × 32 mm with a channel number of 15 in each row for both fluids, and is made of aluminum. Figure 11 shows the simulation results of the temperature profile for Hex-B with the final design.

To assess the effectiveness of the design of Hex-B, the heat transfer density and the pressure drop of Hex-B are compared with those of Hex-A. Figure 12 presents the comparison of the heat transfer density between Hex-A and Hex-B at the specified conditions. Figure 13 shows the comparison of the pressure drop in Hex-A and Hex-B at the specified conditions.

Compared with the Hex-A, the much higher heat transfer density and the much lower pressure shown for Hex-B, affirm the high effectiveness of this compact heat exchanger. The optimized Hex-B is made of aluminum and includes dual flow channels for both hot fluid and cold fluid. Silicone rubber was used as a sealing ring. The weight of the newly fabricated heat exchanger is 0.23kg with all the connecting flanges, which is much less than that for the Hex-A, which weighs 1.20 kg. Additionally, the footprint area of the newly fabricated heat exchanger is much smaller than that of Hex-A, as shown in figure 14. The optimized compact Hex-B has larger heat transfer area ratio and effectiveness.

Another major objective of the design of the liquid cooling system is to reduce the system pressure drop so as to achieve the compactness of the system by selecting the micropump with low pumping power and small size. The variation of the simulated and measured pressure drops versus the flow rate in the heat exchangers and microcooler are presented in figures 15 and 16, respectively. This shows that the experimentally measured pressure drop agrees reasonably well with the simulated value, and the simulated results are slightly lower (5%~10%) than the measured values. The pressure drop in the newly designed and fabricated compact Hex-B is about half of the pressure drop in the Hex-A. It can also be seen that the microcooler with microjet nozzle and microchannels is the main contributor to the pressure drop of the full system, accounting for around 97~99% of the system pressure drop. The proportions of system pressure drop in the microcooler and heat exchanger are shown in figure 17. This indicates that the hydraulic design of this system is efficient, and the pressure drop in the heat exchanger has been reduced to a reasonable level.

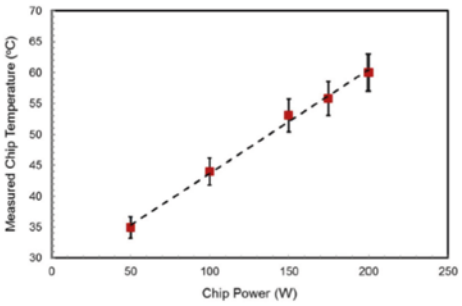

Figure 19. Measured chip temperature through the IR camera for different chip powers.

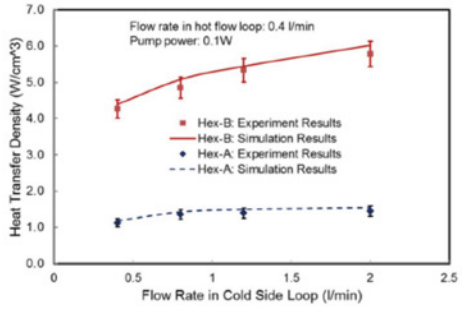

Figure 21. Measured thermal transfer density for commercial heat transfer A and compact Hex -B (a power of 175 W).

The thermal resistance is extracted to evaluate the thermal performance of the full system. The schematic 1-D thermal network of the system is shown in Figure 18. It is seen that the junction to ambient thermal resistance of the system (θ_{ja}) consists of two parts; the first part is the thermal resistance from the junction to microcooler (θ_{jc}), which represents the thermal performance of the microcooler and the other is the thermal resistance from the microcooler to the ambient (θ_{ca}), which represents the thermal performance of the heat exchanger.

The design target for this silicon microcooler system is to have a heat dissipation capability of 350 W/cm^2, which corresponds to a heat power of 175 W on a 7 × 7 mm chip. Assuming the system works in an environment of 40°C, and the allowable junction temperature is 85°C. The design target of the junction to ambient thermal resistance for this system is about 0.25°C/W.

In the tests, the power applied to the thermal test chip varies from 50 to 200 W. The chip temperature under different chip powers is measured, and the results are shown in figure. 19. The flow rate remains 0.4 L/ min in the hot loop and 2 L/min in the cool loop during the test. It can be seen that the chip temperature linearly increases with the increase in the power applied to the chip, while, the overall thermal resistance of the

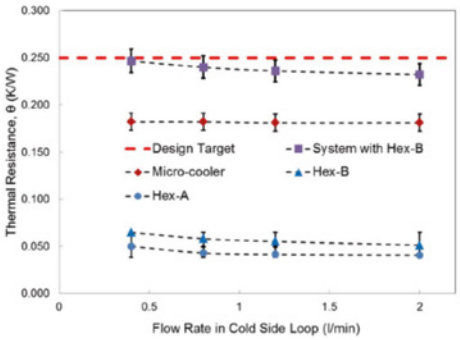

Figure 20. Measured thermal resistance of the heat exchangers, microcooler, and the full system assembled with compact Hex -B (a power of 175 W).

system, including the thermal resistance of the microcooler and the thermal resistance of the heat exchanger, has been obtained. The results are shown in figure 20. The thermal resistance of the heat exchangers decreases when the flow rate in the cool flow loop increases, as such causing the decrease in the overall system thermal resistance with the increase of the flow rate in the cold flow loop. Taking a close examination to figure 20, it shows that the microcooler is the main contributor to the overall system thermal resistance, accounting for around 80~90% of the total thermal resistance, while the heat exchanger only accounts for about 10~20% of the overall system thermal resistance. Additionally, the thermal resistance of Hex-B is slightly larger than that for the Hex-A. While Hex-B is much smaller and lighter than Hex-A. Furthermore, the pressure drop in Hex-B is only half of the pressure drop in Hex-A. Furthermore, as shown in figure 21, the heat transfer density of Hex-B is much higher than that for Hex-A. Hence, it can be concluded that the design of Hex-B is more effective than the design of the Hex-A for the applications in this paper.

Furthermore, the developed compact cooling system is able to meet the design target of 175-W heat dissipation capability with a pumping power of 0.1 W.

Reference:

IEEE TRANSACTIONS ON COMPONENTS, PACKAGING AND MANUFACTURING TECHNOLOGY, VOL. 6, NO. 5, MAY 2016

Development of a Compact and Efficient Liquid

Cooling System With Silicon Microcooler for

High-Power Microelectronic Devices

Gongyue Tang, Yong Han, Boon Long Lau, Xiaowu Zhang, Senior Member, IEEE, and Daniel Min Woo Rhee

Using 1D Computational Models to Predict Automotive Cold-Ambient Warm-up Performance

By Sudhi Uppuluri, Computational Sciences Expert Group

Improved efficiencies. This continues to be the goal of engineers all over the world, especially those in the automotive industry. With all of the focus on new technologies such as fuel cells and fully electric vehicles, it is easy to forget that for at least the next decade the vast majority of new vehicles will still contain the internal combustion engine and all of the systems that support it. It is with this in mind that engineers continue to push designs to be as efficient as possible through the use of computer aided engineering tools. CSEG is doing just that with their novel approach to using a combination of 1D computational models in both Flowmaster and Ricardo Software's WAVE to predict cold-ambient warm-up in vehicles.

When designing a vehicle, one area development teams find challenging is to predict how the heating, ventilation, and air-conditioning (HVAC) system is going to perform in cold environmental conditions. There are number of different scenarios the vehicle needs to perform while under these extreme conditions and its effectiveness can be compromised by several factors including a varying engine heat rejection, calibration changes, and underperforming components due to higher viscosity coolant. The approach to address this challenge using computational models is for the CSEG engineers to first develop and validate an engine thermal model based on a 2L turbocharged direct injection engine using Ricardo Software's WAVE. This model is then used to calculate the engine heat rejection based on various design parameters such as spark timing, air-fuel ratio, manifold pressure, and cylinder wall temperature. The resultant heat rejection can then be used as an input to the cooling system model constructed in Flowmaster, where the ultimate effect on cabin comfort can be predicted.

Engine Thermodynamic Model

The thermodynamic model of the engine was based on the specifications in Table 1, and includes a 1D fluid dynamic model and a predictive combustion model. To calibrate the computational model, representative test data from a 2 liter, 4 cylinder turbocharged direct injection gasoline engine with cooled exhaust gas recirculation was used. The model as shown in Figure 1, was created with three assumptions:

1. The cold ambient conditions did not have any engine knock,
2. Correlating the model to warm conditions would be accurate enough for predications at cold conditions, and
3. The turbocharger waste-gate is open and the EGR valve is closed for cold conditions.

The model was first run under warm conditions to validate against test data. These simulations were run across a range of engine operation conditions from low idle to rate power. Two inputs were tested as part of the model validation including spark timing and air-fuel ratio. The result was that all critical parameters were within acceptable tolerance for the project. The next step was to use the validated engine model under cold ambient conditions. As in the warm ambient condition, the two input variables for the cold model were, spark timing and air-fuel ratio. From the simulations, the predicted engine heat rejection for a range of each of these values was obtained.

Vehicle Cooling System Model

The vehicle cooling system constructed in Flowmaster consisted of five sub-systems based on that of a sports utility vehicle with front and rear cabin heaters. Figure 2, shows the model consisted of a cabin heater including cabin prediction, an engine coolant loop, and engine oil coolant circuit, a transmission oil coolant loop, and an airside path delivering cooling air to the heat exchangers. The engine was modeled as a lumped mass with the heat rejection for each scenario determined by the results of the engine thermal model.

The ultimate goal of the vehicle cooling system model was to calculate the cabin heater coolant inlet temperature as a measure of the system performance. Two main criteria were used to evaluate the design, first how long it took for the coolant to reach 50°C and second the absolute temperature of the coolant at ten minutes into the warm-up cycle. While both criteria measure the same effect, how the vehicle is designed can have a marked effect on either or both of these criteria which needed to be evaluated.

The first scenario of evaluating spark timing was carried out in Flowmaster with results from WAVE at three different spark timings; 0, 15, and 25 degree crank angle adjustment. Figure 3, shows the significant difference in time to 50°C and temperature at ten minutes can be seen from the 25 degree timing.

Displaced volume	1998 cc
Stroke	83.1 mm
Bore	87.5 mm
Connecting Rod	155.75 mm
Compression ratio	9.3:1
Number of Valves	4

Table 1. Engine Specifications

The second scenario evaluated the effect of air-fuel ratio using a stoichiometric ratio, a reduction of 3 basis points, and 5 basis points from stoichiometric. As shown in Figure 4, the reduction in the air-fuel ratio had significant reduction in heat generation and thus a reduction in time to reach 50°C and overall temperature after ten minutes.

In the final scenario, the engine idle speed was adjusted from 1500rpm to 1700rpm. Not surprisingly the increase in speed led to an increase in heat rejection. This difference led to a 21% improvement in the time it took to reach 50°C and increased the coolant temperature after ten minutes by 10°C as shown in Figure 5.

As a result of the analysis, CSEG engineers were able to quantify the effects of several different design parameters for the vehicle. By leveraging simulation technology like Flowmaster they were able to do this very early in the design phase before significant physical testing needed to be done. Combining this technology with engine heat rejection characterization from Ricardo Software's WAVE meant they could improve the fidelity of their simulations and deliver the most accurate analysis possible.

Reference

"Cold-Ambient Warm-Up Predictions: A Novel Approach Using 1D Computational Models," SAE Technical Paper 2016-01-0198, 2016,

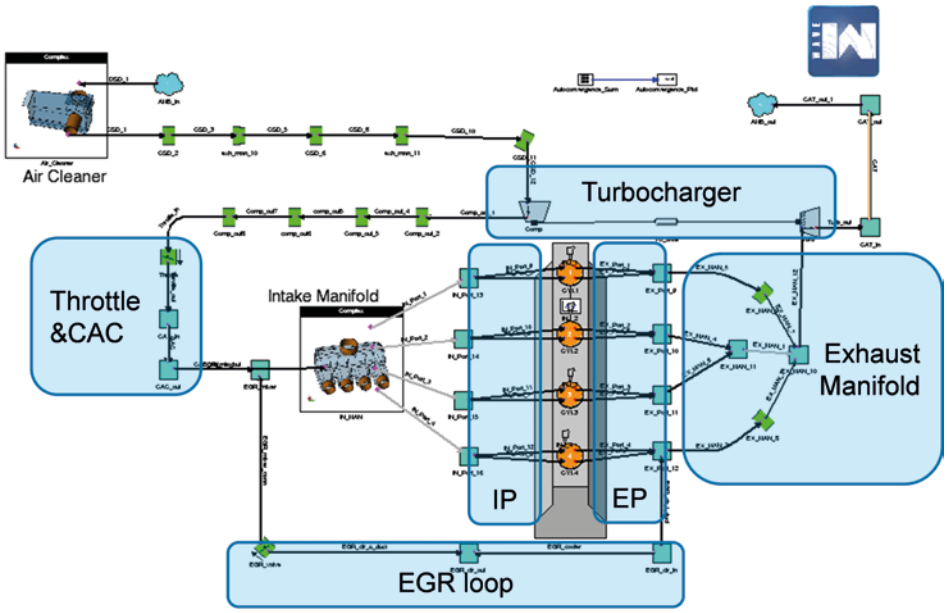

Figure 1. Ricardo Wave Model Map of 2L Gasoline Direct Injection Turbocharged Cooled EGR Engine

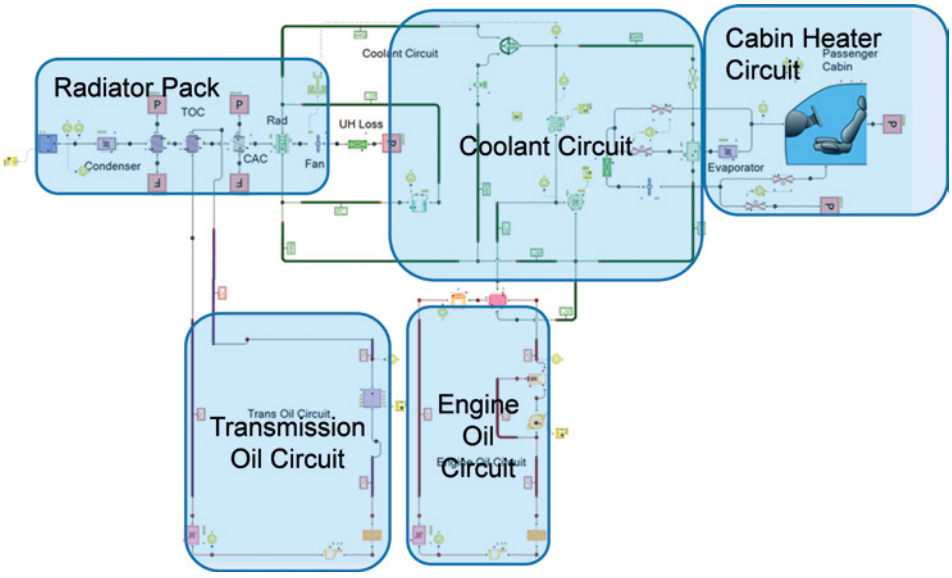

Figure 2. Flowmaster Model Map for Typical Compact Sedan Cooling System

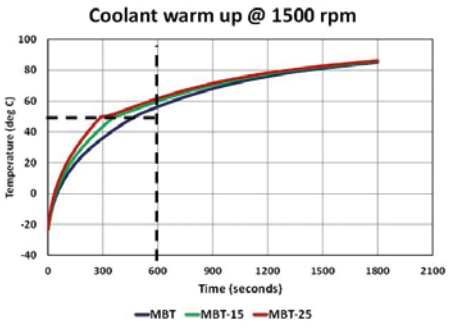

Figure 3. Effect of Spark Timing Retard on Coolant Warm Up

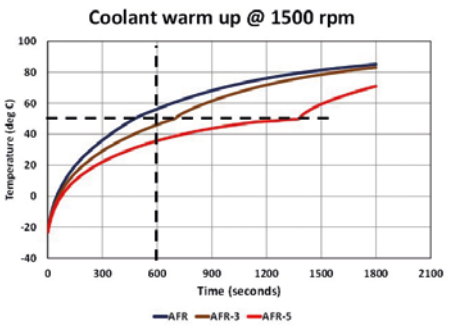

Figure 4. Effect of Rich Air-fuel Ratio on Coolant Warm Up

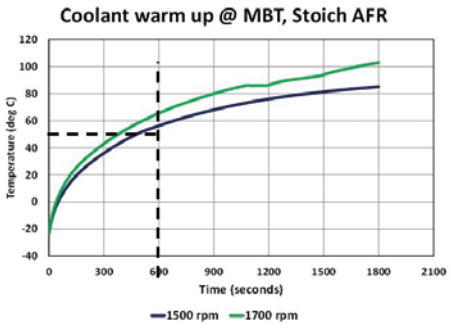

Figure 5. Effect of Engine Speed on Coolant Warm Up

Predicting EV Drive Range

By Doug Kolak, Technical Marketing Engineer, Mentor Graphics

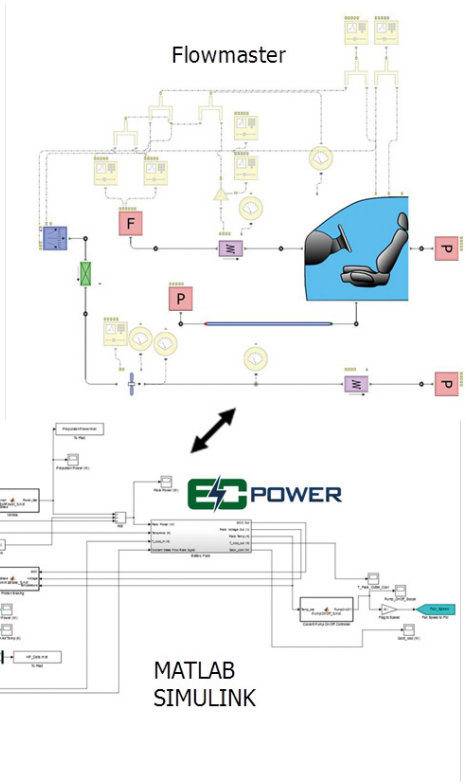

Could the era of the electric car finally be upon us? The answer is yes, but there is still a long way to go. A major concern for consumers of electric vehicles has been that the range of these vehicles has shown to be extremely variable with ambient temperature, [1,2] The ability to understand the effects that potential factors will have to the range of any EV is critical to creating a better design and thus improving the product for customers, ultimately driving increasing adoption. For this reason, the earlier an engineer is able to quantify how different factors will affect the EV, the better, and one of the most efficient ways to do this is through computer simulation.

The purpose of this study was to quantify the ability to capture at least some of these effects using a co-simulation approach to represent different segments of the vehicle. The results were then compared against published empirical data collected by Charged[3] magazine to determine how well the approach fits real world test results. The co-simulation was done using three different software packages to model different parts of the vehicle.

Parameter	Value
Energy	24 kWh
Cells in Series	96
Cells in Parallel	2
Cell Shape	Prismatic
Cathode	70/30 LMO/NMC
Anode	Graphite

Table 1. Battery Design Parameters

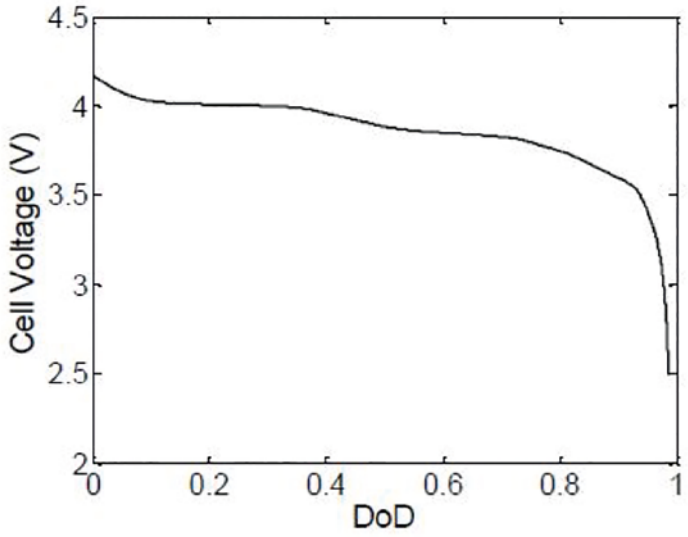

Figure 1. C/3 Discharge Curve for a Single 70/30 LMO/NMC 33Ah Cell

Battery Pack Model

The performance of the battery was modeled using EC Power's AutoLion-ST™. The pack and cells were loosely configured to represent the first generation Nissan Leaf design. The model was responsible for handling three aspects of the simulation, calculating the temperature of the battery pack, calculating the pack voltage, and calculating the State of Charge (SoC).

From the vehicle model, the battery model received a total pack power requirement with the simulation continuing until the battery model reached a SoC state of 20%.

Vehicle Model

The vehicle portion of the model was constructed in MATLAB Simulink®. The vehicle model acted as the platform for the entire co-simulation collecting and distributing data between models. As part of this task, the model also set several of the initial conditions including: ambient, cabin, and battery temperatures; cabin set-point; drive cycle and driver aggressiveness factor.

The vehicle model was also responsible for determining the total power requirement of the vehicle. This included the effects of drag, braking, drivetrain inefficiencies, and propulsion/regeneration from the electric motor. The model also separately determined the cooling fan on/off state with the required power added to the total requirement if necessary.

Cabin Thermal & Battery Cooling Model

The cabin and battery cooling air portions of the model were constructed in Mentor Graphics 1D Computational Fluid Dynamics tool, Flowmaster. The primary purpose of the Flowmaster model was to calculate the power required to maintain the given set-point temperature of the cabin at the different ambient temperatures and vehicle velocities. To accomplish this, the Automotive 1D Cabin component was used to calculate the average cabin temperature as a function of inlet airflow rate, air temperature, and vehicle velocity. The model was able to account for the difference in external heat transfer based on when the vehicle was moving or stationary as well as the heat input due to solar radiation.

The HVAC system was modeled as a simplified heating or cooling generation component. This component added or removed heat to the airflow entering the cabin based on the feedback from Flowmaster's PID controller. A Coefficient of Performance (CoP) of two was used to account for the inefficiencies in the HVAC system.

The Flowmaster model was also responsible for calculating the temperature of the battery pack cooling air and the cooling fan power requirement. If the temperature rose high enough, the vehicle model would signal that the fan should be running. Under these circumstances, Flowmaster would calculate the heat added to the airflow due to the fan inefficencies as well as the power the fan required. The overall Flowmaster power requirement fed back to the vehicle level model to be included in the total power requirement of the battery.

Factor	Values
Driver Aggressiveness	0.8, 1.0, 1.2
Cabin Set Point Temperature	15, 20, 24 (°C)
Ambient Temperature	-10, 0, 10, 20, 30, 40, 50 (°C)

Table 2. Study Factors and Values

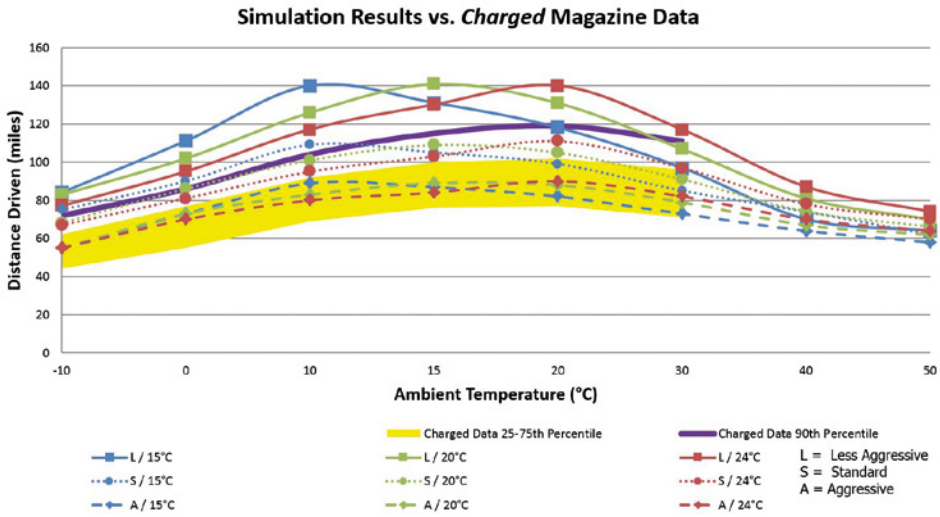

Figure 2. Predicted Drive Range for different Ambient Pressures vs. Published Data

Results and Conclusions

The purpose of the study was to understand how different factors effected the overall drive range of the vehicle through simulation. The three factors chosen for the study were driver aggressiveness, cabin set point temperature, and ambient temperature. Several values for each factor were used in the study as a full factorial study:

Each co-simulation ran for between five and ten minutes ending once the SoC of the battery model reached 20%. In total, the seventy-two studies were run over two days requiring approximately eight hours of engineering time.

The results can also be shown against the data publish in Charged magazine. In figure 2, the yellow band represents the middle 50% of test data collected while the solid purple line represents the longest 10% of drive ranges.

Overall the trends seen from the analysis, are what was expected before the study began. As shown in figure 2, the results were on the upper end of what was seen by Charged magazine as part of their data collection. Further refinement to the estimates for drive cycle and driver aggressiveness could improve this correlation. The model could also be further developed, including more accurate data for the cabin materials as well as the performance of the HVAC system.

With improvements to the model the spread of distance results would likely decrease to be more consistent with test data. The study showed that while drive range information can be determined through test, using a co-simulation approach, a reasonable approximation was possible from a full factorial of driving scenarios in less than one engineering day.

Literature

[1] Heather Hunter, AAA News Room, "Extreme Temperatures Affect Electric Vehicle Driving Range, AAA Says," March 20, 2014 http://newsroom.aaa.com/2014/03/extreme-temperatures-affect-electric-vehicle-driving-range-aaa-says/

[2] Consumer Reports News, "Winter chills limit range of the Tesla Model S electric car," February 15, 2013. http://www.consumerreports.org/cro/news/2013/02/winter-chills-limit-range-of-the-tesla-model-s-electric-car/index.htm

[3] "FleetCarma Goes Deep into the Data", Charged. Pg. 56-61. Jan/Feb 2015.

[4] Kolak, D., Shaffer, C., Marovic, B., Sinha, P. Prediction of EV Drive Range Reduction under Extreme Environmental conditions using Computer Aided Engineering Tools June 2016, EEHE2016

T3Ster® Investigation of Thermal Effects of Surface Roughness on TIMs

By Toshiharu Morimura, Shin-Etsu Chemical Co., Ltd.

Shin-Etsu Chemical Co., Ltd. was founded 90 years ago in Japan and is the largest chemical company in the country, with the world's top share in polyvinyl chloride (PVC) and semiconductor silicon and the top domestic share for silicones. One of Shin-Etsu's main products is silicone which is used in a wide range of industrial fields, including electrical and electronic applications, automobiles, construction, cosmetics and chemicals.

About 40 years ago, Shin-Etsu decided to move into manufacturing TIMs (Thermal Interface Materials). TIMs help to move heat away from electronic components and are an integral part of electronic product design. The challenge with TIMs is usually associated with how effective the interface attachment is to the electronic components especially air gaps that may appear – the so-called "heat resistance" of such materials to heat flow from hot components to their cooling systems (Figure 1).

Silicone is a highly effective TIM because it is both soft and stable and it can be used over high and low temperature ranges. It is an artificial polymer compound that has an inorganic siloxane bond (Si-O) repeating as a main chain, along with various organic groups in its side chains (Figure 2). A spider diagram of its physical and chemical properties can be seen in figure 3 where it can be seen to be excellent in most of its properties and suitable as a base material for TIMs.

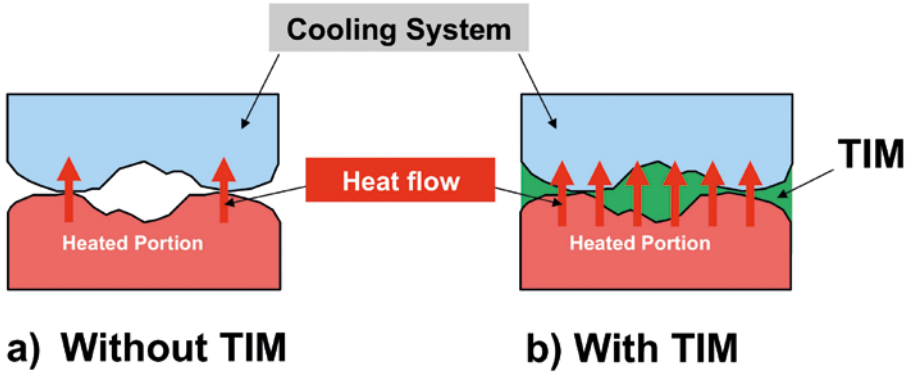

Figure 1. Principle of Operation of an electronics TIM

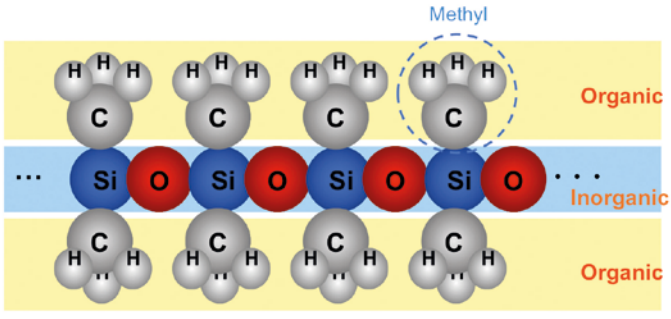

Structural schematic view of a polydimethyl silicone

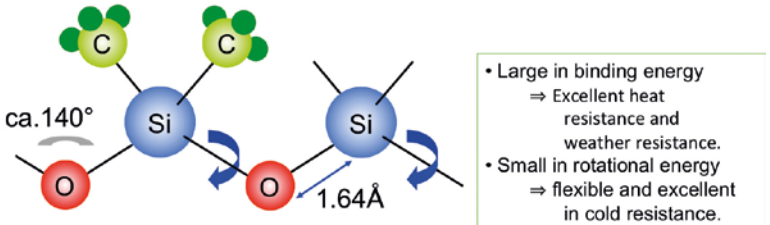

Silicone has a helical structure rich in flexibility.

Bonding	Bond distance	Bond angle	Rotational energy	Binding energy
Siloxane bond (Si-O)	1.6Å	*ca.*140°	<0.8 kJ/mol	444kJ/mol
C-C bond C-C	1.54 Å	*ca.*110°	15.1 kJ/mol	356kJ/mol

Figure 2. Molecular Composition of Silicone and the polymer's Physical Properties

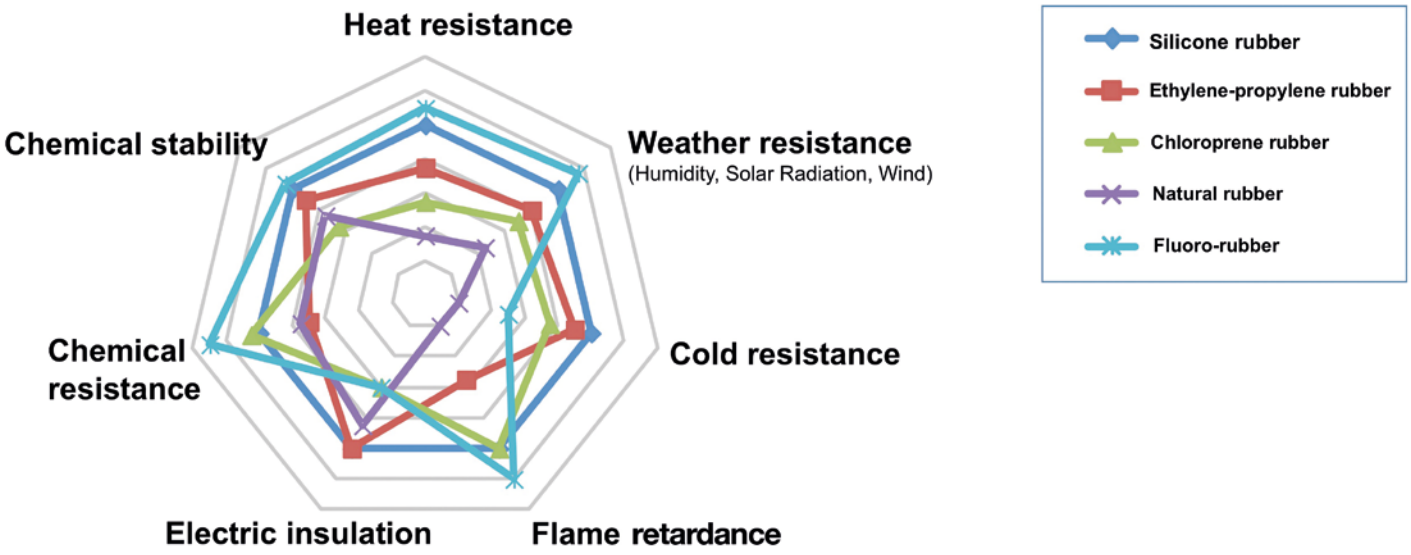

Figure 3. Physical & Chemical Properties of Silicone versus other Rubber Materials

Up to 2015, Shin-Etsu employed in-house test equipment to measure thermal resistance of their TIM products within their laboratories. However, they recently acquired a Mentor Graphics T3Ster transient thermal tester unit in order to capture complex transient thermal features during testing of their TIM products. A series of benchmark tests were devised to validate the MicReD T3Ster™ hardware for a range of TIM variables, some of which involved T3Ster being connected to in-house equipment:

a) Thickness of TIM layers,

b) Hardness of TIM layers, and

c) Roughness of layers TIMs attach to.

The powerful T3Ster Master software from MicReD and its "Structure Function" approach to quantifying thermal resistance for TIMs was employed to good effect in assessing (a) and (b) first. For TIM hardness and thickness Shin-Etsu were able to confirm with T3Ster measurements that the heat releasing performance of silicone based rubbers depends on the pressure the TIM is under during normal operation. In addition, Low Hardness TIMs performed better for heat spreading than High Hardness TIMs, plus thin TIMs produced better heat release than thick TIMs. This article will deal with item (c) in detail, that is, roughness effects on thermal performance of TIMs using T3Ster thermal test methods.

To assess the impact of the roughness of an aluminum plate attached to a TIM (heat release sheet) between the plate and a

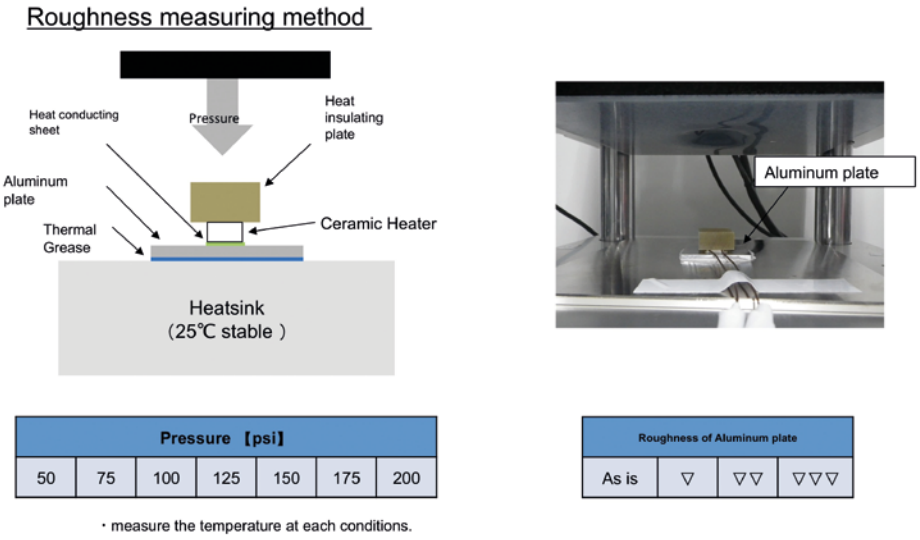

Figure 4. Test Equipment used to assess the effects of aluminum plate roughness is contact with various hardness TIMs

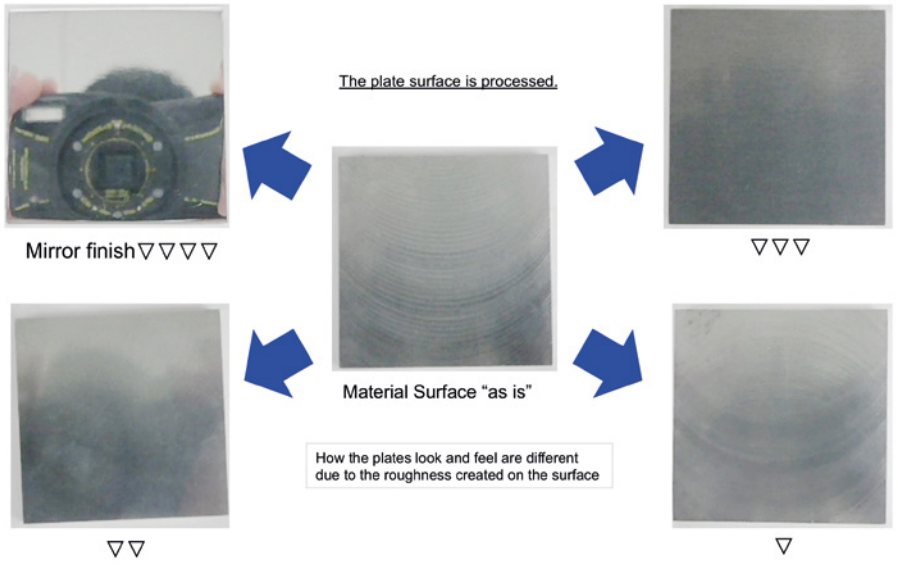

Figure 5. Photos of the five surface roughnesses of the aluminum plates used in the test

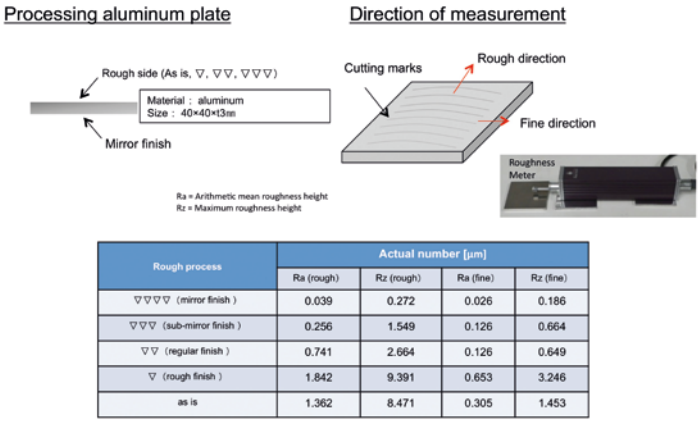

Rough process	Actual number [μm]			
	Ra (rough)	Rz (rough)	Ra (fine)	Rz (fine)
▽▽▽▽ (mirror finish)	0.039	0.272	0.026	0.186
▽▽▽ (sub-mirror finish)	0.256	1.549	0.126	0.664
▽▽ (regular finish)	0.741	2.664	0.126	0.649
▽ (rough finish)	1.842	9.391	0.653	3.246
as is	1.362	8.471	0.305	1.453

Figure 6. Details of the Aluminum Plate surface roughnesses and measurements taken

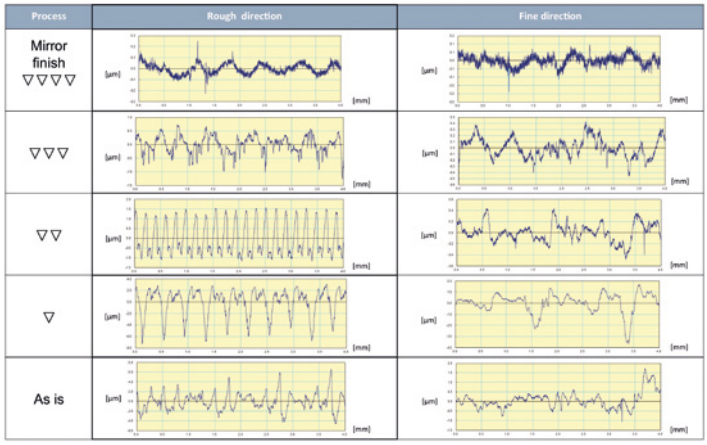

Figure 7. Details of the Aluminum Plate surface roughnesses in the rough and fine directions

ceramic heater, a test was devised (Figure 4) whereby identical plates had varying degrees of roughness etched onto them (Figure 5) and various pressures applied to the test unit while it was heated by a ceramic heater.

Shin-Etsu measured to submicron levels of accuracy the aluminum plate surfaces for four plate smoothness levels. Maximum roughness levels were found to be between 0.2 to 9 microns in height in the samples tested (Figure 6) and actual roughness cross-sections typically showed peaks and troughs illustrative of repeated surface roughness patterns (Figure 7).

Shin-Etsu chose two TIM products, TC-30TAG-8 and TC-100CAF-40 to be applied to the set of aluminum plates to evaluate the influence of roughness. Both materials had similar heat dissipation performance when there was no aluminum plate in position but TC-100CAF-40 had a low hardness (that is, it was relatively soft) and TC-30TAG-8 was of high hardness; see figure 8. There is clearly a small spread in temperature for the plates of different roughness with TC-100CAF-40 in place. However, figure 8 does show a significant difference in temperature due to the different aluminum roughnesses in touch with TC-30TAG-8: the high hardness TIM.

Figures 9 and 10 show the same aluminum plates measured in T3Ster for low and high hardness TIMs at both a high applied pressure (200psi) and a low pressure (75psi). The diagnostic T3Ster structure functions show not much influence due to the difference in roughness with the lower hardness TIM product probably due to less contact heat resistance. With the high hardness TIM product however, heat resistance is different according to the aluminum plate roughness due to the contact heat resistance being larger on the

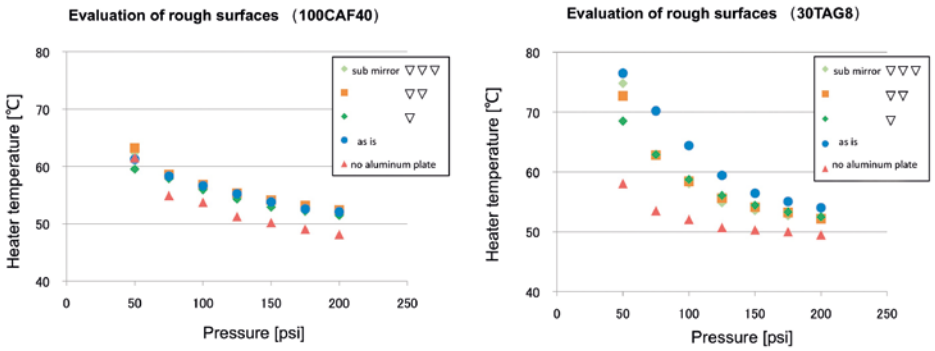

Figure 8. Evaluation of Surface Roughnesses for TC-100CAF-40 and TC-30TAG-8 TIM products heated and under various pressure loadings

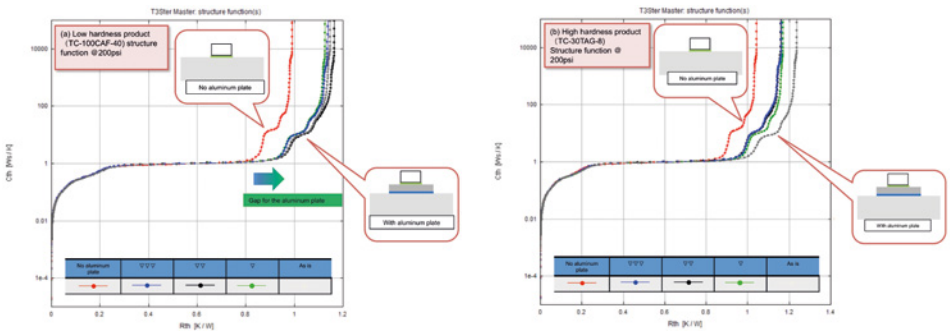

Figure 9. T3Ster Structure Function plots of Low Hardness TC-100CAF-40 and High Hardness TC-30TAG-8 TIM products on aluminum plates of different roughnesses for a 200psi loading

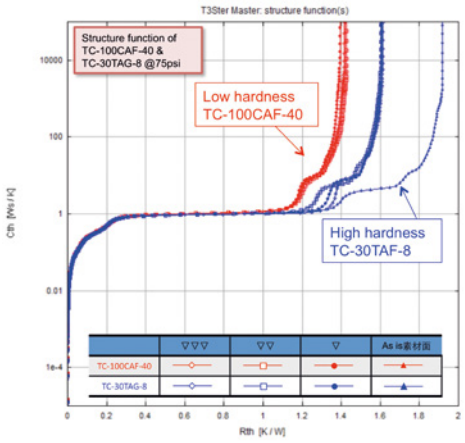

Figure 10. T3Ster Structure Function plots of Low Hardness TC-100CAF-40 and High Hardness TC-30TAG-8 TIM products on aluminum plates of different roughnesses for a 75psi loading

material surface (Figure 9). When comparing the low pressure to high pressure tests, high and low hardness heat release sheets showed obvious differences in structure function (Figure 10) in "as is" condition.

One conclusion from this study is that figure 11 shows that the aluminum plate surface roughness depths (Ra, Rz) cannot be the sole determinant of a TIM's heat spreading performance; rather, the cross sectional roughness curve of the plate needs to be considered too. Figure 12 illustrates the underlying issues schematically where an off-the-shelf "as is" surface of a typical aluminum plate will have peaks that are erratic and with relatively large distances between them. Hence, with "as is" surface, the more air that enters the gap, the larger the contact heat resistance if compared with other smooth surfaces. Comparing a low hardness heat spreading TIM sheet with a high hardness heat spreading sheet, the low hardness TIM by virtue of its softness can fill the gap caused by the surface's roughness thereby reducing the overall contact thermal resistance. Not surprisingly, the same contact thermal resistance can be reduced by pressurizing a TIM by applying a high pressure (of, say, 200psi).

This experimental study clearly shows that with the help of a Mentor T3Ster™ transient thermal tester, Shin-Etsu are now able to supply their customers much more detailed thermal Data Sheets for their TIM products. This approach is much easier to do than was the case with previous in-house solutions and more automated. The company can assess hardness effects of TIMs much better than before plus T3Ster can give much more diagnostic information on the thermal layers under test in a dynamic manner. In effect, Shin-Etsu can now generate a much richer data set than a few years ago which allows it to produce better TIM products for its customers.

Rough process	Roughness curves	Influence of surface roughness	Characteristics of roughness curves
▽▽	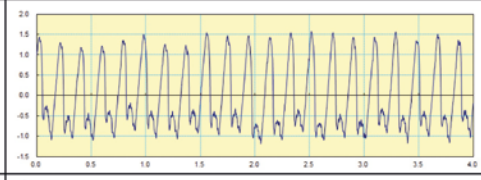	little	· smaller distance · sharp peaks · cyclic nature
▽	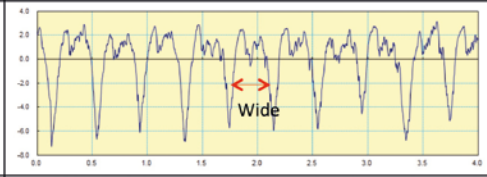	little	· wider distance · cyclic nature
as is material surface	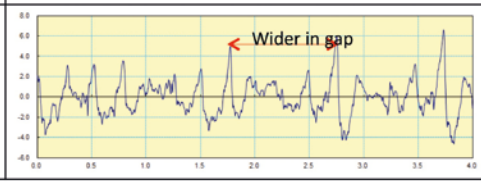	more	· wider in distance · no cyclic nature

Figure 11. Typical effects of Surface Roughness Cross sectional curves for rough to smooth plates

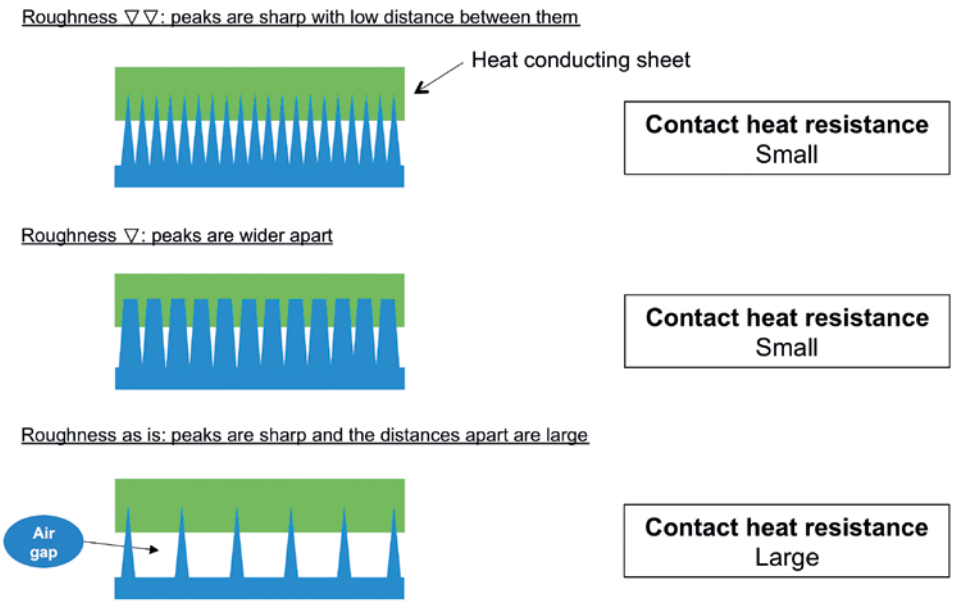

Figure 12. Schematic effects of Surface Roughness Cross sections on resultant surface contact heat resistances

About Shin-Etsu Chemical

Shin-Etsu Chemical Co., Ltd. is the largest chemical company in Japan. Shin-Etsu Chemical produces the key materials that modern industry demands. These business activities are divided into six segments: PVC/Chlor-Alkali Business, Semiconductor Silicon Business, Silicones Business, Electronics and Functional Materials Business, Specialty Chemicals Business and Diversified Business. In each of these fields, they have products with strong market share, with the world's top share in polyvinyl chloride (PVC) and semiconductor silicon and the top domestic share for silicones.

About Shin-Etsu Silicone

In 1953, Shin-Etsu Chemical became the first firm in Japan to venture into the silicones business. In the decades since, Shin-Etsu has created a diverse line of products designed to exploit the unique and useful properties of silicones. Today, their lineup includes over 5,000 products that meet user needs in a wide range of industrial fields, including electrical and electronic applications, automobiles, construction, cosmetics and chemicals.

Voxdale and Flanders' Bike Valley build a Wind Tunnel using FloEFD™

By Mike Gruetzmacher, Technical Marketing Engineer, Mentor Graphics

In April 2016, the Flanders' Bike Valley wind tunnel in Beringen, Belgium was unveiled. The eye-catching structure attracted more than 400 spectators to the opening event. The wind tunnel, with a surface area of around 600 square meters, is the latest project co-created by Voxdale BVBA, and Flanders' Bike Valley. The purpose of the wind tunnel is to provide cyclists, the growing cycling industry and its manufacturers, product developers and athletes with accurate test data to improve product and athlete performance. The tunnel will also be used for additional low speed aerodynamic testing like sports equipment, clothing, drones etc.

The open circuit wind tunnel, also known as an "Eiffel" or NPL Tunnel, is constructed in such a way that air is sucked from the ambient into the test section. The Flanders' Bike Valley wind tunnel is housed in a purpose built hanger measuring 50m x 16m x 10m. The tunnel itself has a length of approximately 50m.

The tunnel comprises several sections: the contraction section, the test section, and the diffusor section. The test section is 2.5m x 2.5m x 6.5m and the maximum wind speed is 108 km/h. The wind tunnel design enables a high level of laminar flow, which leads to very accurate and repeatable results. The test section is equipped with a balance measuring system to determine weight and drag forces and a PIV (Particle Image Velocimetry) system to visualize velocity and the direction of the air.

Marc Hufkens, Chairman Board of Directors of Bike Valley Innovation Center said, "The first idea for a common wind tunnel facility came in Spring of 2012 and we took a few years of preparation to find the right partners, Voxdale is one of them. We started with the construction of the infrastructure in April 2015 and were happy to celebrate the inauguration in April 2016. The wind tunnel is unique, because we have a very exact measurement system. This is unique for cyclist and also for ski and alpine sports applications to determine the exact gain in cm or seconds with the optimized aerodynamics"

Koen Beyers, CEO of Voxdale said, "One of the main challenges we have in our work is the validation of our results and that is the reason why we participated in the Flanders'

Figure 1. Test Section

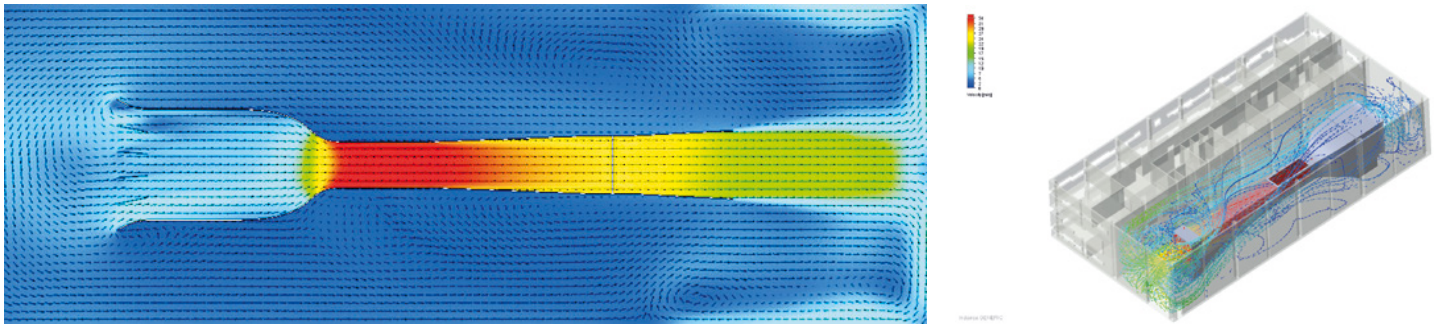

Figure 2 a+b. Wind tunnel simulation set up inside the building

Bike Valley Wind Tunnel project". Additional founding companies include BioRacer, Flanders Make, Lazer Helmets and Ridley with the support of Agentschap Ondernemen, Province Limburg and the European Regional Development Fund.

Voxdale built a very early mockup of the Flanders' Bike Valley Wind Tunnel and building. Many aspects have to be considered during the conceptual phase, for example, the type and size of wind tunnel, performance, velocity and naturally the budget. Voxdale was involved from the beginning in the conceptual design of the wind tunnel as well as in the aerodynamics. Mentor Graphics' FloEFD 3D Simulation Tool was used in the very early design phase. The contraction section, the test section and the diffusor section were modeled, simulated and designed directly in PTC Creo embedded FloEFD. Furthermore the entire hall around the wind tunnel was simulated because it is an open return wind tunnel.

One of the main challenges was the positioning of the wind tunnel inside the brand new building. The flow back from the fans to the contraction section was simulated and visualized. At the same time the laminar flow in the test section and the wind tunnel design were simulated.

Patrick Vlieger, Engineer at Voxdale commented, "At first we did a concept design of the Flanders' Bike Valley wind tunnel. We simulated inside the building to analyze the backflow inside the building and then we could also see the laminar flow in the test section. So we positioned the wind tunnel a little bit higher, a little bit more to the back or to the front of the building. We checked how this influences the laminar flow inside the test section and inside the building itself".

The height and the distances to the walls were optimized taking into consideration the effect on the flow conditions inside the wind tunnel. Hence, the FloEFD simulations ensured a good detailed engineering of the wind tunnel as well as a reliable and efficient design of the hall because an overdesign would lead to unnecessary expenses for the building.

The next stage is to create a digital replica of the test section in FloEFD to prepare the tests virtually. "With that we will be able to facilitate the preparation of the wind tunnel use. We can decide how many runs and which configuration we will do", says Koen Beyers. The correlated results can then be used also for further development in FloEFD. By doing this the time spent in the wind tunnel can be reduced noticeably.

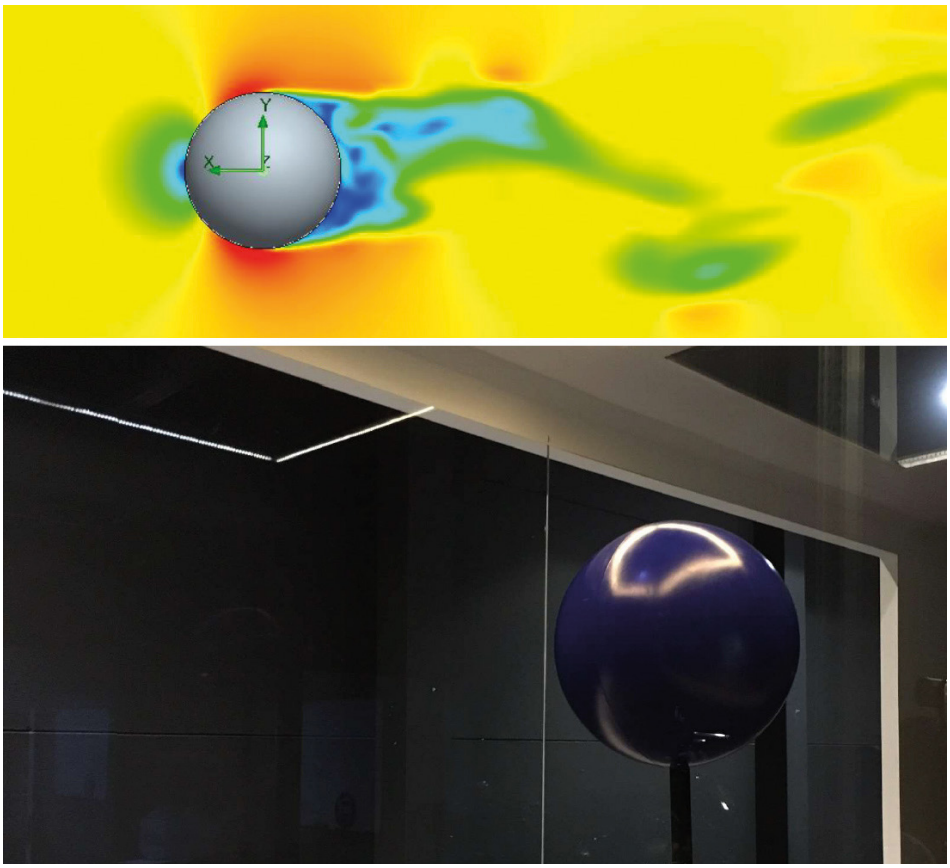

Figure 3. Sphere calibration picture and corresponding FloEFD simulation

Figure 4. The "Aerobar"

Besides all the strictly technically focused solutions the engineers elaborated an additional idea, they found a way to install a bar bellow the wind tunnel contraction section, which is called the "Aerobar".

Koen Beyers sums up, "You have to imagine, this is a multi-million Euro project. You have to come up with the design and then you have to step-by-step really build it. And that might be a risk, imagine that it does not perform as expected or it does not work very well. That's why we stepped in with FloEFD. That gave us enough confidence to validate the design of the tunnel itself and to have the correct dimensions of the hall. We are really proud of this project and it's almost unbelievable what we have materialized in this short period of time to end up with this F1-like facility".

References

https://issuu.com/mtss5/docs/201604fbv

http://www.flandersbikevalley.be/windtunnel/

https://www.grc.nasa.gov/www/k-12/airplane/tuncret.html

https://www.grc.nasa.gov/www/k-12/airplane/tunor

http://bit.ly/2dtwazF

Cleared for Landing

Numerical Methods for the Definition of the Hinge Moments of the Nose Landing Gear Doors of the Commercial Aircraft

By O.V. Pavlenko, TsAGI, A.V. Makhankov, A.V. Chuban, Irkut Corporation

To investigate the impact of the fluid flow on the aircraft's units CFD (Computational Fluid Dynamics) methods based on the numerical calculation of the hydrodynamic equations becomes widely used along with the conventional analytical approaches and experimental tests. Continuously developed and improved CFD methods can serve as a good alternative of the natural experiments in solving many practical problems [1].

Thus, at the design stage of the landing gear doors production often without being able to carry out the natural experiment, designers need to have level of aerodynamic loads acting on the closed doors at high speed of aircraft as well as during aircraft's maneuvers with the opened doors and gear release/retraction. The aerodynamic loads data obtained from CFD analysis gives the possibility to estimate the doors strength and define characteristics of the opening actuator, run the optimization of the kinematic connection between small rear doors with the landing gear strut. For instance, for the considered aircraft the initial variant of the small landing gear door rod mounting to the landing gear main fitting has been replaced

Aerospace

by the mounting to the landing gear strut to reduce the loads on the rod. The calculation results obtained for the selected variant of the doors were confirmed experimentally that indicates good accuracy of the modern software.

The results of the numerical study of aerodynamic loads on the nose landing gear doors demonstrated in this paper were obtained in ANSYS® Fluent and Mentor Graphics FloEFD™ software, based on the solution of the Reynolds averaged and Favre averaged Navier-Stokes equations accordingly.

The calculation in ANSYS Fluent software (license number 501024) was done using the structured computational mesh (about 6 million cells) with « κ - ε realizable» turbulence model (κ - ε method based on a simultaneous solution of the momentum transport equations, the kinetic energy and the dissipation rate equations) with the enhanced modeling of turbulence parameters near the wall and with taking into account the influence of the pressure gradient. The solved equations were approximated with a finite-volume scheme of the second order.

The numerical study in FloEFD software was performed using rectangular computational mesh adapted to the surface (about 2.5 million cells) [3]. To speed up the calculations the local meshes with the increased mesh resolution around the nose of the fuselage and landing gear doors were used. The automatically adapting computational mesh with concentration in the areas of high gradients of velocity was applied. It should be noted that FloEFD uses a relatively small number of cells of the computational mesh as far as in case of a low resolution of the boundary layer the theory based on the Prandtl boundary layer hypothesis is applied. Turbulence model used in FloEFD bases on the modified model with damping functions proposed by Lam and Bremhorstom [4].

The calculations of the hinge moments of the nose landing gear doors were performed for the three-dimensional model of the part

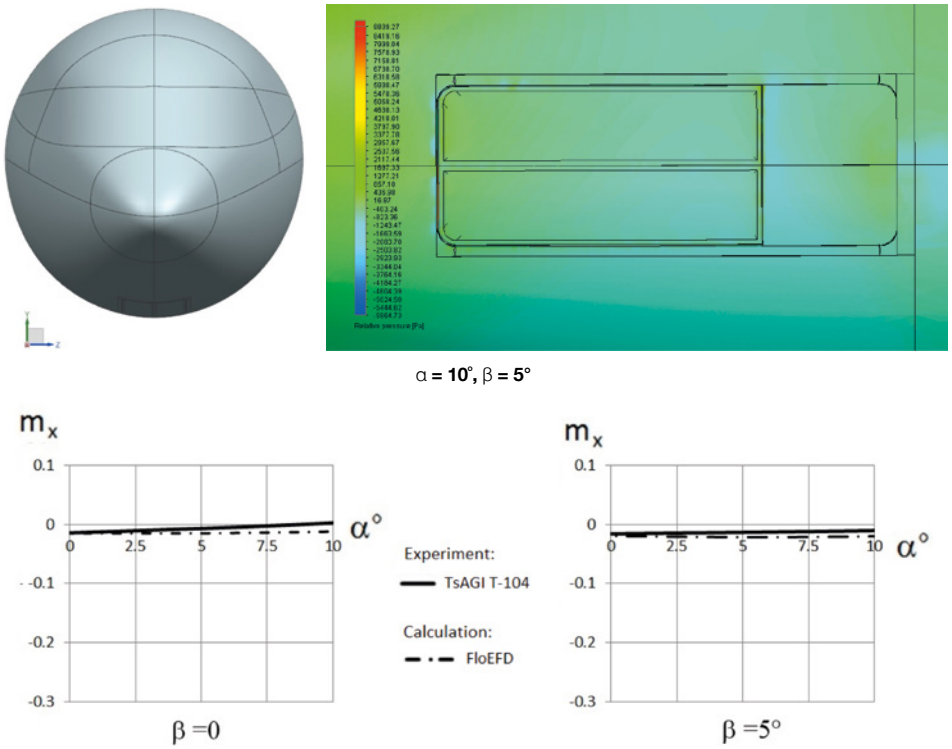

Figure 1. The model with the closed landing gear doors and hinge moments of the large left nose landing gear doors at $\delta_{door1} = 0°$, $\delta_{door2} = 0°$, $\delta_{strut} = 0°$, $\beta = 0°$ and $\beta = 5°$.

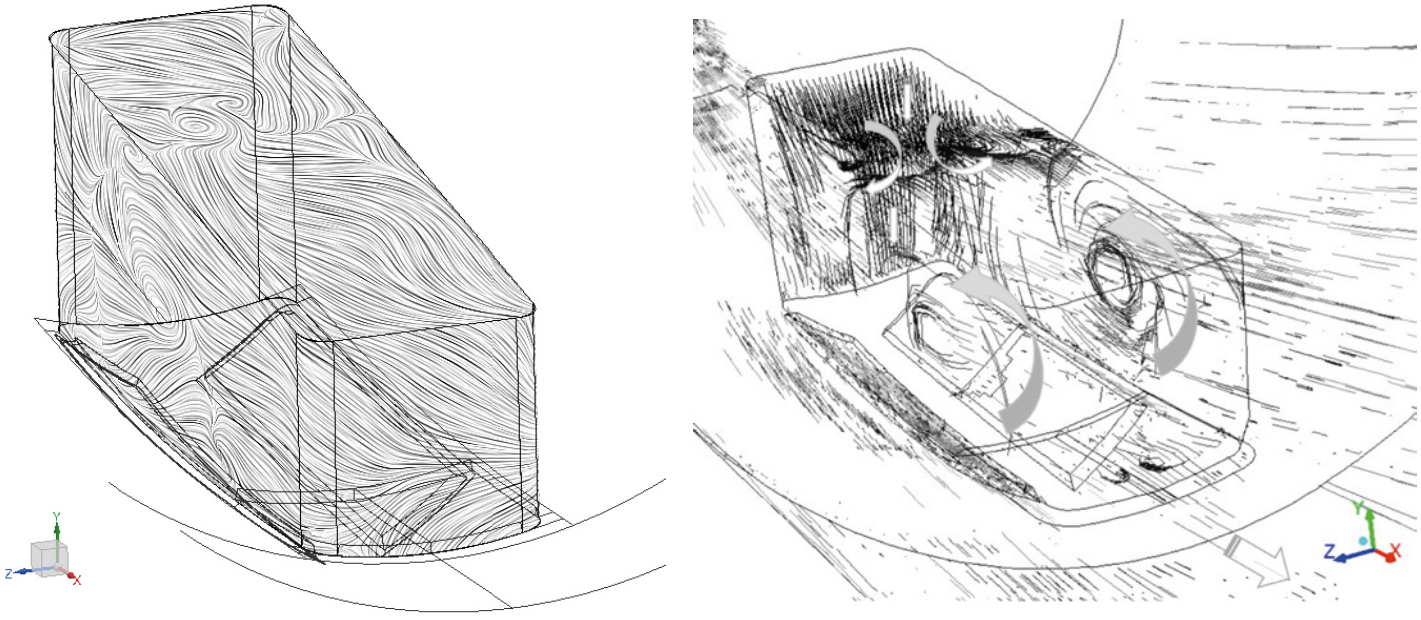

FloEFD

Fluent

Figure 2. Streamlines on the doors and in the niche at $\delta_{door1} = 30°$, $\delta_{door2} = 0°$.

of the commercial aircraft in the scale of 1:1 which includes the fuselage, large front and small rear nose landing gear doors as well as the nose gear and the wheel well. The calculation results were obtained for the stage of release – retraction of the landing gear at Mach number M = 0.34 and impact air pressure q = 771 kg/m^2. Experimental data was obtained by Andreev G.T. in the TsAGI wind tunnel T-104 for the full aircraft model in the scale of 1:8.16 at Mach number M = 0.2. All of the graphs below are related to the left landing gear doors, hinge moments of the right (windward) landing gear doors are less usually.

1. Flow around the large nose landing gear doors at their opening

The calculations and the experimental investigations have shown that in the closed position (δ_{door1} = 0°, δ_{door2} = 0°, δ_{strut} = 0°) hinge moments of the nose landing gear doors are minimal (Figure 1).

This fact is due to the presence of gaps along the doors which balance the static pressure on the outer surfaces of them near their edges and in the landing gear niche. A calculation of the loads without taking into account these gaps leads to an overestimation of normal forces acting on the detachment of the doors because nose gear of the considered aircraft are located in the flow acceleration zone from the nose of the fuselage to the regular part. Since at the sideslip angle of 5° nature of the flow around the fuselage nose does not change much the hinge moments of the closed doors are practically independent on the sideslip angle within a specified range.

During opening of the large doors (δ_{door1} = 30°, δ_{door2} = 30°, δ_{strut} = 0° - experiment, δ_{door1} = 30°, δ_{door2} = 0°, δ_{strut} = 0° - calculation) airflow circulation occurs in the niche of the landing gear (Figure 2), which leads to slow down the flow over the doors and increase the pressure on the inner surfaces of them.

As a result, the hinge moments of the opened doors are significantly higher than of the closed ones even in the absence of the sideslip angle, which is confirmed by the results of calculations as well as experiments (Figure 3). The right chart in figure 3 shows the influence of the sideslip angle on the loads. It is seen that even at the initial stage of opening of the doors the presence of sideslip angle of 5° leads to the drastic (up to 4 times) growth of the hinge moments.

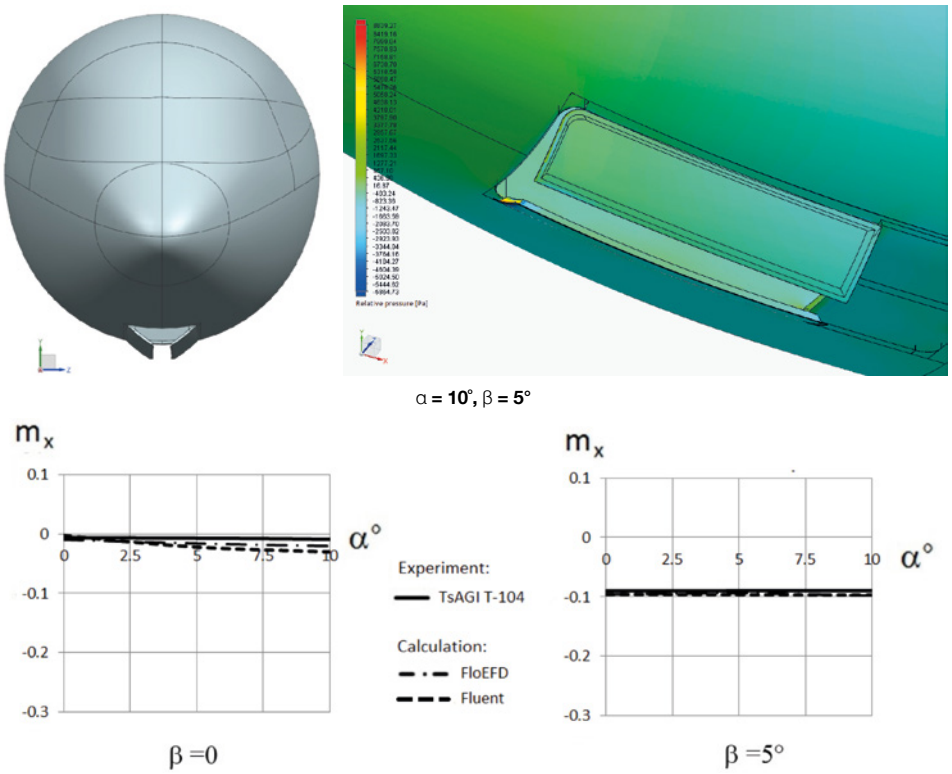

Figure 3. The model with the opened large landing gear doors and the hinge moments of the large nose landing gear doors at δ_{door1} = 30°, δ_{door2} = 30°, δ_{strut} = 0° for the experiment, δ_{door1} = 30°, δ_{door2} = 0°, δ_{strut} = 0° for the calculation, β = 0° and β = 5°.

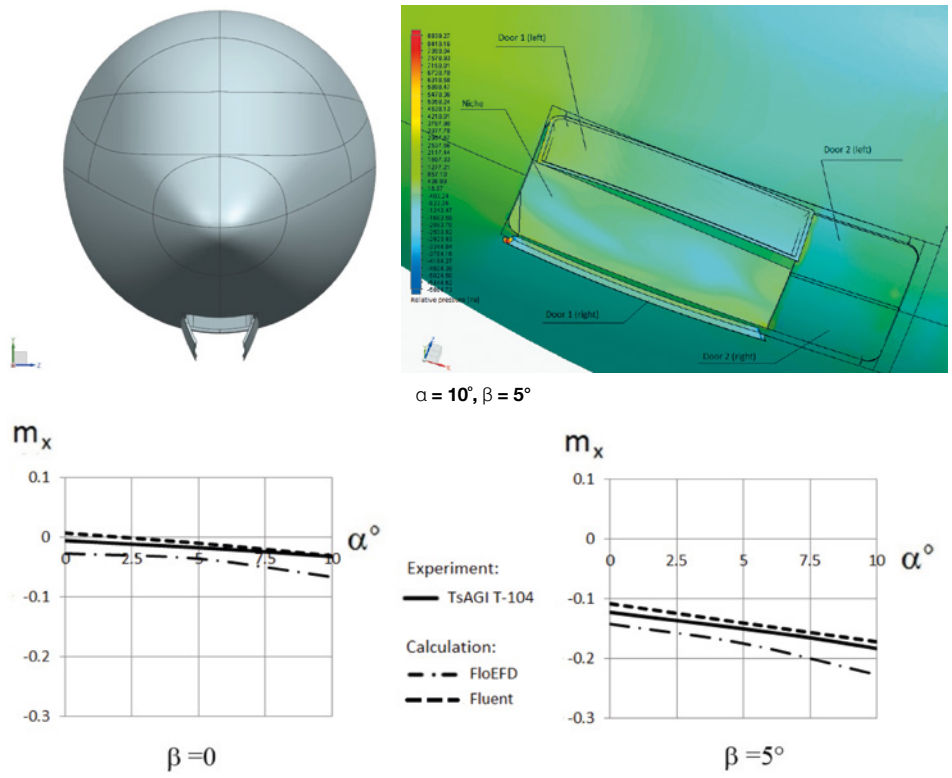

Figure 4. The model with opened large landing gear doors and the hinge moments of the large nose landing gear doors at δ_{door1} = 60°, δ_{door2} = 60°, δ_{strut} = 0° for the experiment, δ_{door1} = 60°, δ_{door2} = 0°, δ_{strut} = 0° for calculation, β = 0° and β = 5°.

From the calculations and the experiments it was obtained that the greatest values of the hinge moments of the doors are observed in their open position in a range of angles δ_{door1} = 60° ÷ 90° (Figures 4 and 5).

Increasing of the sideslip angle up to 5° leads to increase values of the hinge moments approximately in four times. It can be concluded about the constancy of the relative increase of the aerodynamic loads on the doors in the presence of the sideslip angle at all stages of their opening. This pattern can be observed on the charts of the hinge moment coefficients of the nose landing gear doors depending on the angle of their opening as shown on Figure 6. Presented dependencies relate to the angle of attack of 12° in the experiment and 10° in the calculations. The chart below for the sideslip angle of 5° shows nearly linear dependence of growth of hinge moments on the deflecting angle of the doors (with a slight dip in the region of δ = 60° in FloEFD).

2. Flow around the small landing gear doors during the release of the nose landing gear

The computational models of the small rear doors at the release of nose landing gear are shown on figure 7.

The models are made in strict accordance with the kinematics of the connection between the strut and the small door. The hinge moment coefficients of the small door depending on its angle of deflection are shown on figure 8.

Since the left door considered in the article is in the "shadow" of the landing gear by having a kinematic connection with the strut at all stages of the opening, the dependence of the hinge moment on the opening angle of the door is not obvious. The increase of the sideslip angle up to 5° leads to increase of loads only in two times. There is no experimental data of wind tunnel tests for the small doors considering simultaneous release of the landing gear strut.

Conclusions

Computational study of flow around the large and small nose landing gear doors of the commercial aircraft showed that the effect of increasing of the sideslip angle and the opening angle is the most noticeable

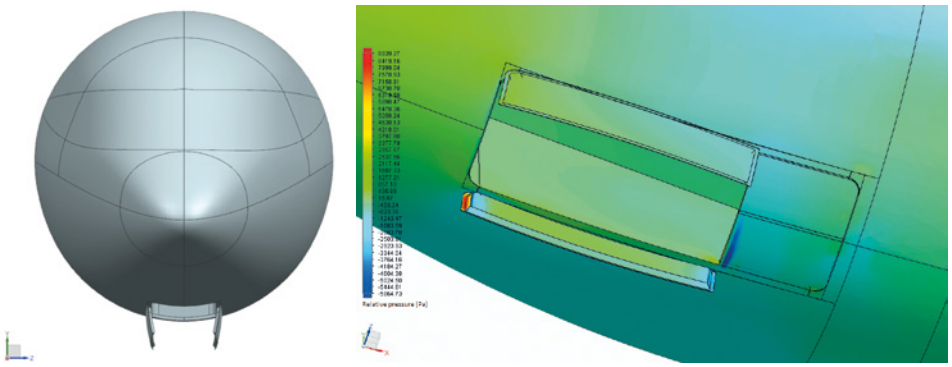

α = **10°,** β = **5°**

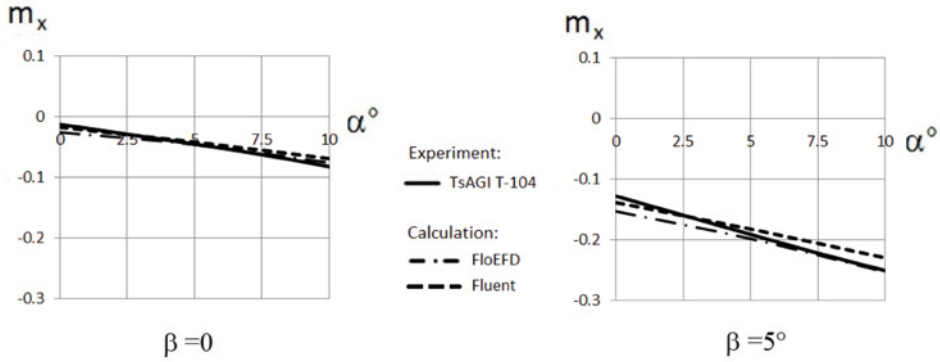

Figure 5. The model with opened large landing gear doors and the hinge moments of the large nose landing gear doors at δ_{door1} = 90°, δ_{door2} = 90°, δ_{strut} = 0° for experiment, δ_{door1} = 74°, δ_{door2} = 0°, δ_{strut} = 0° for calculation, β = 0° and β = 5°.

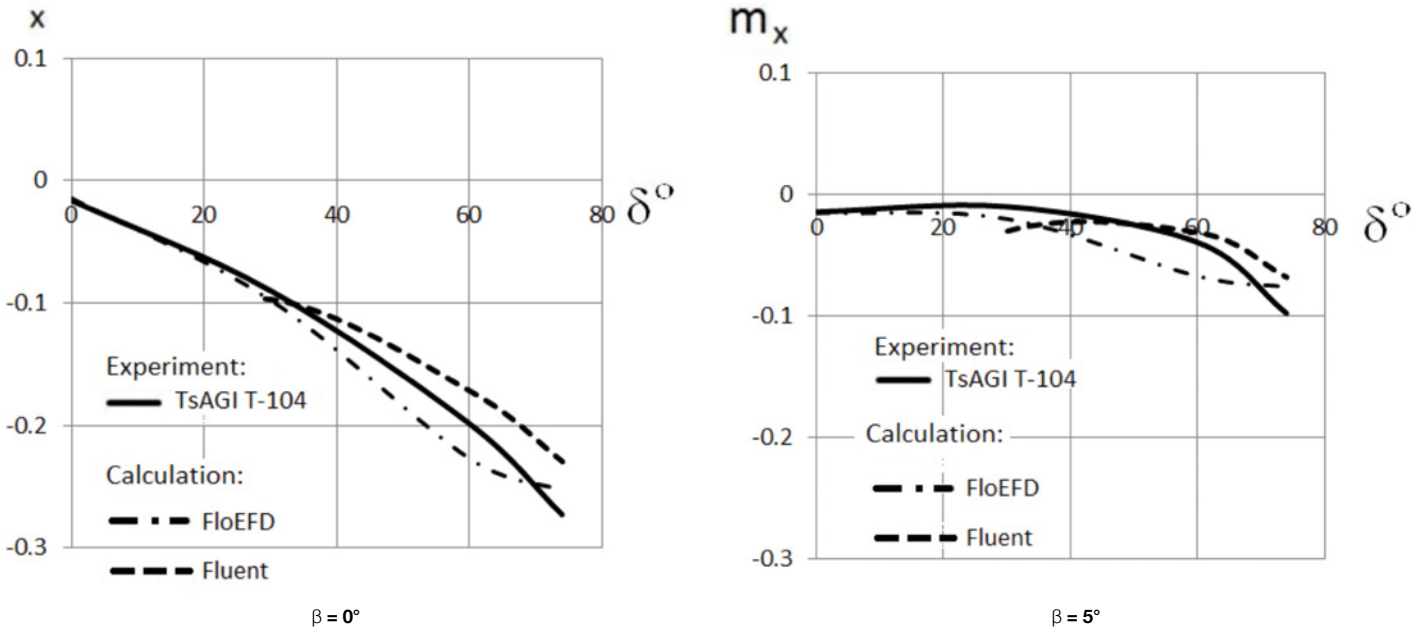

Figure 6. The hinge moment coefficients of large left nose landing gear doors depending on their deflecting angle.

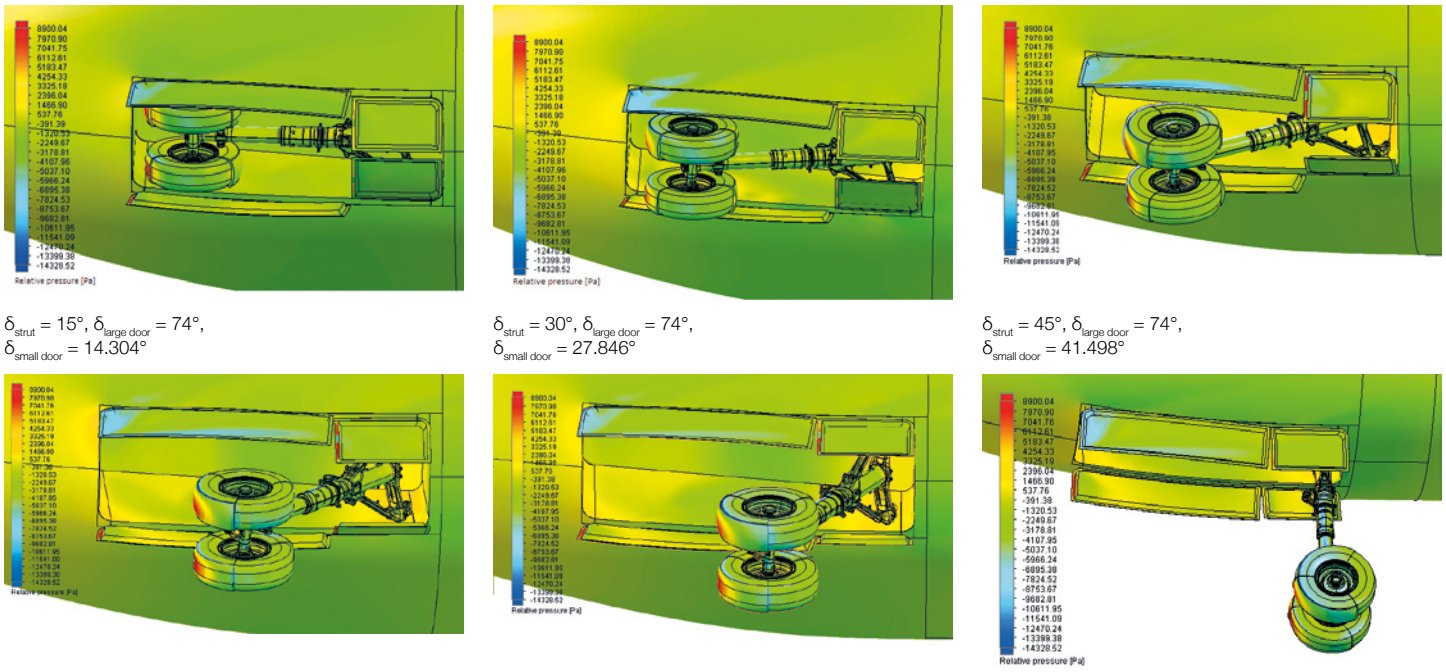

δ_{strut} = 15°, $\delta_{large\ door}$ = 74°, $\delta_{small\ door}$ = 14.304°

δ_{strut} = 30°, $\delta_{large\ door}$ = 74°, $\delta_{small\ door}$ = 27.846°

δ_{strut} = 45°, $\delta_{large\ door}$ = 74°, $\delta_{small\ door}$ = 41.498°

δ_{strut} = 60°, $\delta_{large\ door}$ = 74°, $\delta_{small\ door}$ = 55.378°

δ_{strut} = 75°, $\delta_{large\ door}$ = 74°, $\delta_{small\ door}$ = 68.125°

δ_{strut} = 100°, $\delta_{large\ door}$ = 74°, $\delta_{small\ door}$ = 72.232°

Figure 7. The computational models with different angles of the strut, large and small doors.

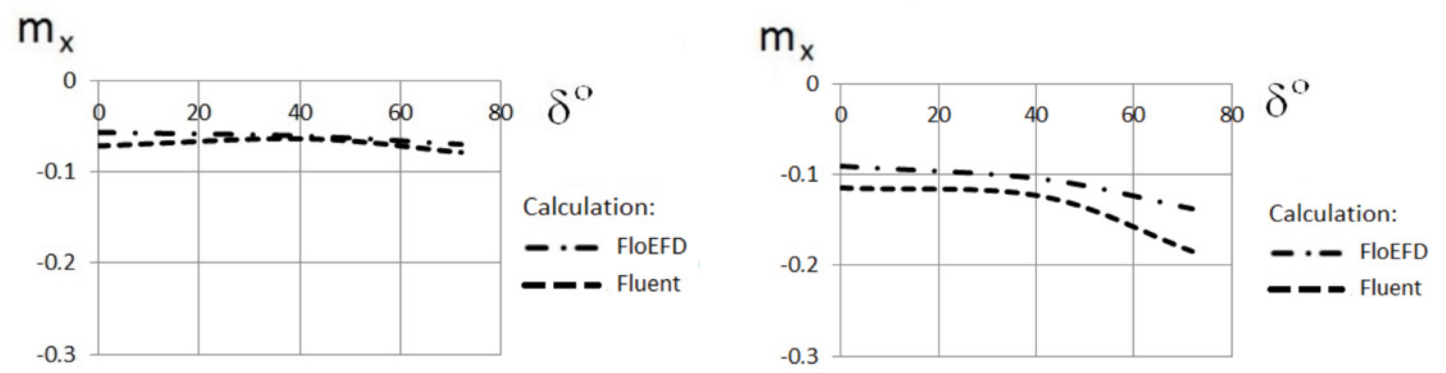

Figure 8. The hinge moment coefficients of small left nose landing gear doors depending on their deflecting angle.

for the large doors with a big aerodynamic surface.

Loads acting on the small doors kinematically connected with the landing gear strut depend on the sideslip angle much less. The dependence of the loads on the small doors on their opening angle occurs only in the presence of sideslip angle.

The results of calculations performed in Fluent and FloEFD presented in this article show good agreement with the experimental data and demonstrate the ability to use these software for the calculation of the loads on the landing gear doors during the design stages.

The use of FloEFD software does not require thorough preparation of the computational model as far as this tool uses an automatic meshing and it is embedded in all modern CAD-software. On the contrary the use of Fluent software with structured mesh requires long preparation of the computational model but allows to perform a fast calculation.

References

[1] Platonov D.V., Minakov A.V., Dekterev A.A., Kharlamov E.B., Comparative Analysis of CFD-packages SigmaFlow and Ansys Fluent on the solution of the laminar problems // Bulletin of the Tomsk State University, 2013, №1 (21)

[2] Pavlenko O.V., Determination of loads on the nose landing gear doors and strut of a commercial aircraft based on the numerical solution of the Navier-Stokes equations // TVF. 2011, Volume LXXXV, №2 (703), p. 19-25

[3] Dr. A. Sobachkin, Dr. G. Dumnov Numerical Basis of CAD-embedded CFD, NAFEMS World Congress 2013

[4] Lam, C.K.G. and Bremhorst, K.A. (1981) Modified Form of Model for Predicting Wall Turbulence, ASME Journal of Fluids Engineering, Vol.103, pp. 456-46

Achieving a 60% Efficient Laser Diode Design With Optimized Thermal Management

By Roberto Mostallino, M. Garcia[1], Y. Deshayes[2], A. Larrue[1], Y. Robert[1], E. Vinet[1], L. Bechou[2], M. Lecomte[1], O. Parillaud[1], and M. Krakowski[1]
1 III-V lab, France 2 Laboratoire IMS, Université de Bordeaux, France.

The demand of high power Laser diodes is ever increasing. Especially devices in the 910-980nm range are used for fibre laser pumping, material processing, solid-state laser pumping, defense and medical/dental applications.

Critical to the device's operation is its ability to convert the input electrical power into output optical power with high efficiency, since such devices need a stable wavelength that is affected by the device temperature.

Researchers at III-V Lab/THALES Research Technology in Palaiseau, France have recently developed a structure for a diode laser based on a Al-free Large Optical Cavity (LOC), [1], and a uniform distributed feedback grating (DFB) and processing techniques that are able to achieve the best up-to-date optical performances with an optimized thermal management through one of the lower thermal resistance. In such a context, low thermal resistance of the entire assembly (< 2K/W) is difficult to measure through classical optical techniques. Detail and precise characterizations of the high power Laser diode assembly have been carried out at IMS Laboratory (CNRS UMR 5218) from the University of Bordeaux. Regular practice is to use an infrared camera, spectral measurements vs temperature and the pulse electrical method. Infrared cameras are not particularly accurate or required emissivity calibration and spectral measurements that monitor temperature variations versus drifts of the central wavelength, are not well-suited for these high power laser diodes mainly due to their spectral multimode behavior. Therefore, the two research teams devised a new measurement approach based on Mentor Graphics' T3Ster® equipment. The method is well-known for conventional electronic devices and LEDs, being a crucial technique for understanding both the thermal management of the structure and its improvement through design for reliability. Part of this approach involved mixing 2D finite element modeling of the Laser diode and structure functions created using the T3Ster-Master software in order to correctly predict the temperature distribution within the structure.

Many papers have been recently published on the use of T3Ster, especially in the field of thermal resistance extraction of high-power GaN-based LEDs, as reported in references 2 to 4. However, application to laser diodes, particularly for a high-power diode laser emitting at 975nm, has been published publicly very recently (See reference in acknowledgements).

The epitaxial construction of the laser is complex, and so not described in detail in this article. It uses a double trench planar structure that is then built up using standard semiconductor processing techniques. The Laser diodes are mounted epi p-side down onto a dedicated C-mount copper heatsink that is mounted on a copper tungsten submount onto which the Laser diode is soldered using gold-tin eutectic solder.

T3Ster uses the Electrical Test Method, as standardized by JEDEC more than 20 years ago. The technique involves heating the device under test using a constant supplied current until the power dissipation and temperature of the device within the test environment, normally mounted on a cold plate, stabilizes. The heating current is then stepped down to a much smaller sensing current, which measures the change in the diode's forward voltage over time, allowing the measurement of this temperature sensitive parameter to be directly related to the junction temperature. From this a one-dimensional thermal model (Foster model) can be derived that for instance shows the cumulative thermal capacitance vs. cumulative thermal resistance from the heat flow path from the heat source at the PN-junction to the ambient. Hence, the technique can give a detailed picture of the heat flow and its spreading crossing the whole device – laser, sub-mount, heatsink, and solder interfaces.

The diode's forward voltage (ΔV_F) is calibrated as a function of temperature beforehand in an oven, by applying the same sensing current used during the measurements, in this case 10mA. This is done by reducing the temperature in the oven from 80°C to 20°C in 10°C steps, waiting for the diode laser's junction temperature (T_J) to reach thermal equilibrium at each oven temperature before the measurement is taken. The results are plotted on a graph, and the K-factor, which relates change in junction temperature to the change in the device's forward voltage, is then calculated as:

$$K = \Delta T_J / \Delta V_F$$

By a suitable fit to the graph's data that needs not necessarily be a linear fit, as the T3Ster-Master software supports non-linear K-factors. Each diode laser tested is separately calibrated to ensure the highest accuracy from the measurements.

To ensure the greatest quality of thermal resistance extraction, the mounting of the device must be repeatable. Various materials have been considered for the interface sheet, including thermal pad, graphite sheet, and indium foil. Tests showed that the thermal resistance of the thermal pad was too high (around 10°C/W), while both graphite sheet and indium foil demonstrate the best repeatability. Graphite sheet was finally chosen and the three screws shown in figure 1 were tightened to a mechanical torque of 0.25Nm.

T3Ster's Structure Function allowed us to quantify the thermal resistance of the laser itself, and layers within the structure. The values are more reliable than using classical optical methods, plus we can identify degradation in the structure of the laser

Roberto Mostallino, PhD Student/ Research engineer, III-IV Lab - Palaiseau/IMS Laboratory, University of Bordeaux - Talence France

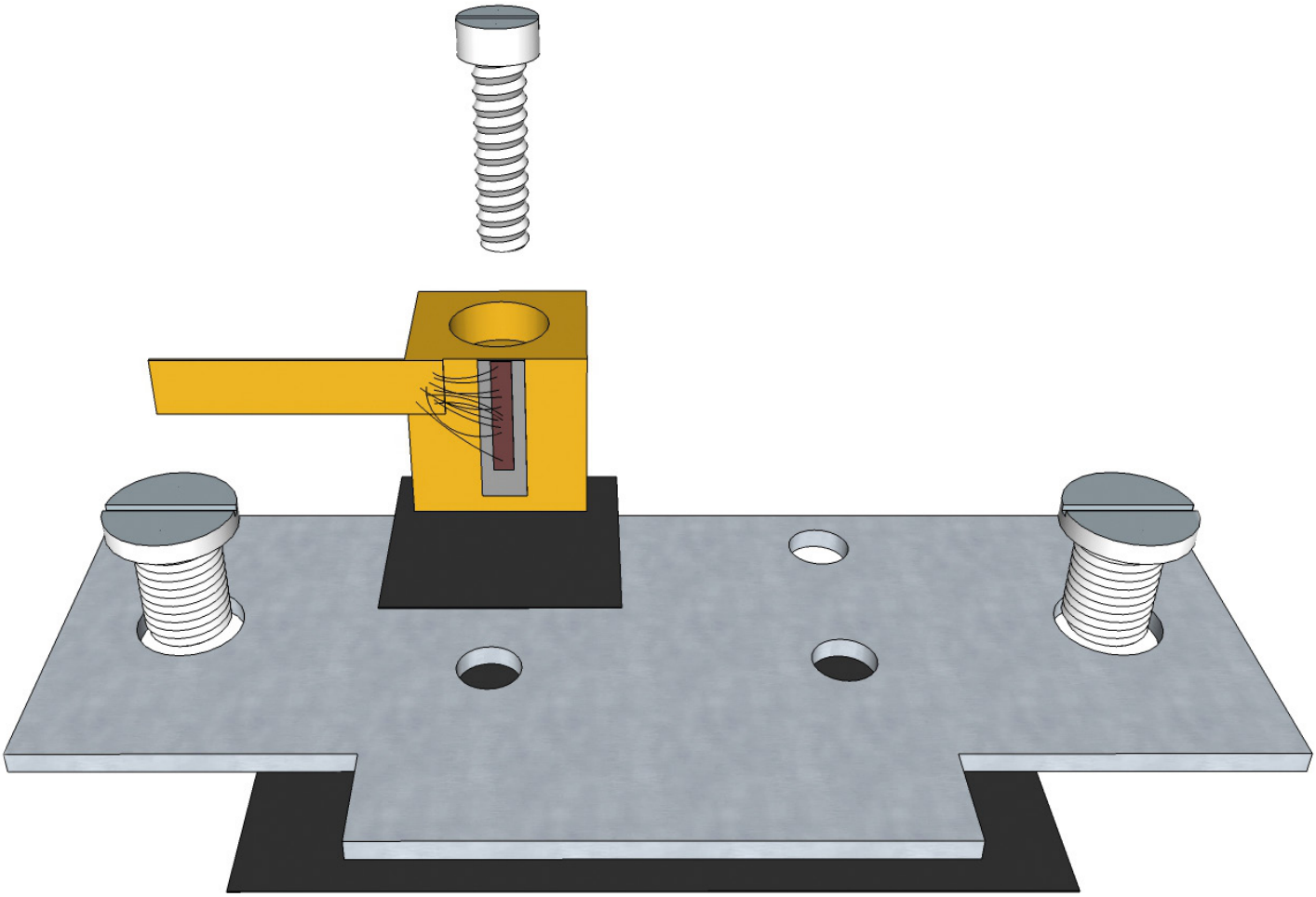

Figure 1. Dedicated fixture used to hold the whole assembly for T3Ster measurements

To ensure a repeatable measurement process, the researchers investigated the measurement time needed for the entire structure to cool down from its powered-on state, investigating times from 200s to 2400s. It was found that a cool-down period of 800s was sufficient to achieve a temperature for the C-Mount copper heatsink to fall to within 0.25°C of the ambient temperature. The level of the heating current was also investigated. If the heating current is too low the laser will not heat sufficiently. If the heating current is too high, lasing is activated and some of the supplied electrical power is thus converted into light. The heating current must be less than or equal to the threshold current. A range of currents from 100mA to 800mA were investigated for lasers with 2mm, 3mm and 4mm cavity lengths. Different cavity lengths have been considered to demonstrate the high level of output optical power under normal operating conditions. The authors highlight that the thermal resistance of the Laser diode chip, calculated from the T3Ster, varies linearly with the laser diode cavity length. Other factors, such as contribution from the mounting, etc. remain the same, thereby helping to identify any problems with the experimental setup. From this, it was determined that the powering currents for the 2mm, 3mm and 4mm cavity lengths should be 300mA, 450mA and 600mA,

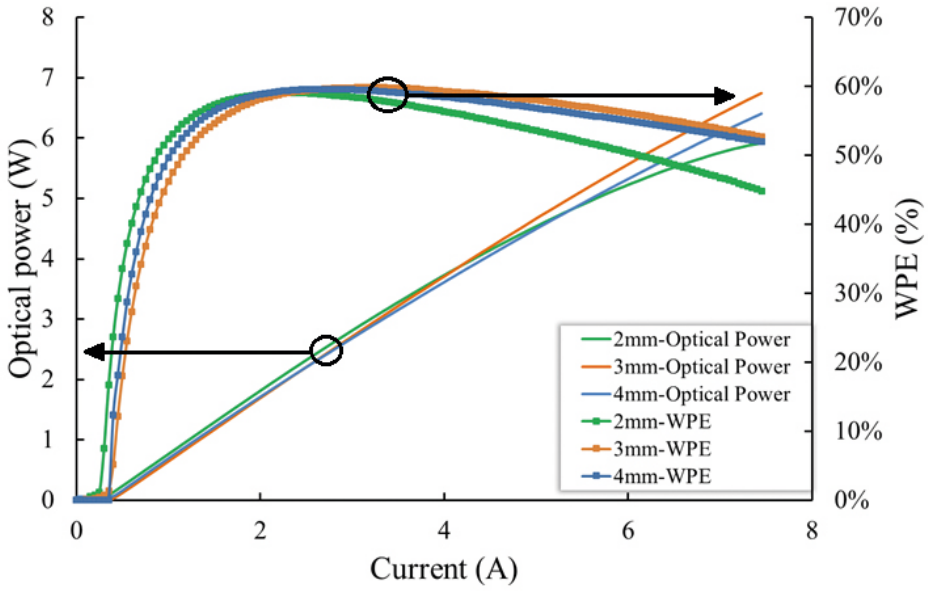

Figure 2. Optical Power and Wall Plug Efficiency vs. Supplied Current

which can be seen to be below the lasing threshold as displayed in figure 2.

In order to reach high levels of optical power output, thermal management of the structure is a key point, so thermal modeling was used to optimize each step of the assembling process. One predominant factor in high power Laser diode is Joule heating, with optical re-absorption also contributing to heating within the laser itself.

Results of the characterization with T3Ster aim to establishing design for robustness and reliability rules, consisting in a feedback into the fabrication process to improve both the epitaxial process and the assembling process. The main outcome of the work

emphasizes a laser diode that has a wall plug efficiency above 60%, that remains stable when driven with a current of up to 8A, exhibits a side mode suppression ratio greater than 30dB (so that emits strongly at 975nm and much more weakly either side of that peak frequency). The spectral line width at 975nm is less than 1nm, putting this device among the very few laser diode with stabilization wavelength thanks to internal gratings (DFB). This laser diode shows also one of the best thermal resistance reported in literature [5].

The Structure Function is shown in figure 4, in which each part of the structure can be identified by the numbers corresponding to those in figure 1. From the Structure Functions it is possible to extrapolate the thermal resistance of the 2, 3 and 4mm cavity length laser diode chips to be 3.2, 2.8 and 1.5°C /W respectively, dealing with a more reliable approach than using the classical optical method. Such technique allows to investigate the contribution of each part of the laser diode assembly. Moreover, T3Ster provides the opportunity to identify any atypical behavior for the device, such as assembly interface degradation.

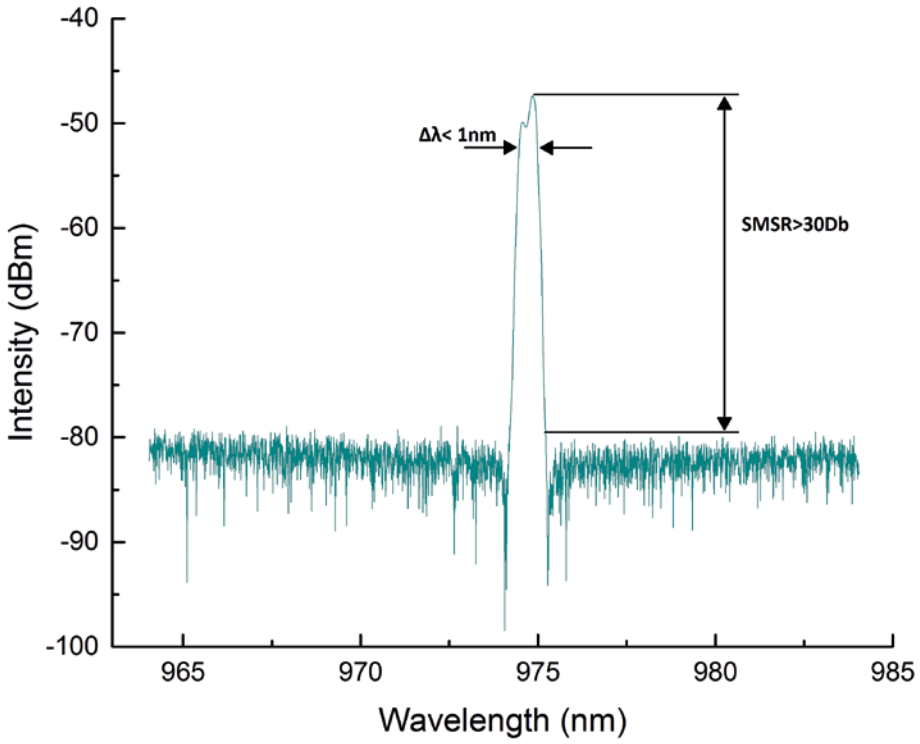

Figure 3. Optical spectrum of a DFB 4mm cavity laser at 60°C in CW operation at 5A.

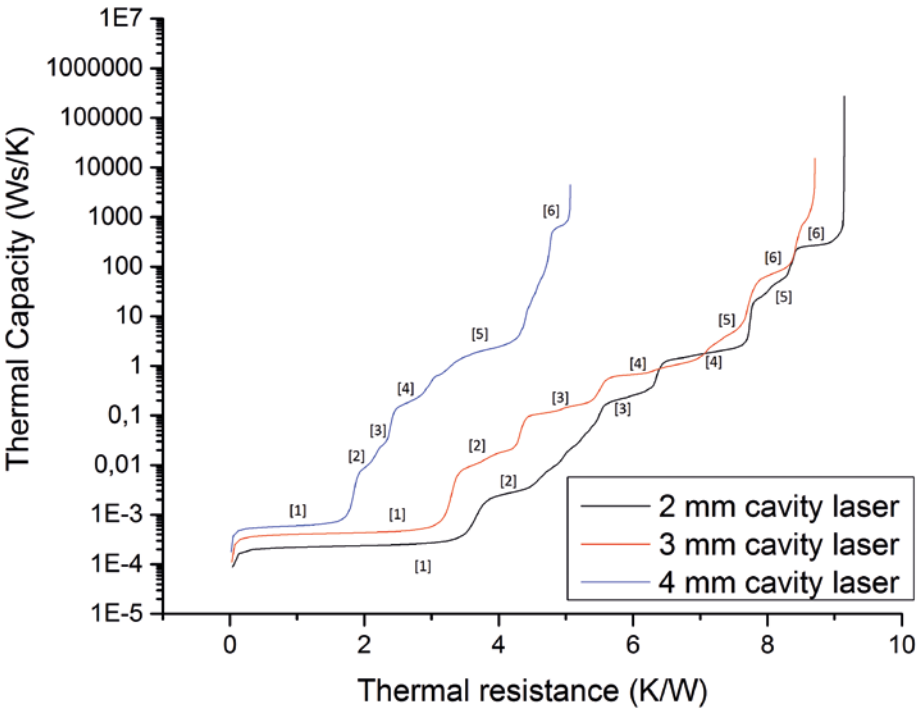

Figure 4. Cumulative Structure Function of three-cavity length laser. The numbers on the plot correspond to the different parts in figure 1.

Acknowledgements:

This article is abstracted from the paper "THERMAL INVESTIGATION ON HIGH POWER DFB BROAD AREA LASERS AT 975nm, WITH 60% EFFICIENCY" by R. Mostallino[1,2], M. Garcia[1], Y. Deshayes[2], A. Larrue[1], Y. Robert[1], E. Vinet1, L. Bechou[2], M. Lecomte[1], O. Parillaud[1], and M. Krakowski[1]

1 III-V lab, 1 avenue Augustin Fresnel 91767 Palaiseau, France

2 Laboratoire IMS, Université de Bordeaux, CNRS UMR 5218, 351 Cours de la Libération, 33405 Talence Cedex, France.

References:

[1] N. Michel, M. Calligaro, M. Lecompte, O. Parillaud, and M. Krakowki, "High wall-plug efficiency diode lasers with an Al free active region at 975nm," in Photonics West Conference, San Jose, USA, 2009, vol. Paper 7198–53.

[2] S. Shanmugan and D. Mutharasu, "Thermal transient analysis of high power led employing spin coated silver doped zno thin film on al substrates as heat sink," J. Optoelectron. Biomed. Mater., vol. 7, no. 1, pp. 1–9, 2015.

[3] S. Shanmugan and Mutharasu, D., "Thermal transient analysis of high power LED tested on Al2O3 thin film coated Al substrate," Int. J. Eng. Trends Technol., vol. 30, no. 6, p. 6, 2015.

[4] C. Jong Hwa and S. Moo Whan, "Thermal investigation of LED lighting module," Microelectron. Reliab., vol. 52, no. 5, pp. 830–835, 2012.

[5] A. Pietrzak, R. Hülsewede, M. Zorn, O. Hirsekorn, J. Sebastian, J. Meusel, P. Hennig, P. Crump, H. Wenzel, S. Knigge, A. Maaßdorf, F. Bugge, and G. Erbert, "Progress in efficiency-optimized highpower diode lasers," in SPIE, 2013, vol. 8898, pp. 08–22.

Geek Hub

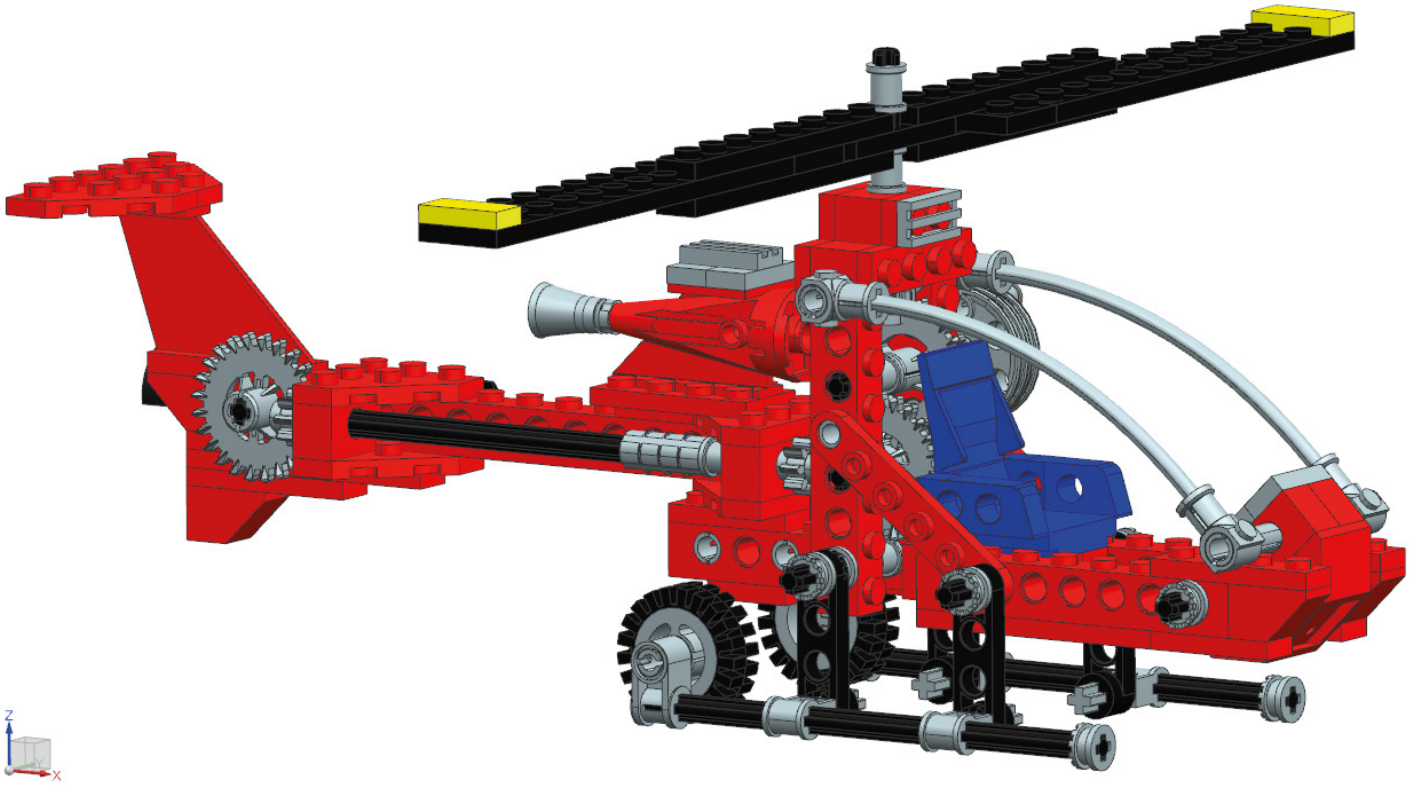

Figure 1. LEGO Technic Aero Hawk. The CAD model of the Aero Hawk was obtained from http://www.GrabCAD.com.

Ever wondered if a LEGO Aero Hawk Helicopter could actually fly?

By Karl du Plessis, Technical Specialist Esteq

Remember that LEGO Aero Hawk from your seventh birthday? Remember how it did loops, flew upside down and even reached warp speed? In the imagination of a seven-year-old anything is possible. But being all grown-up, combined with harsh reality and a degree in engineering, you know that anything is indeed possible, but sadly everything isn't. So you set out to apply your engineering knowledge to determine if there is even the slightest possibility of a LEGO Aero Hawk managing some form of flight. You dive into your vast engineering toolbox and pull out your traditional Computational Fluid Dynamics (CFD) tool.

At first glance, the geometry is quite complex. The LEGO parts being modeled in meticulous detail, which the designer in you can definitely appreciate, but knowing what you know about CFD simulation, immediately you start to think "How on earth am I going to build the mesh for this model?" You consider doing some serious CAD clean-up to reduce the complexity but consequently realise that you would lose too much of the authenticity of the LEGO model when simplifying the geometry down to the level typically required to perform CFD simulations. You are faced with a conundrum. It is time to revive and even stretch a little further that imagination that is long lost due to the doctrine of what is and what isn't possible in the world of CFD… Imagine a world in which one can open up a

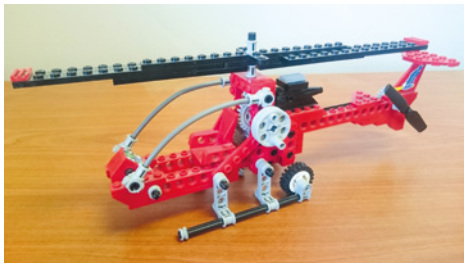

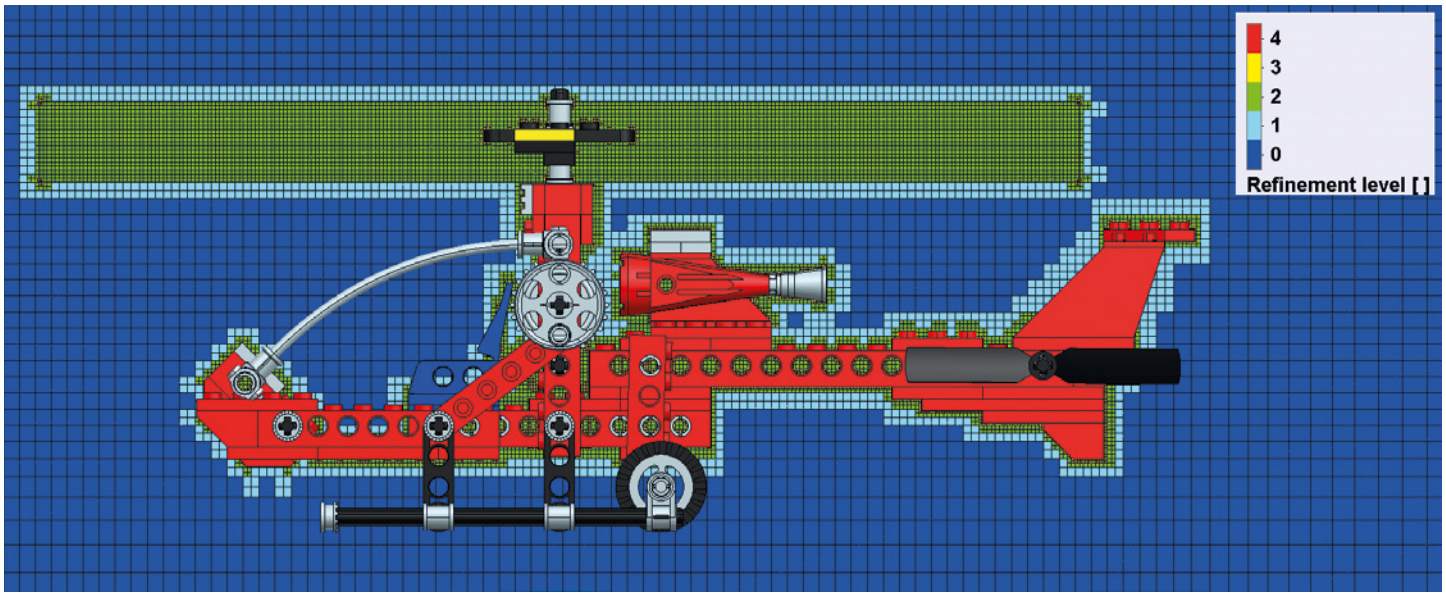

Figure 2. FloEFD Immersed Boundary Cartesian Mesh Cut-plot showing Level of Refinement

CAD model, specify the mesh settings, apply boundary conditions and start solving within a matter of minutes. Sounds like a bit of a stretch of the imagination, doesn't it? Enter FloEFD™!

FloEFD as integrated in Siemens NX was selected to analyse the LEGO Aero Hawk helicopter, making use of the new Sliding Mesh technology in FloEFD to simulate the rotation of the main rotor. This serves as a good test to see how FloEFD would handle the rotation of more complex geometry. You load the model into NX as-is, with only an additional rotating region part (simple cylindrical component) modeled to represent the rotation region that encapsulates the main rotor. You apply a rotor speed of 300rpm. You set the computational domain size and make use of a relatively coarse base mesh as a start with local mesh refinements to control the level of mesh resolution in the rotating region and on the helicopter. You are satisfied with the resulting mesh resolution as in the image below, with approximately one million cells being generated. You are completely amazed at the fact that FloEFD had no trouble creating the mesh even with all of the small geometric features and unnecessary narrow channels between the stacked LEGO blocks. This is obviously wasteful and one would spend some time cleaning up the CAD model in this regard. Nonetheless, you are curious as to how FloEFD will cope with this and proceed, leaving the model as-is in order to test the solver stability. When you are ready to solve you notice that you have access to all of your CPU cores. You select all 16 cores to your availability (or four if you don't have that luxury) and press the "Solve" button and leave the simulation to run overnight. The sliding rotation option requires a transient analysis to be conducted and of course you do have to sleep at some point…

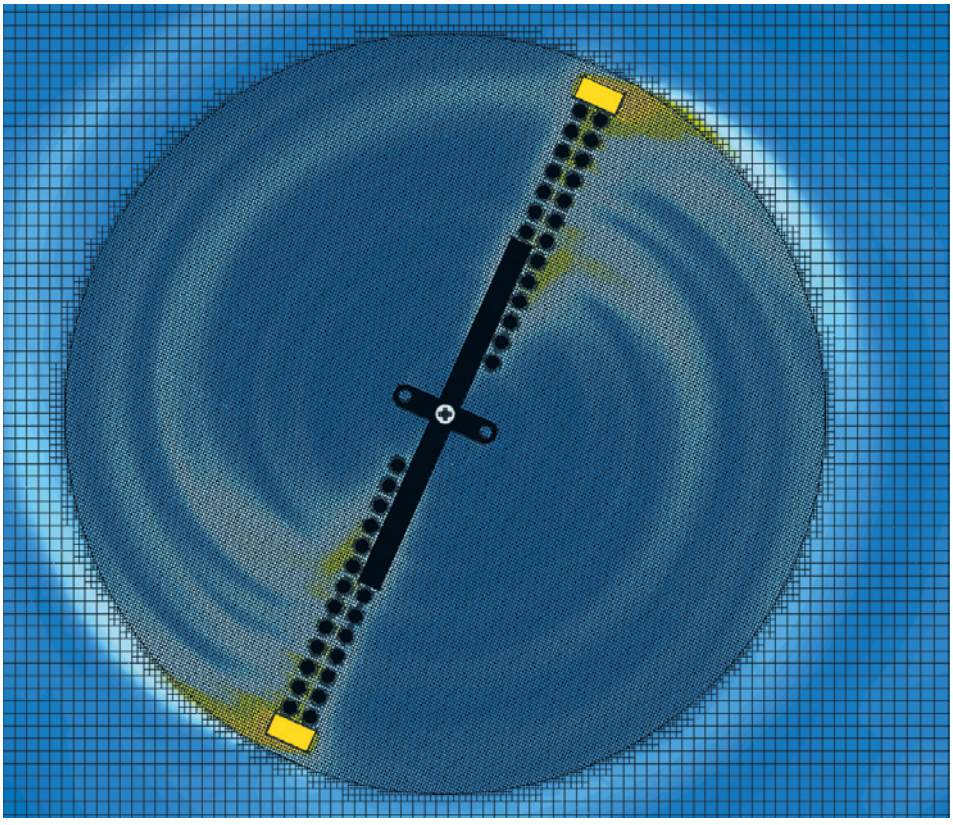

Figure 3. FloEFD Sliding Mesh Rotation

Come morning, the simulation has finished solving without error or divergence. Again you find yourself quite impressed. You play around with the animations post-processing feature and record videos of the velocity field in the plane of the propeller rotation as shown in figure 3, shows the rotation of the mesh within the rotating region just moments after the initial start-

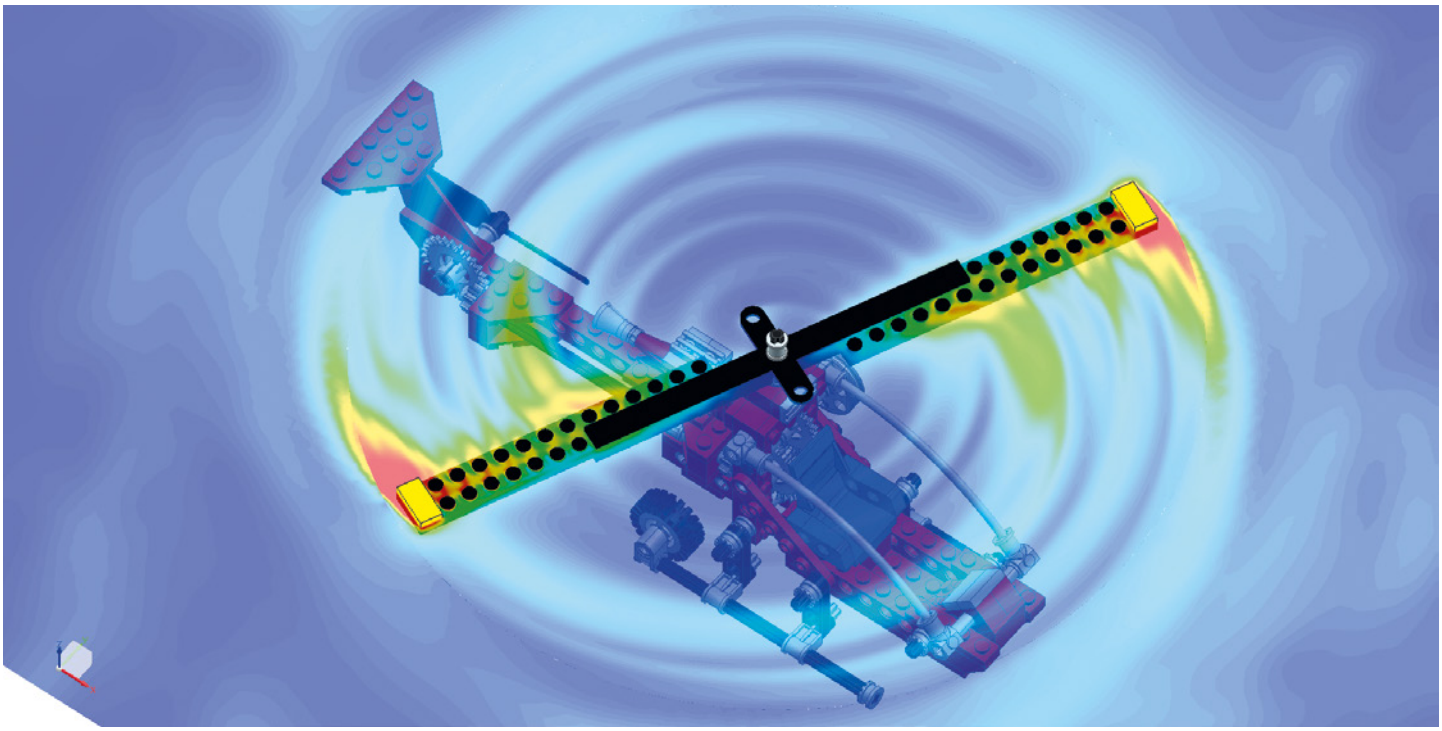

Figure 4. Velocity contour plot with rotor blade rotation

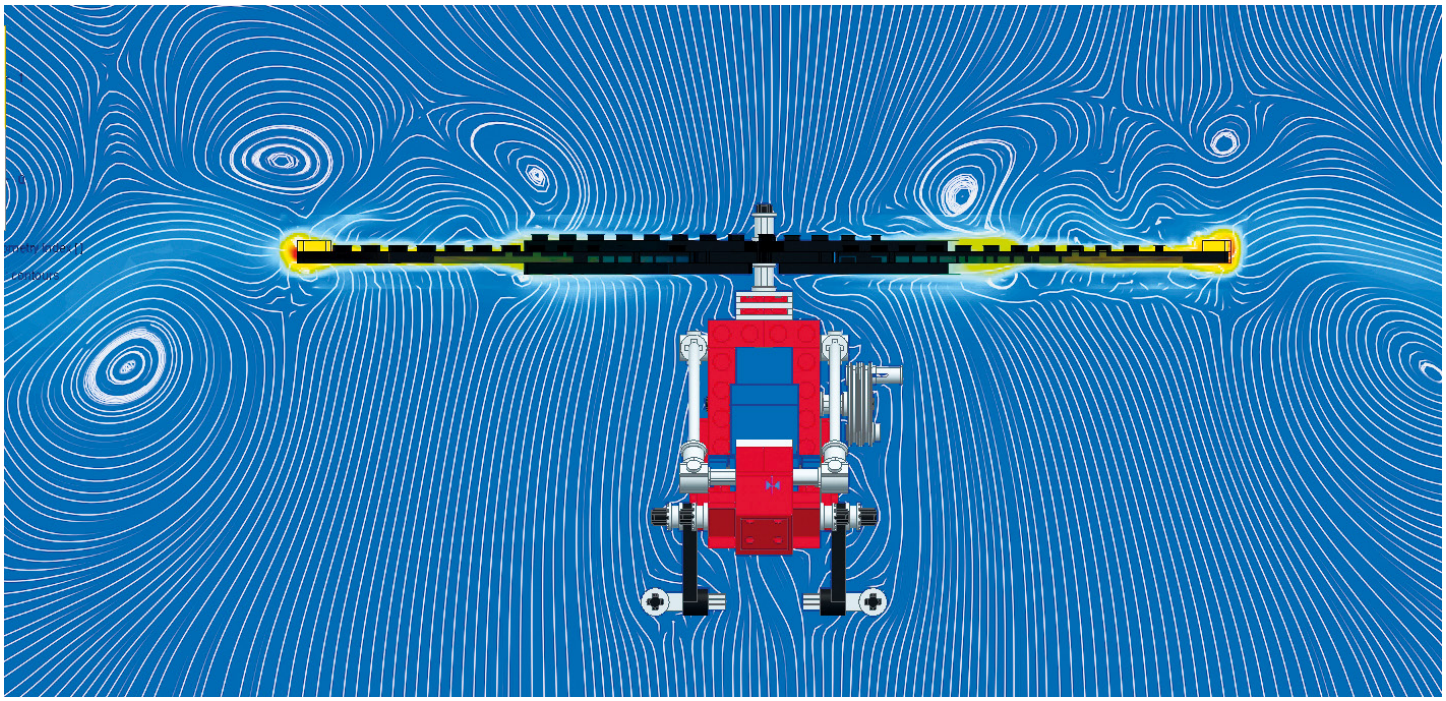

Figure 4. Velocity contour plot with rotor blade rotation

up. Figure 4 shows the velocity field as developed after a few rotations. You make cut-plots of the velocity over the propeller blades and you note in these images the development of the boundary layer at the propeller surfaces, one of the key technologies within FloEFD that make it possible to perform simulations with such complex geometry.

There is still the question – Can this LEGO Aero Hawk actually fly? You make a time-history plot of the propeller lift force. After close inspection you can see a definite positive offset in the average lift force, albeit fairly small, definitely not enough to lift the helicopter off the ground in the real world, but still a positive lift force nonetheless, enough to revive that youthful imagination that knows no bounds. You start to think like the seven-year-old you once were, thinking "if I can develop a strong lightweight material, lighter than anything known to man…or if I can spin the propeller at 3,000,000 rpm, then this LEGO Aero Hawk from my childhood just might actually be able to fly"! Thanks to FloEFD this whole new world of CFD has been unlocked. A world not confined to simplified geometry or constrained by meshes and convergence issues. What seemed hard to imagine in the past has

become a reality, giving the engineer in you free reign to imagine more…(It goes without saying that the very low lift force is due to the fact that the LEGO propeller does not represent an airfoil very well)

FloEFD (Engineering Fluid Dynamics) is a highly sophisticated CFD tool aimed at Engineers. The main objective of FloEFD is to enable engineers to make design decisions as quickly and simply as possible, without having to ask the resident CFD specialist (if one should be so lucky to employ one of these very rare specimens) to perform the thermal-fluid analyses that traditionally required a lot of expertise and patience. FloEFD transcends almost all of the inherent obstacles of traditional CFD through innovative and ingenious technologies that truly stretch the imagination. Some of these technologies include,

- CAD Embedded
- Immersed Boundary Adaptive Cartesian Mesh
- Two-scale Modified Wall Functions
- Enhanced k-ε Turbulence Model.

These technologies are what make FloEFD the efficient and productive engineering tool that it is. Now hopefully the engineer in you is starting to imagine again a world of possibilities that seemed lost in translation and that it is easy to imagine a CFD tool that is easy to use, makes meshing a breeze, is highly tolerant of complex geometry and provides quick, stable, accurate and converged solutions. So in closing, if I may borrow the theme song from The LEGO Movie…

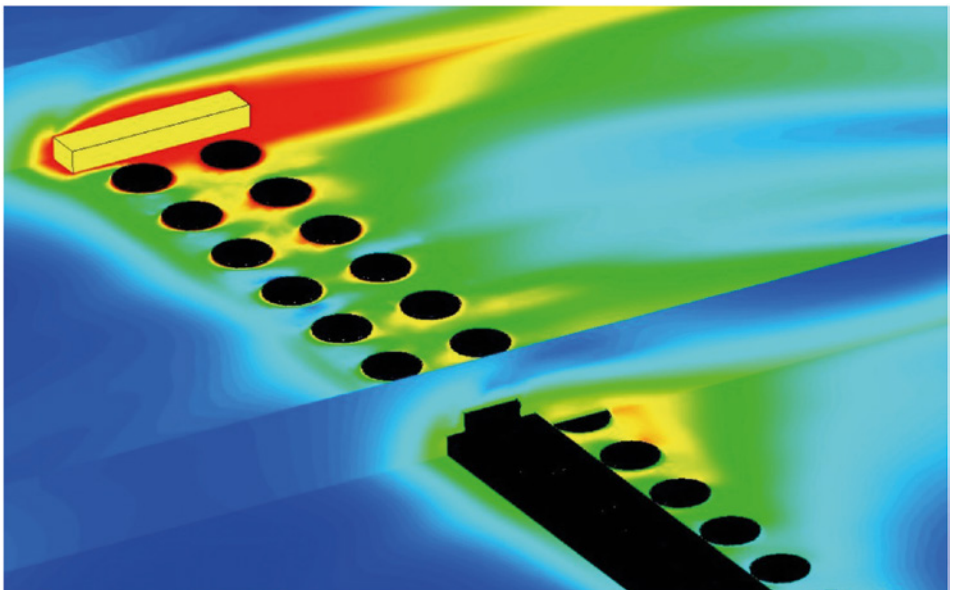

Figure 5. Velocity Cut-plots around rotor blade detail

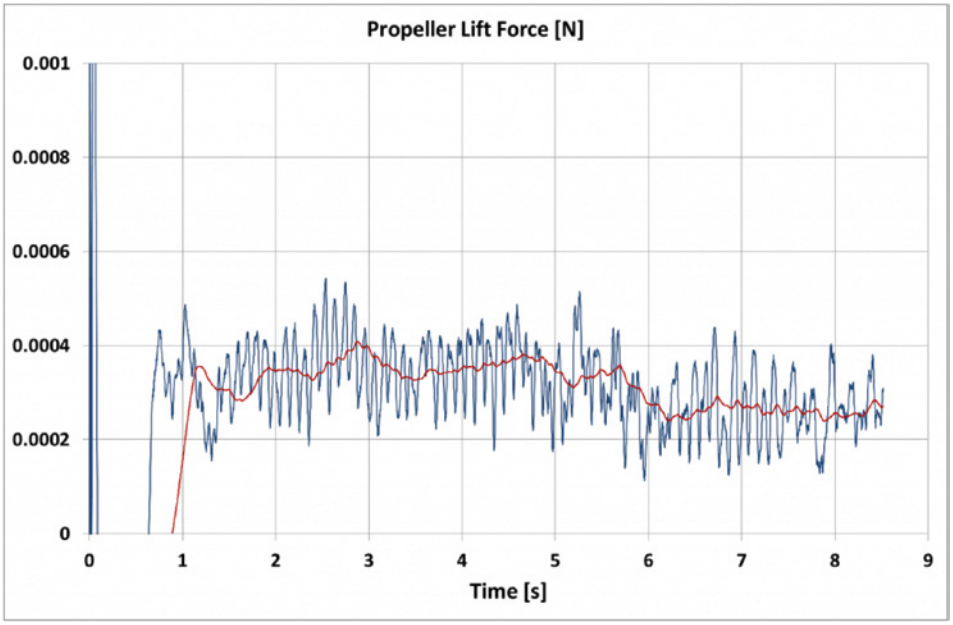

Figure 6. Time-history graph of rotor blade lift force

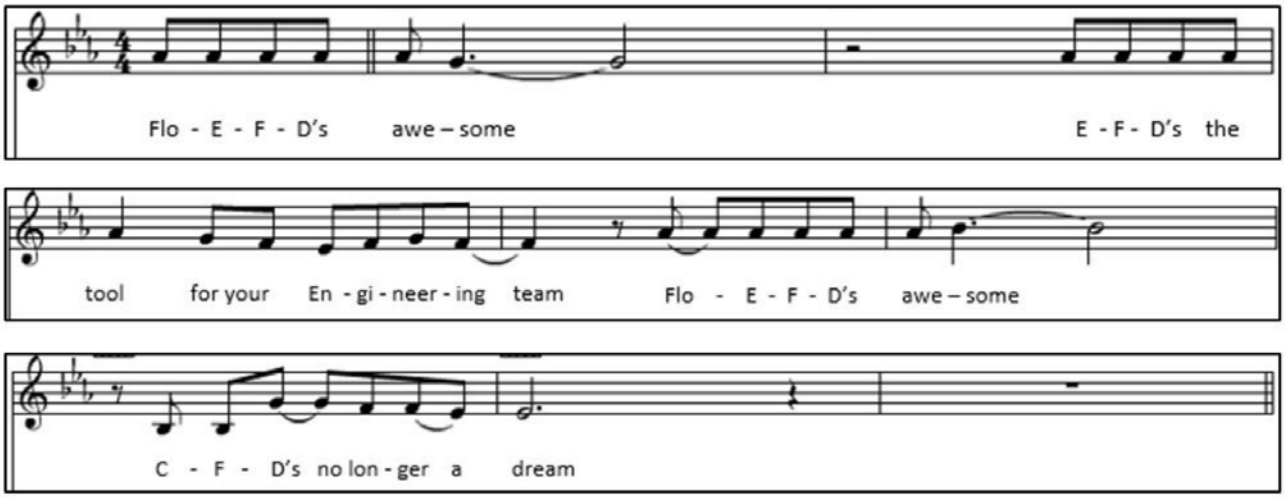

Brownian Motion...

The random musings of a Fluid Dynamicist

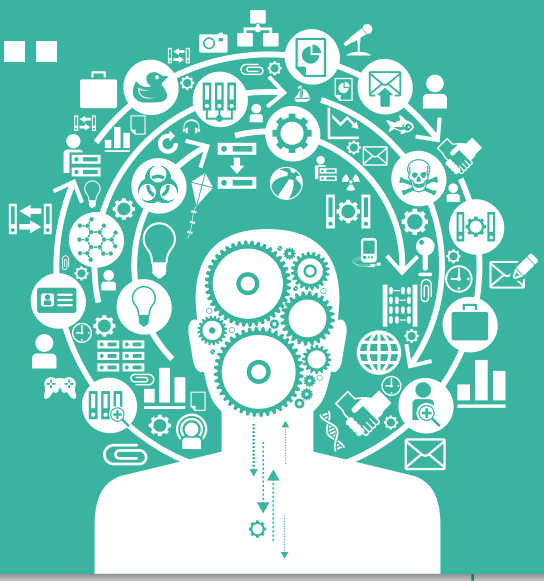

Brownian Motion or **Pedesis** (from Greek: πήδησις Pεdε:sιs 'leaping') is the presumably random moving of particles suspended in a fluid (a liquid or a gas) resulting from their bombardment by the fast-moving atoms or molecules in the gas or liquid. The term 'Brownian Motion' can also refer to the mathematical model used to describe such random movements, which is often called a particle theory.

Not now, I'm Busy

I'm on a train, it's late, around 10pm, and yet there are still a fair number of people on it who have obviously just left the office. The guy opposite me opens his bag and gets some documents out. Across the aisle, a woman is similarly spreading out a vast array of paperwork on the table in front of her.

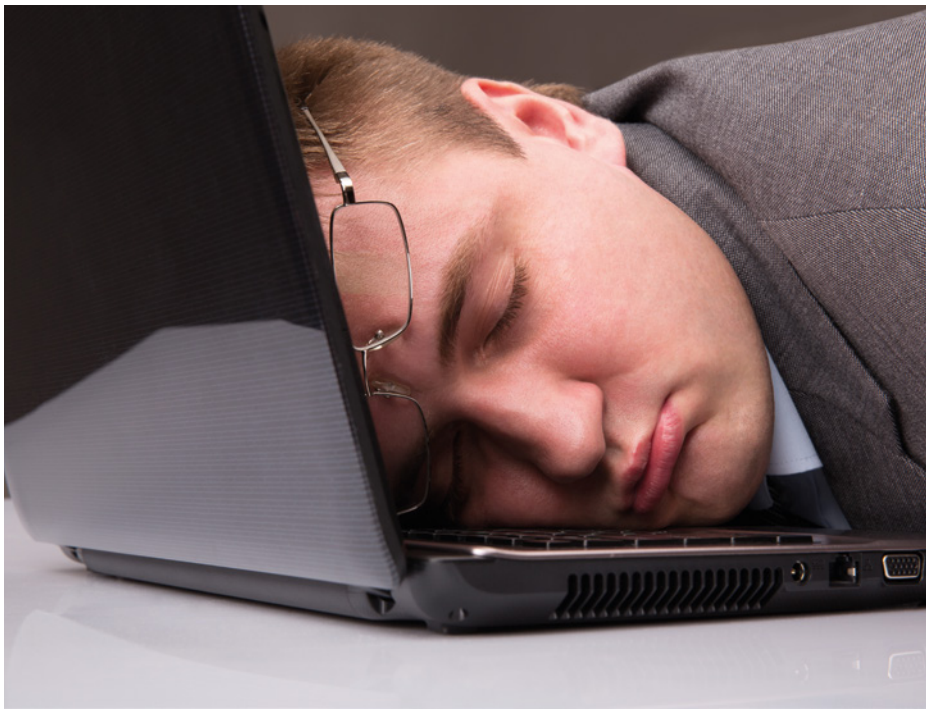

Within ten minutes, both are fast asleep. The guy is snoring across an impressive range of frequencies and the woman is dropping off in a series of improbable and uncomfortable looking poses before startling herself awake and glancing around guiltily. She then goes back to looking at her work.

Only to drift off again.

All the while, the guy opposite me continues to do a decent impression of a saw-mill being inexpertly run by someone who is also snoring loudly. His paperwork remains untouched.

Now, I'm all for going the extra-mile for work, but as the saying goes; you can't pour from an empty cup. These people were exhausted, and yet still felt compelled to at least maintain the pretence of working even when it must have been obvious to them that their brains had thrown the towel in for the day. There are often peaks in work as deadlines approach, but even then I'd have thought the goal is best achieved by knowing when enough is enough and making sure that you can come back to it the next day with a clear mind?

I've read that some companies are going so far as to switch office lights off in an attempt to get particularly zealous employees to go home, which is quite an interesting turn of events; our employers now need to actively step in to stop us working ourselves to a standstill? Whatever would Ebenezer Scrooge make of that, I wonder?

One final thought. I'm going to stick my neck out and say that my fellow travellers had decent jobs that they got in no small part because they're smart, and possibly ambitious, people. I'm not in a position to filter out the cod science from the good when it comes from understanding creativity and productiveness, but I'm going to put money on the fact that neither are helped by being exhausted.

Now, having finished this treatise on taking it easy, it's time to take my own advice.

FloEFD™ Fully CAD Embedded CFD

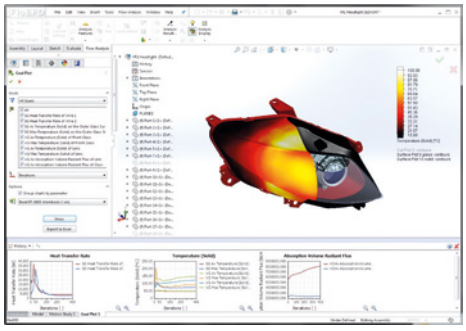

FloEFD - Built on SolidWorks® OEM

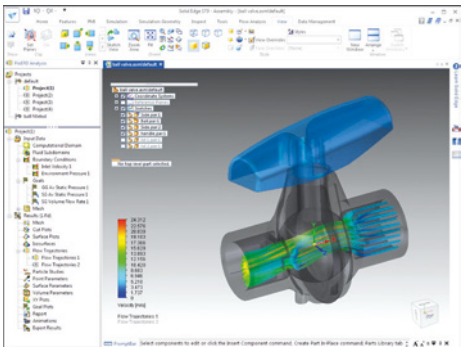

FloEFD for Solid Edge®

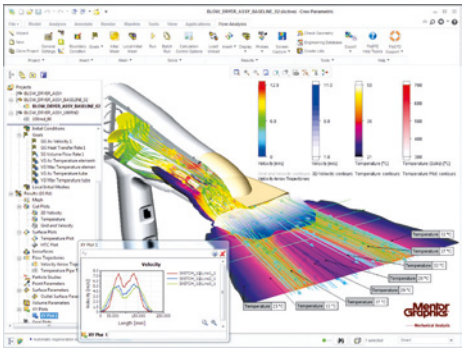

FloEFD for PTC Creo®

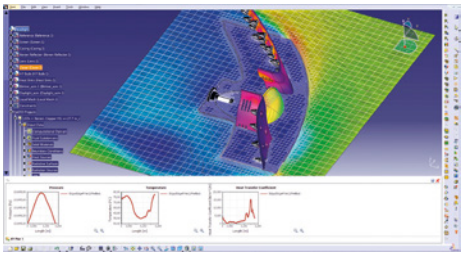

FloEFD for CATIA V5

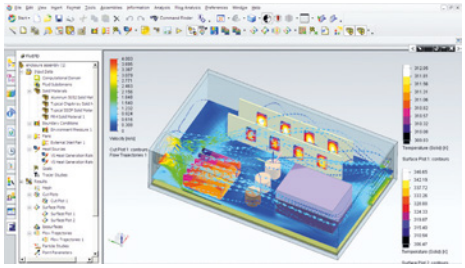

FloEFD for Siemens NX®

Test-drive fully featured FloEFD standalone software with over 20 tutorials within a cloud computing environment: **http://bit.ly/2d2JFdo**

Mentor Graphics®
Mechanical Analysis

Waste Heat Recovery Modeling with FloMASTER™ V8

FloMASTER V8

- Highly Accurate Geometric-Based Plate Frame Heat Exchangers
- Validated against Academic Test Rig
- Quick & Easy System Optimization through Circuit Manager
- Computationally Efficient Shell & Tube Heat Exchangers
- Organic Rankine Cycle Physics

Simple ORC System Modeled in FloMASTER

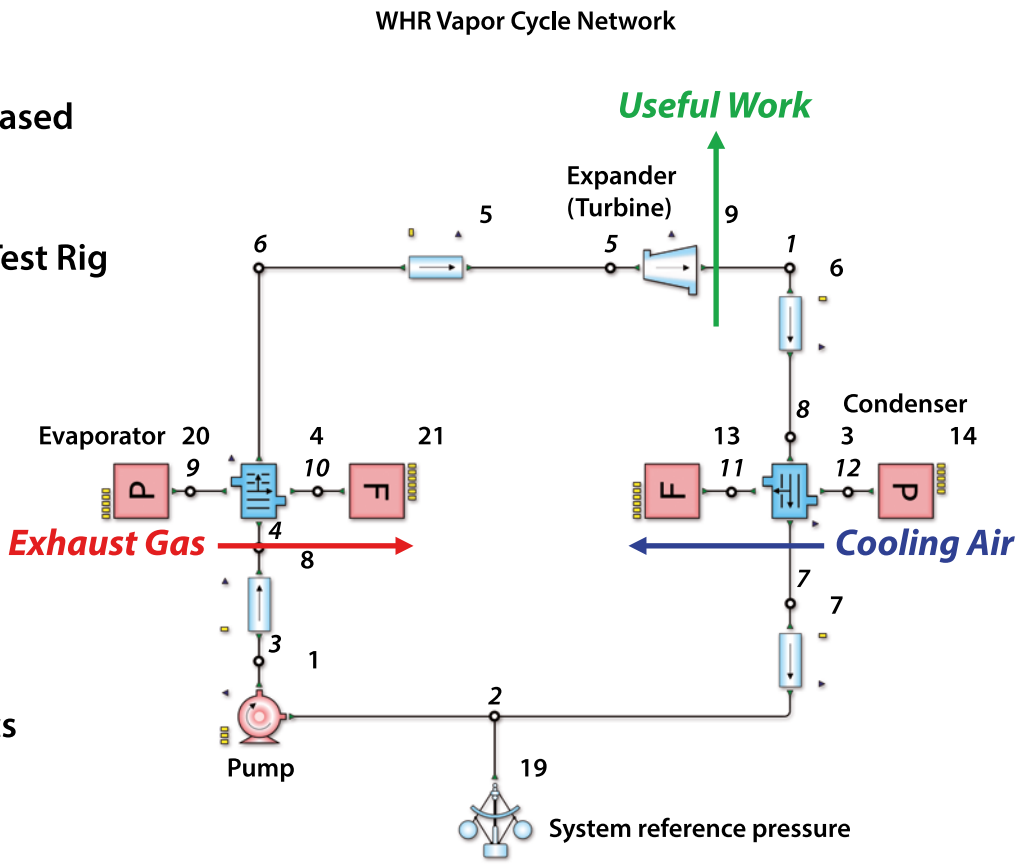

Visit the website for more:
www.mentor.com/mechanical

Mentor Graphics®

Mechanical Analysis